

ATWS-I Analysis Methodology for BWRs Using RAMONA5-FA

ANP-10346NP
Revision 0

Topical Report

December 2017

AREVA Inc.

Copyright © 2017

**AREVA Inc.
All Rights Reserved**

Nature of Changes

Item	Section(s) or Page(s)	Description and Justification
1	All	Initial Issue

Contents

1.0	INTRODUCTION AND SCOPE	1-1
2.0	SUMMARY	2-1
3.0	REGULATORY REQUIREMENTS	3-1
3.1	Compliance with Standard Review Plan, Chapter 15, Section 15.0.2	3-2
3.2	ATWS-I Transient Scenarios	3-2
3.2.1	Turbine Trip	3-3
3.2.2	Two Recirculation Pump Trip	3-4
4.0	PHYSICAL PHENOMENA	4-1
4.1	Unstable Oscillations in General	4-1
4.2	Density Waves in a Boiling Channel	4-2
4.2.1	Density Waves in Parallel Channels between Two Plena	4-4
4.2.2	Density Wave with Power Oscillations due to Density-Reactivity Coupling	4-5
4.3	Oscillation Modes – The Global Mode	4-6
4.4	Oscillation Modes – The Regional Mode	4-7
4.5	Oscillation Modes – The Rotational Mode	4-8
4.6	Oscillation Modes – Axial Power Shape	4-9
4.7	Large Amplitude and Limit Cycles of Global Mode Oscillations with Linearized Hydraulics	4-10
4.8	Large Amplitude Regional Mode Oscillations with Linearized Hydraulics	4-10
4.9	Large Amplitude Pure Thermal-Hydraulic Density Waves	4-11
4.10	Very Large Nonlinear Oscillations of Global and Regional Types	4-13
4.11	Prompt-Criticality	4-15
4.12	Effect of Bypass Flow with Possible Boiling	4-15
4.13	Cyclical Dryout and Rewetting	4-16
4.13.1	Impact of Cyclical Dryout and Rewetting on Very Large Oscillations	4-18
4.14	Vessel Considerations	4-19
4.15	Phenomena Ranking	4-21

4.16	Major Assumptions	4-27
5.0	CODE DESCRIPTION	5-1
5.1	Neutronics	5-1
5.1.1	Adaptive Two-Group 3-D Neutron Kinetics	5-2
5.1.2	Numerical Solution	5-7
5.1.2.1	Interfacial Diffusion Coefficient Approximation	5-8
5.1.2.2	Steady State and Initialization	5-11
5.1.2.3	Time Integration Procedure	5-12
5.1.3	Cross Section Representation	5-15
5.1.4	Power Generation	5-15
5.1.4.1	Prompt Fission Heat	5-16
5.1.4.2	Decay Heat	5-17
5.1.5	Power Deposition	5-19
5.2	Fuel Thermodynamics	5-20
5.2.1	ATWS-I Fuel Pin Heat Conduction	5-21
5.2.2	ATWS-I Heater Rod Heat Conduction	5-30
5.2.3	Heat Transfer Coefficient	5-36
5.2.4	Hot Fuel Pin Model	5-42
5.2.5	Material Properties	5-43
5.2.6	Pellet-Clad Gap Heat Transfer Coefficient	5-45
5.2.7	Radial Power Deposition Distributions in Fuel Pellets	5-51
5.3	Thermal-hydraulic Model	5-52
5.3.1	General Description of the System Considered	5-53
5.3.2	[]	5-56
5.3.3	Vapor generation rate	5-60
5.3.4	Mass conservation	5-62
5.3.5	Energy Conservation	5-63
5.3.6	[]	5-67
5.3.7	[] Momentum Conservation	5-69
5.3.7.1	[] Formulation in the Vessel Components	5-74
5.3.7.2	[] Formulation in the Core	5-76
5.3.8	Pressure Calculation	5-78
5.3.9	Steam Dome Equations	5-81
5.3.10	Recirculation Flow	5-83
5.3.11	Constitutive Equations	5-86
5.3.11.1	Friction and Two Phase Friction Multiplier	5-86
5.3.11.2	Local Pressure Loss Models	5-88
5.3.11.3	Abrupt Contraction/Expansion Pressure Change Model	5-89

5.3.11.4 []	5-90
5.3.11.5 Thermodynamic Steam-Water Properties	5-91
5.3.11.6 []	5-91
5.3.12 Numerical Integration Techniques	5-93
5.4 Steam Line Flow Dynamics	5-94
5.5 SPECIAL MODELS	5-97
5.5.1 Recirculation Pump Model	5-97
5.5.1.1 Pump Model 1	5-98
5.5.1.2 Pump Model 2	5-98
5.5.1.3 Pump Model 3	5-99
5.5.2 Jet Pump Model	5-100
5.5.3 Steam Separator Model	5-102
5.5.3.1 Flow Inertia	5-103
5.5.3.2 Carry under Flow	5-103
5.5.4 Feedwater Sparger Condensation Model	5-107
5.5.5 Dryout and Rewetting Model	5-108
5.6 PLANT CONTROL AND PROTECTION SYSTEMS	5-116
5.6.1 Pressure Control System	5-117
5.6.1.1 Turbine Valve Regulator	5-117
5.6.1.2 Bypass Valve Regulator	5-117
5.6.2 Feedwater Controller	5-118
5.6.3 Safety and Relief Valves	5-118
5.6.4 Main Steam Isolation Valve (MSIV)	5-119
5.6.5 Plant Protection System (PPS)	5-120
5.6.6 Manual Operator Actions	5-120
5.7 NUMERICAL TIME INTEGRATION	5-120
5.7.1 Neutron Kinetics	5-121
5.7.2 Fuel Thermodynamics	5-121
5.7.3 Vessel Hydraulics	5-121
5.7.4 Coupling of the Neutronics and Hydraulics Integration	5-122
6.0 CODE VALIDATION	6-1
6.1 Test Suite and Acceptance Criteria	6-2
6.2 Benchmarking to Void Fraction Tests	6-4
6.3 Benchmarking to KATHY Pressure Drop Tests	6-7
6.4 Benchmarking to KATHY Stability Tests	6-11
6.5 Benchmarking to KATHY Dryout/Rewet Tests	6-14
6.6 Benchmarking to Linear Reactor Stability Benchmarks	6-27
6.6.1 []	6-27

6.6.2	[]	6-28
6.6.3	[]	6-28
6.6.4	[]	6-29
6.7	Benchmarking to Non-Linear Reactor Benchmarks	6-29
6.7.1	Oskarshamn Nonlinear Instability	6-29
6.7.2	BWR A Feedwater Transient with Non-Linear Instability	6-34
7.0	SAMPLE PROBLEMS	7-1
7.1	Turbine Trip	7-1
7.2	Two Recirculation Pump Trip	7-8
8.0	CALCULATION PROCEDURE	8-1
9.0	REFERENCES	9-1
Appendix A	Steady State Dryout Correlation CPROM	A-1
A.1	DESCRIPTION OF CPROM CORRELATION	A-1
A.2	CPROM CORRELATION FOR ATRIUM 10XM	A-5
A.3	CPROM BOUNDS OF APPLICABILITY	A-19
A.4	CPROM COEFFICIENT GENERATION FOR NEW FUEL DESIGNS	A-20
Appendix B	Heat Transfer Data from KATHY Loop Stability Testing of ATRIUM 10XM	B-1
B.1	SUMMARY OF HEAT TRANSFER COEFFICIENT DATA AND OBSERVATIONS	B-1
B.2	HEAT TRANSFER COEFFICIENT UNDER WETTED CONDITIONS	B-3
B.3	[]	B-3
B.4	REFERENCES	B-6
Appendix C	Investigation of the Dynamic Effects of Interfacial Friction	C-1

Tables

Table 4-1: Ranking of Phenomena and Processes 4-23

Table 5-1: Summary of State Equations..... 5-94

Table 5-2: Homologous Pump Curves Definition 5-100

Table 6-1: Summary of Void Fraction Test Conditions 6-5

Table 6-2: Summary of Pressure Drop Test Conditions 6-8

Table 6-3: Dryout and rewetting ATRIUM 10XM KATHY test runs 6-17

Table 7-1: TTWB Sensitivity Study Results 7-4

Table 7-2: 2RPT Sensitivity Study Results 7-9

Table 8-1: ATWS-I Limitation and Conditions 8-4

Figures

Figure 5-1: Fuel rod discretization	5-24
Figure 5-2: Heater rod discretization	5-32
Figure 5-3: Loop Parts in the Vessel Hydraulics Model.....	5-54
Figure 5-4: Recirculation Loop	5-84
Figure 5-5: Steam Line Model	5-95
Figure 5-6: The Loop Parts of the Vessel Hydraulics	5-105
Figure 6-1: Validation of [] using FRIGG, ATRIUM-10 and ATRIUM 10XM Void Data.....	6-6
Figure 6-2: Validation of Pressure Drop Prediction versus KATHY ATRIUM-10 Measured Data	6-9
Figure 6-3: Validation of Pressure Drop Prediction versus KATHY ATRIUM 10XM Measured Data.....	6-10
Figure 6-4: Validation of Decay Ratio Prediction versus KATHY Measured Data	6-13
Figure 6-5: Validation of Frequency Prediction versus KATHY Measured Data.....	6-13
Figure 6-6: Limiting Temperature for KATHY ATRIUM 10XM []	6-18
Figure 6-7: Limiting Temperature for KATHY ATRIUM 10XM []	6-18
Figure 6-8: Limiting Temperature for KATHY ATRIUM 10XM []	6-19
Figure 6-9: Limiting Temperature for KATHY ATRIUM 10XM []	6-19
Figure 6-10: Limiting Temperature for KATHY ATRIUM 10XM test []	6-20
Figure 6-11: Limiting Temperature for KATHY ATRIUM 10XM []	6-20
Figure 6-12: Limiting Temperature for KATHY ATRIUM 10XM []	6-21
Figure 6-13: Limiting Temperature for KATHY ATRIUM 10XM []	6-21
Figure 6-14: Limiting Temperature for KATHY ATRIUM 10XM []	6-22
Figure 6-15: Limiting Temperature for KATHY ATRIUM 10XM []	6-22
Figure 6-16: Limiting Temperature for KATHY ATRIUM 10XM []	6-23
Figure 6-17: Limiting Temperature for KATHY ATRIUM 10XM []	6-23
Figure 6-18: Limiting Temperature for KATHY ATRIUM 10XM []	6-24
Figure 6-19: Limiting Temperature for KATHY ATRIUM 10XM []	6-24
Figure 6-20: Limiting Temperature for KATHY ATRIUM 10XM []	6-25
Figure 6-21: Limiting Temperature for KATHY ATRIUM 10XM []	6-25
Figure 6-22: Limiting Temperature for KATHY [].....	6-26

Figure 6-23: Limiting Temperature for KATHY []	6-26
Figure 6-24: Oskarshamn-2 Non-Linear Stability Simulation Core Power, Imposed Pump Speed	6-31
Figure 6-25: Oskarshamn-2 Non-Linear Stability Simulation Core Power - Zoom, Imposed Pump Speed	6-31
Figure 6-26: Oskarshamn-2 Non-Linear Stability Simulation Recirculation Flow, Imposed Pump Speed	6-32
Figure 6-27: Oskarshamn-2 Non-Linear Stability Simulation Core Power, Match Recirculation Flow	6-32
Figure 6-28: Oskarshamn-2 Non-Linear Stability Simulation Core Power - Zoom, Match Recirculation Flow	6-33
Figure 6-29: Oskarshamn-2 Non-Linear Stability Simulation Recirculation Flow, Match Recirculation Flow	6-33
Figure 6-30: BWR [] Transient Non-Linear Stability Simulation.....	6-35
Figure 7-1: TTWB Base Case Core Power	7-5
Figure 7-2: TTWB Base Case Core Inlet Flow	7-5
Figure 7-3: TTWB Base Case Core Inlet Subcooling	7-6
Figure 7-4: TTWB Base Case Limiting Channel Inlet Flow	7-6
Figure 7-5: TTWB Base Case Vessel Water Level	7-7
Figure 7-6: TTWB Base Case Limiting Channel PCT.....	7-7
Figure 7-7: 2RPT Base Case Core Power	7-9
Figure 7-8: 2RPT Base Case Core Inlet Flow	7-10
Figure 7-9: 2RPT Base Case Limiting Channel Inlet Flow	7-10
Figure 7-10: 2RPT Base Case Core Inlet Subcooling	7-11
Figure 7-11: 2RPT Base Case Vessel Water Level	7-11
Figure 7-12: 2RPT Base Case Limiting Channel PCT.....	7-12

Nomenclature

Acronym	Definition
2RPT	Two Recirculation Pump Trip
ANS	American Nuclear Society
ATWS	Anticipated Transient Without Scram
ATWS-I	Anticipated Transient Without Scram With Instability
BOC	Beginning of Cycle
BWR	Boiling Water Reactor
CFR	Code of Federal Regulations
CHF	Critical Heat Flux
CPR	Critical Power Ratio
CPRM	Critical Power Reduced Order Model
DC	Downcomer
DNB	Departure from Nucleate Boiling
DIVOM	Delta over Initial Versus Oscillation Magnitude
EFW	Extended Flow Window
EM	Evaluation Model
EOC	End of Cycle
EOI	Emergency Operating Instructions
EOP	Emergency Operating Procedure
EPU	Extended Power Uprate
FoM	Figure of Merit
GDC	General Design Criteria
HPCI	High Pressure Coolant Injection
HTC	Heat Transfer Coefficient
KATHY	Karlstein thermal-hydraulic loop test facility
LCA	Limit Cycle Amplitude
LHGR	Linear Heat Generation Rate
LP	Lower Plenum
LPRM	Local Power Range Monitor
MCPR	Minimum Critical Power Ratio

MELLLA	Maximum Extended Load Line Limit Analysis
MSIV	Main Steam Isolation Valve
OI	Oscillation Inception
PBDA	Period Based Detection Algorithm
PCT	Peak Clad Temperature
PDO	Post Dryout
PHE	Peak Hot Excess
PIRT	Phenomena Identification and Ranking Table
PPS	Plant Protection System
PWR	Pressurized Water Reactor
QA	Quality Assurance
RCIC	Reactor Core Isolation Cooling
SLC	Standby Liquid Control
SP	Standpipe
SRP	Standard Review Plan
SRV	Safety/Relief Valve
SS	Steam Separators
TR	Topical Report
TTWB	Turbine Trip With Bypass
UP	Upper Plenum
USNRC	United States Nuclear Regulatory Commission

Abstract

This report presents a generic methodology for licensing the Extended Flow Window (EFW) operation of BWR3 to BWR6 plants with regard to Anticipated Transient without Scram with Instability (ATWS-I). The method aims at addressing the fuel specific impacts of the ATWS-I event. The methodology presented in this report utilizes the RAMONA5-FA computer code. The presented version of RAMONA5-FA has been modified to be capable of simulating the severe power and flow oscillations associated with core instabilities unsuppressed with scram. The code applies advanced models for post-dryout heat transfer for the calculation of the cladding temperature excursion. These post-dryout models are based on, and benchmarked against, data obtained from the Karlstein thermal-hydraulic loop (KATHY) test facility where a full scale electrically heated ATRIUM 10XM bundle was tested under realistic ATWS-I conditions of severe unstable density waves with simulated reactivity and power feedback.

The RAMONA5-FA code has been benchmarked against both single bundle KATHY measurements as well as regional and global oscillations in actual BWR plants. The KATHY benchmarks include pressure drop, void fraction, and stability measurements for several bundle designs. The plant stability benchmarks include benchmarks in both the linear and nonlinear instability domains.

In addition to benchmarking, sample ATWS-I transients, along with selected sensitivities are presented to better understand the event. Finally, a calculation procedure is described to define the process and conservatisms to be used in licensing calculations.

1.0 INTRODUCTION AND SCOPE

This document presents a description of BWR instability transients that are not terminated by scram, and thus power and flow oscillations grow to large amplitudes (see References 1 and 2). This class of transients is referred to as Anticipated Transients Without Scram with Instability (ATWS-I). This report documents a RAMONA5-FA based method for evaluating the fuel-related aspects of these events.

The methodology complies with the USNRC requirements of Section 15.8 of NUREG-800, Reference 3. The method is applicable to the limiting ATWS-I events covering the event from the initiation through inception of oscillations and final suppression through operator action.

Section 2 presents a summary of the method and its intended application. Section 3 identifies the regulatory requirements, as well as the potential limiting ATWS-I transients. Section 4 is devoted to a detailed qualitative discussion of the physical phenomena pertinent to the ATWS-I evaluation. With this background, the development campaign to prepare the transient system code, RAMONA5-FA, for the task of calculating ATWS-I transients is put in perspective. The modifications to the approved RAMONA5-FA code (Reference 22) are presented in Section 5. The validation of the code capabilities with regard to reactor oscillations as well as transient hydraulic test loop measurements is presented in Section 6. Having demonstrated the capability of the code to calculate an ATWS-I transient, Section 7 presents the sensitivity to important phenomena to demonstrate that the methodology is robust. The remaining element of the methodology is the ATWS-I licensing basis procedure for demonstrating that the ATWS/Stability Mitigation Actions are effective in maintaining core coolability described in Section 8.

Appendices present special topics; Appendix A is devoted to presenting a step by step derivation of the new critical power reduced order model (CPROM) formulation, Appendix B presents the special topic of [

[

]

2.0 SUMMARY

A new generic methodology for the evaluation of Anticipated Transients Without Scram with Instability (ATWS-I) is presented. This report documents a RAMONA5-FA based method for evaluating the fuel specific portion of the event. This method is intended to cover the initial ATWS-I event through the time that operator actions suppress core oscillations for BWR3 through BWR6 plants. This method is not intended for use in evaluating containment effects or over pressurization during the event.

A key improvement of the RAMONA5-FA code is the addition of [

]

RAMONA5-FA has been benchmarked against both linear and non-linear stability transients. These benchmarks include hydraulic-only oscillations at the KATHY test facility as well as full core reactor transients. These benchmarks demonstrate that RAMONA5-FA can adequately predict oscillatory behavior.

A sample ATWS-I application problem based on the Brunswick BWR4 reactor has been presented. Various sensitivities have been performed to examine the sensitivity to important parameters and to help validate the conclusions of the PIRT.

3.0 REGULATORY REQUIREMENTS

The regulatory requirements for the ATWS-I event are defined in 10 CFR 50.62. Specifically, 10 CFR 50.62 lays out the required design features and the requirements for the assessment of their adequacy. Additional regulatory requirements that could be affected by fuel design for these events are compliance with General Design Criteria (GDC) 12 and 35 in Appendix A to Part 50 of Title 10 of the Code of Federal Regulations (10 CFR Part 50). Specifically:

“GDC 12: The reactor core and associated coolant, control, and protection systems shall be designed to assure that power oscillations which can result in conditions exceeding specified acceptable fuel design limits are not possible or can be reliably and readily detected and suppressed.”

“GDC 35: A system to provide abundant emergency core cooling shall be provided. The system safety function shall be to transfer heat from the reactor core following any loss of reactor coolant at a rate such that (1) fuel and clad damage that could interfere with continued effective core cooling is prevented and (2) clad metal-water reaction is limited to negligible amounts.”

While NUREG-0800 Standard Review Plan (SRP) Chapter 15, Section 15.8 (Reference 3) also identifies GDC 14, 16, 38, and 50 as applicable to an ATWS-I event. These general design criteria define requirements for the vessel and containment and [] and are therefore not addressed in this report.

The ATWS-I event was originally addressed generically for operation within the MELLLA domain (Reference 1), SRP 15.8 states:

“BWRs that implement both extended power uprate (EPU) and expanded power-flow domains (e.g., MELLLA+), the licensee will demonstrate that the ATWS/Stability Mitigation Actions are effective in maintaining core coolability.”

The modification of the RAMONA5-FA evaluation model (EM), that was originally developed and approved for application to DIVOM linear instabilities in Reference 7, has been extended to be the transient simulator that will be used to assess the fuel specific impact of the mitigation actions on the ATWS-I event. This methodology is not intended to cover system or containment impacts of the ATWS-I event.

3.1 ***Compliance with Standard Review Plan, Chapter 15, Section 15.0.2***

NUREG-0800 Chapter 15, Section 15.0.2 provides guidance to the Nuclear Regulatory Commission (USNRC) reviewer with respect to reviewing the technical contents of a submittal, typically a Topical Report (TR) pertinent to transient and accident analysis methodology. To accomplish this task, the USNRC provided the reviewer a list of criteria in Chapter 15.0.2 of the SRP as a means of arriving at a sound technical conclusion. The areas of considerations listed in Chapter 15.0.2 are provided below:

- Item 1. Documentation. This document satisfies this requirement.
- Item 2. Evaluation Model. Refer to Section 5.0.
- Item 3. Accident Scenario Identification Process. Refer to Section 3.2.
- Item 4. Code Assessment Database. Refer to Section 3.2.
- Item 5. Uncertainty Analysis. Refer to Section 8.0.
- Item 6. Quality Assurance (QA) Plan. Refer to Reference 4. Reference 4 is the basis for quality assurance in both the development and application of RAMONA5-FA for ATWS-I.

3.2 ***ATWS-I Transient Scenarios***

Two events are considered as potentially limiting. Both events result in a trip of the recirculation pumps. This trip reduces core flow to natural circulation while core power remains high which can quickly put the reactor deep within the instability region. These two events are (1) Turbine Trip With Bypass (TTWB), and (2) Two Recirculation Pump Trip (2RPT).

3.2.1 Turbine Trip

The first event, the TTWB, is initiated by a turbine trip. The recirculation pumps are tripped either by the turbine stop valve closure, or an ATWS high pressure pump trip. Core flow drops rapidly to natural circulation which drives core power lower. As the core settles at natural circulation, the feedwater temperature begins to decrease due to the loss of extraction steam. The feedwater temperature decrease causes core power to rise. If no action is taken, then core power will rise to the point that it crosses the instability boundary. Without the ability to scram, and if mitigating operator action is sufficiently delayed, oscillations will begin to grow and will reach large magnitudes, accompanied by reverse flow at the inlet of the hot channels. Once the oscillations reach sufficient magnitude, cyclical dryout and rewetting of the cladding surface will begin. If the oscillations continue to grow, they can reach sufficient magnitude that rewetting is no longer possible and large excursions of clad temperature that could potentially challenge acceptance criteria will occur.

In order to prevent large amplitude oscillations plant Emergency Operating Instructions (EOI) or Emergency Operating Procedures (EOP) instruct the operators to reduce water level upon recognition of an ATWS scenario. This reduction in water level has two primary effects. The first is to reduce core flow by reducing the density head on the downcomer side of the loop. The resulting reduction in core flow also serves to reduce core power. In addition, the water level is reduced to a level that is below the elevation of the feedwater spargers. At this point in the transient scenario, the cold feedwater is spraying through a steam environment and falling a significant distance until it reaches the water level. Passing through the steam environment heats the feedwater to the point that it approaches saturation. This significantly reduces the core inlet subcooling, which not only directly adds a stabilizing force to the system, but also reduces core power further stabilizing the system. The suppression of oscillations and reduction in power terminate any temperature excursion in the fuel and ends the fuel-specific portion of the ATWS-I event.

The EOI/EOP also specify that operators initiate boron injection upon recognition of an ATWS condition. Boron injection normally happens after water level reduction due to system delays in the Standby Liquid Control (SLC) system. The boron injection serves to shutdown core power and terminates the ATWS-I event. As this action occurs after the limiting fuel portion of the event, this operator action will not be simulated.

3.2.2 Two Recirculation Pump Trip

The two recirculation pump trip event (2RPT) evolves similarly to the TTWB event with two exceptions, the event initiation and the feedwater temperature excursion. Since the 2RPT event does not involve a turbine isolation, the turbine remains online and extraction steam to the feedwater heaters is maintained so the feedwater temperature remains significantly higher than the TTWB event. Because of this, the power excursion in the 2RPT event is mild which results in a less severe event for the same operator intervention times. One difference between the two transient scenarios is that the TTWB event should generate an automatic scram very early in the event leading to earlier identification of the ATWS scenario by the operators. There may not be a scram signal at the initiation of the 2RPT which means the event may be allowed to progress further due to a delayed identification of ATWS by the operator. As such, the 2RPT may become limiting if operator action in the TTWB event occurs fast enough to suppress oscillations prior to dryout.

4.0 PHYSICAL PHENOMENA

In this section, a review of the basic physical phenomena that occurs during an ATWS-I event is presented. These can be divided into the phenomena leading to power and flow oscillations, and the dryout phenomena under these oscillatory conditions. [

]

4.1 *Unstable Oscillations in General*

A feedback system is unconditionally unstable in the case of positive feedback, i.e., a perturbation in a system parameter results in enforcing the perturbation. This kind of divergence is not oscillatory. In systems with negative feedback, i.e., a perturbation in a system parameter results in reducing the perturbation may or may not be stable depending on other system characteristics. Immediate negative feedback makes the system unconditionally stable. On the other hand, delayed negative feedback may render the system unstable if the magnitude of the feedback is sufficiently large. In the case of strong delayed negative feedback, the corrective effect of the feedback overshoots the original perturbation and the system undergoes oscillations of exponentially increasing magnitude. This type of oscillation is possible in BWRs.

The simple description of the feedback effects outlined above applies to linear systems, or nonlinear systems that behave as a linear system when the oscillation magnitude is sufficiently small. As the oscillation magnitude grows, the magnitude of the feedback is no longer proportional to the original perturbation due to the nonlinear effects. The nonlinear effects can be stabilizing, and in this case an initially exponentially growing oscillation will grow at a slower rate as the oscillation magnitude increases, and finally reach a stable limit cycle. Nonlinear effects may also act in the opposite direction, and an initially exponentially growing oscillation will accelerate its growth rate further as the oscillation magnitude increases. Normally in a complex nonlinear system, like a BWR, there are regions of different nonlinear effects. [

]

[

]

4.2 *Density Waves in a Boiling Channel*

The mechanism capable of inducing a strong and delayed negative feedback in a boiling channel is the propagation of density waves (See Reference 5 for a comprehensive review). The kinematic description of density waves can be best described in the idealized boiling channel where the rate and axial distribution of the heat source remain invariant, and the pressure drop between the inlet and exit of the channel is kept constant. A perturbation of the inlet mass flow rate travels up the channel and its magnitude changes and phase lag increases. The mass flow rate wave generates a corresponding change in the steam quality and void fraction and equivalently the mixture density. The single-phase and two-phase friction components will also respond to the perturbation in the mass flow rate and the resulting steam quality response. In a slow (quasi-steady state) perturbation, the net resulting feedback is negative, that is for a positive inlet mass flow perturbation, the average void fraction decreases lowering the density head that drives the flow and the frictional pressure drop will increase forcing the restoration of the original inlet mass flow. The inlet flow perturbation can take any functional form, which can be linearly decomposed into sinusoidal waves of different magnitudes and frequencies. The variation in density results in gravitational head change, while the mass flux variation results in friction variations. The net pressure drop variation across the channel due to the gravitational and frictional components must be compensated for by flow acceleration in order to satisfy the constant channel pressure drop boundary condition. The feedback strength is maximal for an inlet flow perturbation with a frequency comparable to the inverse of the delay time, and if the magnitude of the feedback is sufficiently strong, the channel hydraulic parameters will oscillate at that preferred frequency with an increasing

magnitude. The hydraulic stability of the density waves depends on the strength of the feedback processes.

The quantitative parameter for measuring the degree of stability is the decay ratio defined as the oscillation magnitude at a given cycle relative to the previous cycle's magnitude. Under typical BWR conditions, the decay ratio is increased (less stable) with the following system variables:

- High power to flow ratio: This increases the density contrast along the channel (and hence the gravity head) which drives the instability.
- Low flow: In addition to being the denominator in the power-to-flow ratio, low flow is destabilizing because it decreases the preferred frequency (because lower flow speed increases bubble transit time) and thus reduces the axial attenuation of the mass flux and void fraction.
- Bottom-skewed power peaking: This power shape results in creating the bubbles at lower elevations which remain for a longer time, thus increasing the average density contrast and thus is destabilizing.
- Low system pressure: Low system pressure is destabilizing as the difference in saturated liquid and vapor densities increases which drives the gravitational component, hence a destabilizing effect.
- [

]

- High inlet subcooling: The inlet subcooling does not have a monotonic effect on stability, as very high and very low inlet subcooling are both stabilizing. Very high inlet subcooling prevents boiling and suppresses density response by preventing

phase change. Reducing inlet subcooling to allow boiling, while remaining sufficiently high such that the boiling boundary is high, the two-phase-to-single-phase pressure drop ratio is low and the system remains stable. [

]

The discussion of the hydraulic density waves, idealized under constant pressure drop and constant rate of heating, remained in the linear small amplitude regime. The large oscillation amplitude effects will be discussed separately.

4.2.1 Density Waves in Parallel Channels between Two Plena

In describing the idealized density wave instability a constant channel pressure drop was imposed as a boundary condition, which can be assured using a recirculation loop much larger than the boiling channel. In the case the recirculation loop is not so large the oscillating flow will result in pressure drop boundary changes which are stabilizing. Two identical boiling channels connected in parallel to the same recirculation plena will be coupled only if the recirculation loop is finite and the common pressure drop responds to the net flow change in the two boiling channels. The coupling results in the two channels oscillating out-of-phase (180 degrees phase shift) such that the pressure drop boundary fluctuation is minimized. For three identical boiling channels connected in parallel to the same plena, the coupling forced by the recirculation loop will result in the channels oscillating 120 degrees apart. However, for four channels, there are two possibilities, either the four channels will oscillate 90 degrees apart, or two channels will oscillate in-phase with each other and out-of-phase with the other two channels. The situation can become very complicated when hundreds of channels are connected to the same plena. In real situations, the channels are not identical and therefore have natural frequencies that are not identical, and their respective degrees of stability are also different. Coherent oscillations where many channels share the frequency and phase depend on the coupling mechanism of the neutron flux in addition to the

recirculation loop. Yet, hydraulically unstable channels, if sufficiently destabilized, may break away and oscillate independently from other channels and experience a superposition of multiple oscillation modes.

4.2.2 Density Wave with Power Oscillations due to Density-Reactivity Coupling

The propagation of the density wave along the boiling channel results in an oscillation of the bundle average coolant density (equivalently void fraction). The change in void fraction changes the neutron absorption and fission cross sections and produces a neutron reactivity response. The reactivity oscillation in turn produces a fission power response. There are two components of the power response, the first is the fission power deposited in the UO_2 pellets, and the second is the power deposited directly in the coolant as gamma radiation and neutron moderation.

The direct energy response is practically immediate, i.e. in-phase, with the original density change and results in an opposing effect on coolant density, i.e. negative feedback. The in-phase negative feedback of the direct energy deposition in response to density change has a stabilizing effect on the density wave.

The fission energy deposition is eventually transported to the coolant via heat conduction through the fuel rod. The dynamics of the transport of heat through the fuel rod to the coolant are governed by the heat capacity and the various thermal resistance components between the pellet interior and the coolant. These thermal resistances include the UO_2 pellet, the Zircaloy clad wall, the gap between pellets and clad, and the coolant in contact with the outer clad wall. The result of the thermal resistance and heat capacity inertia is a delay of the heat transport to the coolant, i.e. phase lag, of slightly less than 90 degrees. It also accounts for considerable attenuation of the heat source to the coolant. The attenuation of the heat flux amplitude relative to the fission power oscillation amplitude is of the order of 10^{-1} and increases with increasing the conduction time constant, which in turn increases with increasing the fuel rod diameter and increasing pellet-gap resistance. Unlike the direct energy deposition in the coolant, the

time lag of the coolant heating response through clad wall heat flux relative to the perturbation of the fission power deposition in the pellet results in destabilizing the density wave.

The void reactivity-to-power feedback not only provides the coupling needed for the different channels to oscillate coherently, but also has a destabilizing effect that makes it possible for the system to be unstable even when every channel in it is stable hydraulically. The coherence is broken if a single channel becomes hydraulically unstable at which point the flow in that channel will reflect a superposition of its intrinsic instability and the driven component via the oscillating power. Unstable single channel oscillations have been observed in unusual situations, for instance when a BWR bundle is not properly seated and deprived of flow (as occurred in Forsmark-I and Brunsbüttel Reference 6). Single channel instability also occurred in Garigliano during a special test (Reference 5). Aside from these unusual situations, single channel instabilities have been predicted and special effort has been made to exclude the possibility of their occurrence in the approved AREVA methodology for DIVOM calculations (Reference 7).

4.3 ***Oscillation Modes – The Global Mode***

As mentioned earlier, several boiling channels connected in parallel to two plena may not oscillate coherently absent a mechanism for coupling the density waves among the individual channels. In the case of a BWR core, the density-reactivity feedback provides the required coupling. The neutron flux in the core responds to reactivity changes anywhere in the core due to neutron diffusion. Thus the reactivity change in one channel results in a corresponding power change not only in that channel but to all other channels - with varying strength.

The oscillation mode where the power in every channel oscillates coherently, and in-phase with the power in all other channels, is called the global mode. The inlet mass flows in all the channels oscillate similarly, with the same frequency and in-phase. As the inlet mass flow rate in all channels is in-phase, the total core inlet mass flow rate

must also oscillate, and similarly for the core exit mass flow rate. The core pressure drop (between the upper and lower plena) must also oscillate. Accordingly, the recirculation loop flow must interact with the core flow, and its dynamics must be considered in the analysis of the global mode oscillations. Generally, the friction and inertia of the recirculation loop exert a stabilizing influence on the global mode, and the extent of this stabilizing effect depends mostly on the dynamics of the steam separator assembly.

In a BWR core oscillating in-phase the fundamental mode of the neutron flux distribution function is excited. The excitation of all the other planar harmonics is not needed for the global mode. The axial flux harmonics must be driven as a result of the density waves causing the observed phase lag between neutron detector responses of the upper core elevation relative to lower elevation. [

]

4.4 ***Oscillation Modes – The Regional Mode***

The regional mode is characterized with half the core bundles oscillating out-of-phase with the other half. The two core halves are separated by a vertical plane, which is also called the neutral line when a planar projection is considered. The net core flow remains unchanged during the regional oscillation provided its magnitude is not so large as to introduce nonlinear effects that do not cancel out.

The main reason the hydraulic channels prefer to oscillate out-of-phase is the cancellation of the recirculation loop damping. The regional mode oscillation in a BWR

is forced to be coherent with half the core bundles oscillating in-phase and the other half oscillating with a 180 degree shift due to neutronics coupling. The half-core oscillation is preferred because it excites the first azimuthal neutron flux mode and thus receives the highest possible amplification. The other flux harmonics that can be excited by other channel groupings are characterized by larger subcritical reactivities, and therefore are significantly damped.

It is important to notice that the decay ratios of the regional and global modes are comparable. The regional mode is preferred for

- Large cores, which result in small eigenvalue separation for the first azimuthal flux mode.
- Low center power peaking (ring of fire), which also decreases the eigenvalue separation.
- Loose inlet orifice, which destabilize the hydraulic channels. This effect favors the regional mode in the absence of recirculation loop damping. It must be emphasized that the regional oscillations are isolated, and thus independent from the recirculation loop.

4.5 ***Oscillation Modes – The Rotational Mode***

In the regional oscillations described above, the neutral symmetry line is stationary. The rotational mode is similar to the regional mode where the neutral line is oscillating or rotating (See Reference 8). The rotational mode essentially results from the simultaneous excitation of two orthogonal azimuthal modes. Assuming the core loading and control rod patterns are symmetric, the first two azimuthal modes are degenerate (approximately equal eigenvalues), and are thus indistinguishable. In the case the stability threshold is crossed with a decay ratio slightly greater than unity, and the core symmetry is not exact, it is expected that only one first azimuthal flux harmonic is excited leading to a regional mode oscillation with fixed neutral line. In the case the core is destabilized further, the orthogonal azimuthal mode is excited next, and interference patterns emerge depending on the relative amplitude and frequency differences between the two modes. The neutral line may oscillate or rotate slowly in

response to unequal magnitude and frequency of the two excited azimuthal modes.

The most interesting case is when the two azimuthal modes are degenerate and oscillate with the same frequency and amplitude, which leads to the neutral line rotating at the same frequency.

[

]

4.6 *Oscillation Modes – Axial Power Shape*

As the density wave propagates upward, not only the total reactivity oscillates, but also the axial reactivity distribution is altered where oscillating reactivity difference between the upper and the lower parts of the core is created. As a result, the axial neutron flux harmonic is driven by density waves. The effect of the axial power shape oscillation on the decay ratio is minimal but it is noticeable as the cause of the phase lag of the upper local power range monitor (LPRM) power signal relative to the power signal from the lower LPRM on the same string.

The axial mode excitation is significant when the global or regional/rotational oscillation amplitude is large and large axial power shape changes are expected during the oscillations. [

]

4.7 *Large Amplitude and Limit Cycles of Global Mode Oscillations with Linearized Hydraulics*

As the oscillation magnitude increases, nonlinear effects are introduced (Reference 9). The neutron kinetics nonlinear effects become significant before the hydraulic nonlinear effects. This is the case because the reactivity oscillations required to induce large neutron flux response can be produced by relatively small coolant mass flow oscillation magnitude. In the idealized case of assumed linear thermal-hydraulics, with only the nonlinear effects of reactivity on the power response being allowed, a stabilizing effect has been observed which eventually leads to saturating the growth of the oscillation until a stable limit cycle is reached. The nonlinear stabilizing effect originates in the negative reactivity shift that is produced in response to the average power increases, the latter is due to the oscillating reactivity where the increase in reactivity during half a cycle increases power more than compensated for by an equal reactivity decrease in the subsequent half cycle. This asymmetric power response to reactivity oscillation is also responsible for generating high and sharp power peaks compared with the flat power minima.

The power drift under oscillatory reactivity results in an average power increase that is balanced by the negative reactivity due to the increased average void fraction. [

]

4.8 *Large Amplitude Regional Mode Oscillations with Linearized Hydraulics*

The power oscillation magnitude considered here is sufficiently large for the nonlinear neutron kinetics effects to manifest, but not high enough for the nonlinear effects of the hydraulics to become important. The regional oscillation of large amplitude differs in

basic ways from a global oscillation (Reference 10). Most importantly, there is no reactivity bias associated with the first azimuthal harmonic excitation and growth, unlike the fundamental flux excitation and growth in the global mode oscillation. The only negative reactivity that reduces the first azimuthal mode growth is the subcriticality associated with its steady state eigenvalue being less than unity, and this subcriticality is not affected by the oscillation magnitude and therefore not a nonlinear effect. The main nonlinear effect of the growth of the first azimuthal mode is the emergence of a driven fundamental mode oscillation component with relative magnitude proportional to the square of the first harmonic magnitude at low oscillation magnitudes and at double its frequency (see References 11 and 12). The double frequency fundamental mode will grow until it becomes equal to the first harmonic in magnitude. A negative reactivity shift is generated, [

]

For growing regional oscillations, unlike the global mode, the nonlinear effects accelerate the rate of growth, and the oscillation magnitude is not self-limited (Reference 10). The eventual arrest of the regional mode oscillation growth is due to [This is one reason why large amplitude regional oscillations are of special interest and can be considered limiting compared with the nonlinearly self-limiting global oscillations.

4.9 ***Large Amplitude Pure Thermal-Hydraulic Density Waves***

Flow in a boiling channel includes highly nonlinear processes. For example, the frictional pressure drop is approximately proportional to the square of the flow rate, and the void fraction dependence on the steam quality is also nonlinear. When unstable density waves in a boiling channel, without neutron kinetic feedback, are allowed to grow the oscillation magnitude may reach a limit cycle [

]

[

]

Detailed numerical models are needed to simulate the behavior of a boiling channel as an integral system whereas purely analytical models are of limited use for understanding the effects of various phenomena particularly for large amplitude oscillations. However, it is still possible to discern the role of these phenomena by observing the behavior of oscillating channels in test loops, and in simulations, and guided by knowledge of the fundamentals of flow dynamics. Using these tools, a qualitative description of the nonlinear effects and their influence on density wave oscillations growth is offered here.

[

]

The main nonlinearly destabilizing effect originates from the [

]

[

] The maximum oscillation amplitude at the channel inlet is negative, where the reverse flow magnitude [

] The inlet flow oscillation has broad peaks and sharp minima signifying the nonlinear processes involved in the generation of these high amplitude oscillations.

4.10 ***Very Large Nonlinear Oscillations of Global and Regional Types***

For small amplitude oscillations, the system behavior is linear and the principle of superposition is applicable. Accordingly, all the possible unstable modes will be manifested without coupling to each other, for example in the case the decay ratios of the global and regional modes are comparable and greater than unity, both types of instabilities will be excited and the resultant oscillations will reflect a superposition mix. This is not the case for large oscillations where nonlinear effects are significant. [

]

[

] An exception for this behavior is the case of two regional modes representing the excitation of a first azimuthal flux harmonic and a nearly degenerate mode where the corresponding neutral lines are orthogonal. The nonlinear effects of the growth of one of these modes will impact both modes, and simultaneous growth of the two modes would lead to oscillating or rotating neutral line, i.e. the mixed mode oscillation of the rotational type is not discouraged by nonlinear effects.

[

]

[

]

4.11 ***Prompt-Criticality***

Very large power oscillations result from very large reactivity oscillations due to the severe flow oscillations. It is important to consider that reactivities in excess of the delayed neutron contribution may occur, i.e. prompt-super-criticality. The possibility of prompt-super-criticality requires the neutron kinetics models to be able to handle it properly with finite neutron velocity and Doppler reactivity feedback. However, from theoretical analysis (see References 9 and 10) and experience with numerical calculations (Reference 2), it has been found that prompt-criticality may be expected only under unrealistically rapid rate of oscillation growth, before the system has time to respond by increasing the average power and shift the average reactivity to a large negative value. Even in this case, the prompt criticality is exceeded by only a few cents, not dollars like in reactivity insertion accidents. No qualitatively distinct power pulses result from small super-prompt-critical reactivity.

[

]

4.12 ***Effect of Bypass Flow with Possible Boiling***

Boiling is possible in the upper part of the core bypass at natural circulation under relatively high power (Reference 13). This effect is modeled in steady state simulators which provide the initial conditions and neutron cross sections to the transient codes

used in this application. The main effect of the bypass boiling is a shift of the axial power shape to more bottom-peaking. The important question here is the transient response of the bypass, with or without boiling, in the presence of large regional mode oscillations. Under regional oscillations, the core pressure drop remains nearly invariant as the effects of flow in the two halves of the core oscillating out-of-phase tend to cancel out. [

]

4.13 *Cyclical Dryout and Rewetting*

Large oscillations of flow and power in a BWR bundle can result in conditions of degraded heat transfer and clad temperature excursions beyond the safe limits designated to maintain fuel coolability.

In steady state operation, the conditions of heat transfer degradation are associated with the inception of dryout. Dryout correlations based on critical heat flux or critical quality concepts are used to obtain the critical power ratio, which provide quantitative measure of allowable bundle power and define the safety margins to protect that limit. Quasi-steady state application of dryout correlations has been the basis for protecting the fuel against dryout. Steady state dryout correlations were extended for applications to DIVOM oscillatory transients (Reference 7), which are rather mild, compared with power and flow oscillations accompanying anticipated transient without scram. [

]

[

]

With the detailed accounting of the phenomena governing the cyclical dryout and rewetting, the limiting consideration for fuel safety is shifted from dryout inception to failure to rewet. Accordingly, cyclical dryout and rewetting is not considered a threat to fuel integrity as long as high clad temperature excursion does not occur. [

]

A detailed [] model for cyclical dryout and rewetting with possible failure to rewet [

]

[

]

4.13.1 Impact of Cyclical Dryout and Rewetting on Very Large Oscillations

The phenomena of large density wave oscillations and cyclical dryout are interlinked. The previous section addresses the cyclical dryout and rewetting, with possible failure to rewet, [

]

[

]

4.14 ***Vessel Considerations***

Aside from the vessel impact on global oscillations as described in Section 4.3, there are several systems that can have a direct impact on the evolution of the ATWS-I event. One such category is the systems involved in pressure control. For a 2RPT, normal pressure control is maintained by the pressure control system through the positioning of the turbine control valves. Pressure change is gradual resulting in minimal effect on the system. For a turbine trip, the turbine is isolated and pressure is controlled by the bypass valves and Safety/Relief Valves (SRV). The fast opening and closing of the SRVs cause pressure to oscillate in the vessel. [

]

[

]

The mitigating actions of the operators will also impact the progression of the ATWS-I event. There are two primary mitigating actions required to shut down the ATWS-I event: water level reduction and boron injection. The water level reduction begins by operator action at an assumed time following entry into the ATWS condition. Water level is reduced to a level that is typically near the top of the core. This reduction in water level to a point significantly below the feedwater spargers means that once water level control is re-established at the lower level, the cold feedwater is now sprayed through a steam environment. The large distance between the spargers and the water level means that the feedwater will be heated to near saturated conditions. This heated water will both reduce core power and stabilize the core terminating oscillations.

The boron injection process begins as soon as the ATWS condition is recognized (same time as the beginning of the water level reduction). However, system delays due to pump run up, the time required to pump boron from the holding tank to the vessel, and the time required for boron to accumulate in the core in sufficient concentration to suppress power mean that this action can be delayed relative to the water level reduction. As such, the water level reduction will mitigate the oscillation prior to boron injection. In this case, the boron injection serves to shut the core down and limit impact of high core power on the containment heat load. The RAMONA5-FA ATWS-I methodology will not include boron injection as the base analysis definition. If, in the unlikely scenario, the boron injection is needed to be modeled, it can be modeled

[

]

4.15 *Phenomena Ranking*

A comprehensive phenomenon identification and ranking process has been performed to identify the dominant phenomena for the target scenario (ATWS leading to core instability). During the development process, this identification and ranking is the basis for determining which closure relations require development or enhancement for the intended application. The process aids in methodology development because it prioritizes the model development activities and defines the types of validation and sensitivity studies that are needed to support the methodology. The culmination of the process is a phenomenon identification and ranking table (PIRT) that summarizes all the phenomena and provides their importance ranking relative to selected figure of merit (FoM). This PIRT utilizes AREVA's extensive history and experience with analyzing and testing density wave phenomena including the core minimum critical power ratio (MCPR) response for both global and regional mode instabilities as a function of the power oscillation magnitude (Reference 7). In the approved EO-III TR (Reference 30) AREVA included [

]. In

addition, AREVA has previously participated in industry efforts to develop a previous ATWS-I PIRT (Reference 31).

When developing the PIRT, it is important to note that the development of very large power and flow oscillations follows a progressive path from the initial inception of instability, exponential oscillation growth from noise level to mild amplitudes, and further growth to large amplitudes that can be prevented from further growth by nonlinear effects. Intuitively, the phenomena and parameters participating in all the stages of the evolution of the transient from inception to maximum oscillation amplitude are ranked such that any important phenomenon at any stage remains important for the ultimate maximum oscillation event under consideration. [

]

[

]

Acceptance criteria for the target scenario are derived from General Design Criteria 35:

"A system to provide abundant emergency core cooling shall be provided. The system safety function shall be to transfer heat from the reactor core following any loss of reactor coolant at a rate such that (1) fuel and clad damage that could interfere with continued effective core cooling is prevented and (2) clad metal-water reaction is limited to negligible amounts."

For the ATWS-I event, maintaining the PCT below the 10CFR 50.46 limit of 2200 °F (1204 °C) ensures that the acceptance criteria of maintaining core coolability is met.

[

]

The first FoM is the oscillation inception (OI). Since the purpose of the evaluation is to demonstrate that operator actions occur in sufficient time to prevent severe overheating of the clad, the method must be able to accurately determine when oscillations would begin relative to the operator intervention.

The second FoM is the limit cycle amplitude (LCA). While not all events will reach the full limit cycle, this point determines the ultimate magnitude of the oscillations and defines the worst case oscillation.

The final FoM is post-dryout (PDO). This FoM encompasses the time between the initial prediction of dryout through to rewet or failure to rewet. The ability to accurately determine dryout and rewetting can directly determine the severity of the event.

The ranking of the phenomenon and processes are presented in Table 4-1.

Table 4-1: Ranking of Phenomena and Processes

H - High
M - Medium
L - Low
N - N/A

Table 4-1: Ranking of Phenomena and Processes (cont.)

H - High
M - Medium
L - Low
N - N/A

Table 4-1: Ranking of Phenomena and Processes (cont.)

H - High
M - Medium
L - Low
N - N/A

Table 4-1: Ranking of Phenomena and Processes (cont.)

H - High
M - Medium
L - Low
N - N/A

4.16 ***Major Assumptions***

Assumptions are necessary measures and approximations needed to create any practical analytical or numerical tool such as done in this work. The listing of the key or major assumptions is desirable, at least in part, to put the accuracy and expectations of the model performance in the right perspective, enlighten the user as to the application limitations, and point to areas of future improvements.

The identification and justification of assumptions is often an exercise of engineering common sense more than a quantitative analysis with objective metrics. Fortunately in this particular case, the RAMONA5-FA ATWS-I model and code are based on a solid foundation of practice and experience with codes of similar nature, namely the previously approved RAMONA5-FA (Reference 22). The assumptions which represent simplifications or improvements or any deviation of significance from the experience base of the original RAMONA5-FA will be listed and discussed. Complementing assumptions in models [] will also be discussed depending on their particular significance to the correspondence between the particular model/assumption and the important ATWS-I phenomena which is the key application of the code.

The key assumptions are listed below along with the associated consequences and justifications. The neutron kinetics representation using []

[

]

New water property functions based on the IF97 formulation are used [

]. The use of the most up-to-date formulation is assumed to imply no significant changes to the nature of the oscillation transient, and any change no matter how small is an improvement. The density of liquid water at temperatures (or equivalently enthalpies) higher [

]

5.0 CODE DESCRIPTION

A detailed description of the theory is given in this section. Description of the various components of the model, the neutron kinetics, the fluid flow, pin heat conduction and heat transfer to the fluid, is given in separate subsections. Notice that the nomenclature is defined in each subsection as the model description is presented and the meaning of symbols may differ within each model. For example, ρ refers to reactivity in the description of the neutron kinetics, while the same symbol is used for density in the fluid flow model.

Model description is brought to the level of discretized formulation, with the aid of governing differential equations [

]

5.1 *Neutronics*

An adaptive 3-D neutron kinetics module has been developed for application to BWR transient codes. [

].

[

]

5.1.1 Adaptive Two-Group 3-D Neutron Kinetics

The adaptive kinetics theory is presented in this section along with a derivation of the 3-D governing equations in two-energy-groups. The two-group neutron diffusion equations in the steady state simulator MICROBURN-B2 are:

$$-\nabla \cdot (D_1(\mathbf{r}) \nabla \Psi_1(\mathbf{r})) + \Sigma_1(\mathbf{r}) \Psi_1(\mathbf{r}) = \frac{1}{k_0} (\nu \Sigma_{f1}(\mathbf{r}) \Psi_1(\mathbf{r}) + \nu \Sigma_{f2}(\mathbf{r}) \Psi_2(\mathbf{r})) \quad (5.1)$$

$$-\nabla \cdot (D_2(\mathbf{r}) \nabla \Psi_2(\mathbf{r})) + \Sigma_{a2}(\mathbf{r}) \Psi_2(\mathbf{r}) = \Sigma_{12}(\mathbf{r}) \Psi_1(\mathbf{r}) \quad (5.2)$$

where

D_1	Fast group diffusion coefficient
D_2	Thermal group diffusion coefficient
k_0	Effective multiplication factor (eigenvalue)
\mathbf{r}	Space vector
Σ_1	Fast neutron removal cross section (by absorption and slowing down)
Σ_{a2}	Thermal neutron absorption cross section
Σ_{12}	Slowing down cross section
$\nu \Sigma_{f1}$	Fast fission neutron production cross section
$\nu \Sigma_{f2}$	Thermal fission neutron production cross section
Ψ_1	Fast flux steady state distribution
Ψ_2	Thermal flux steady state distribution

The transient form is given by

$$\frac{1}{v_1} \frac{\partial \Phi_1(\mathbf{r}, t)}{\partial t} = \nabla \cdot (D_1(\mathbf{r}, t) \nabla \Phi_1(\mathbf{r}, t)) - \Sigma_1(\mathbf{r}, t) \Phi_1(\mathbf{r}, t) + (1 - \beta(\mathbf{r}, t)) \times$$

$$\frac{1}{k_0} (\nu \Sigma_{f1}(\mathbf{r}, t) \Phi_1(\mathbf{r}, t) + \nu \Sigma_{f2}(\mathbf{r}, t) \Phi_2(\mathbf{r}, t)) + \sum_{n=1}^N \lambda_n(\mathbf{r}, t) C_n(\mathbf{r}, t) \quad (5.3)$$

$$\frac{1}{v_2} \frac{\partial \Phi_2(\mathbf{r}, t)}{\partial t} = \nabla \cdot (D_2(\mathbf{r}, t) \nabla \Phi_2(\mathbf{r}, t)) - \Sigma_{a2}(\mathbf{r}, t) \Phi_2(\mathbf{r}, t) + \Sigma_{12}(\mathbf{r}, t) \Phi_1(\mathbf{r}, t) \quad (5.4)$$

$$\frac{\partial C_n(\mathbf{r}, t)}{\partial t} = \frac{\beta_n(\mathbf{r}, t)}{k_0} (\nu \Sigma_{f1}(\mathbf{r}, t) \Phi_1(\mathbf{r}, t) + \nu \Sigma_{f2}(\mathbf{r}, t) \Phi_2(\mathbf{r}, t)) - \lambda_n(\mathbf{r}, t) C_n(\mathbf{r}, t), \quad n=1, \dots, N \quad (5.5)$$

where

t	Time
v_1	Fast neutron velocity
v_2	Thermal neutron velocity
N	Total number of delayed neutron energy groups
β_n	Delayed neutron fraction in the group n
λ_n	Decay constant for the delayed neutron precursor of the group n
C_n	Concentration of the delayed neutron precursor of the group n
Φ_1	Time- and space-dependent fast flux distribution
Φ_2	Time- and space-dependent thermal flux distribution

The total delayed neutron fraction is the sum of the group-wise fractions, thus

$$\beta(\mathbf{r}, t) = \sum_{n=1}^N \beta_n(\mathbf{r}, t) \quad (5.6)$$

The fast removal cross section is the sum of absorption and slowing down components, thus

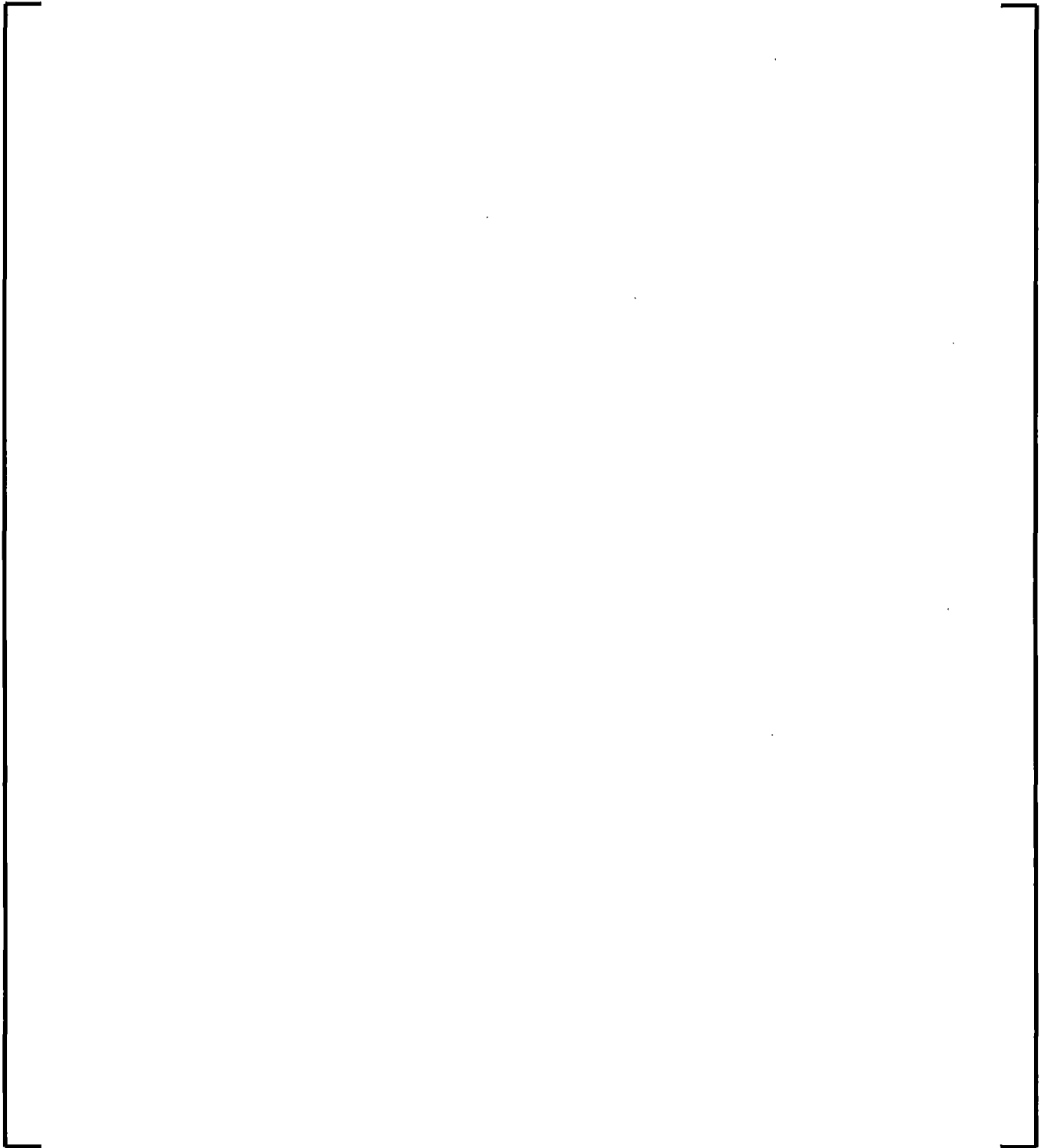
$$\Sigma_1(\mathbf{r}, t) = \Sigma_{a1}(\mathbf{r}, t) + \Sigma_{12}(\mathbf{r}, t) \quad (5.7)$$

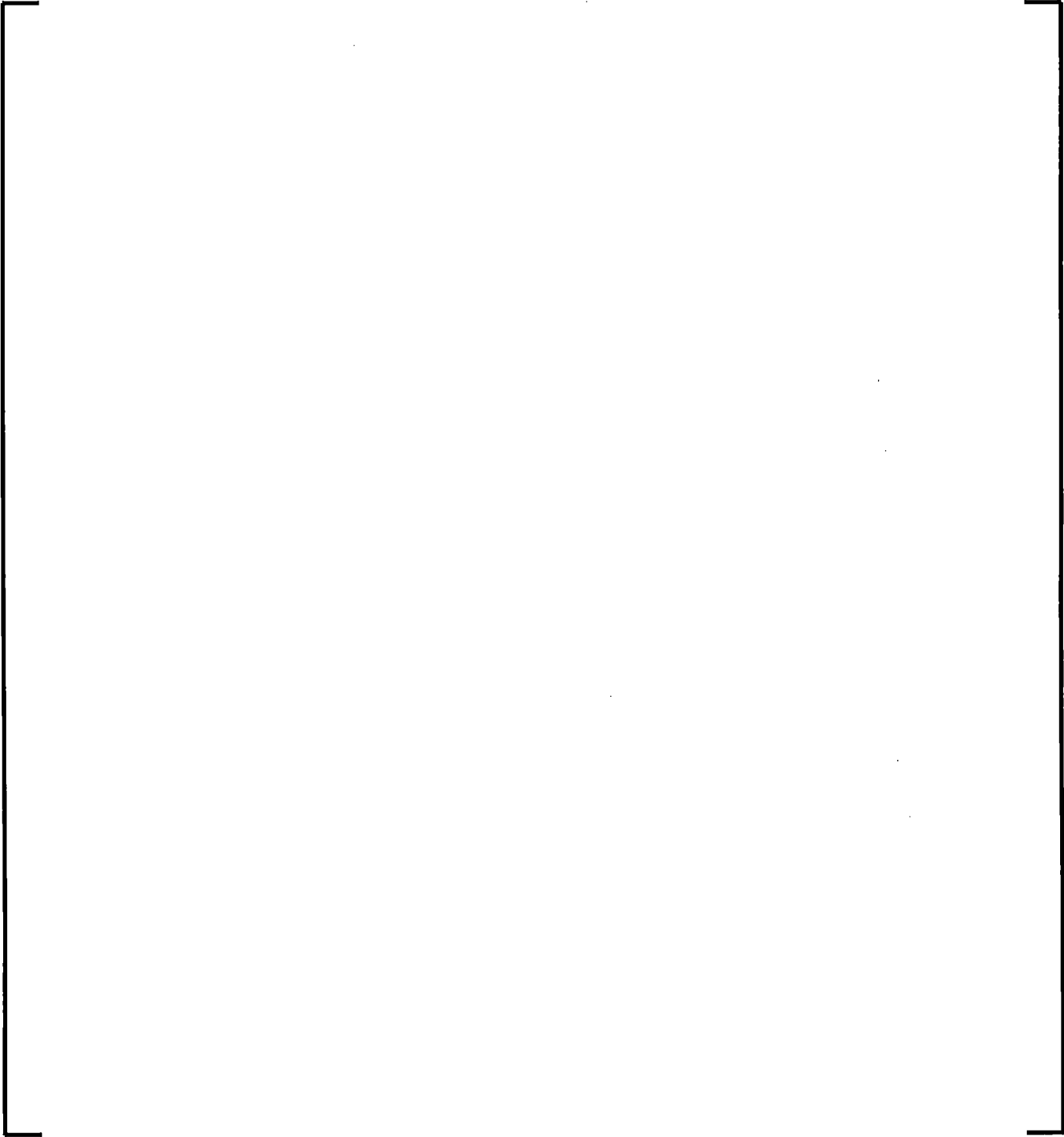
where

Σ_{a1} Fast absorption cross section.

Notice that the eigenvalue, k_0 , is retained to maintain consistency with the steady state cross sections and force the initial condition to exact criticality. [

]





5.1.2 Numerical Solution

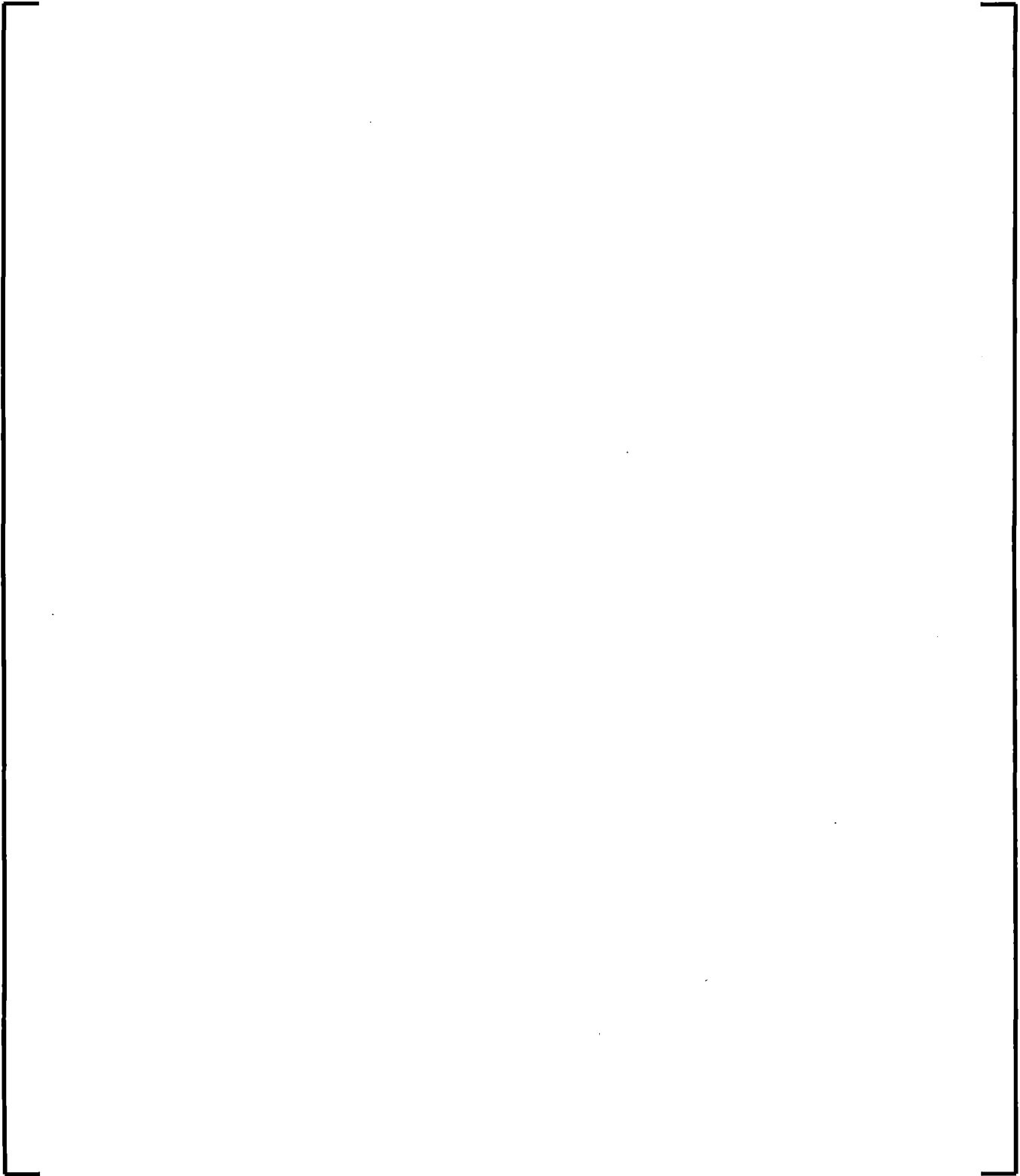
The cross sections and fluxes are defined on the same 3-D mesh as MICROBURN-B2. The x-coordinate is associated with the index i , the y-coordinate with j , and the vertical z-coordinate with k . For example

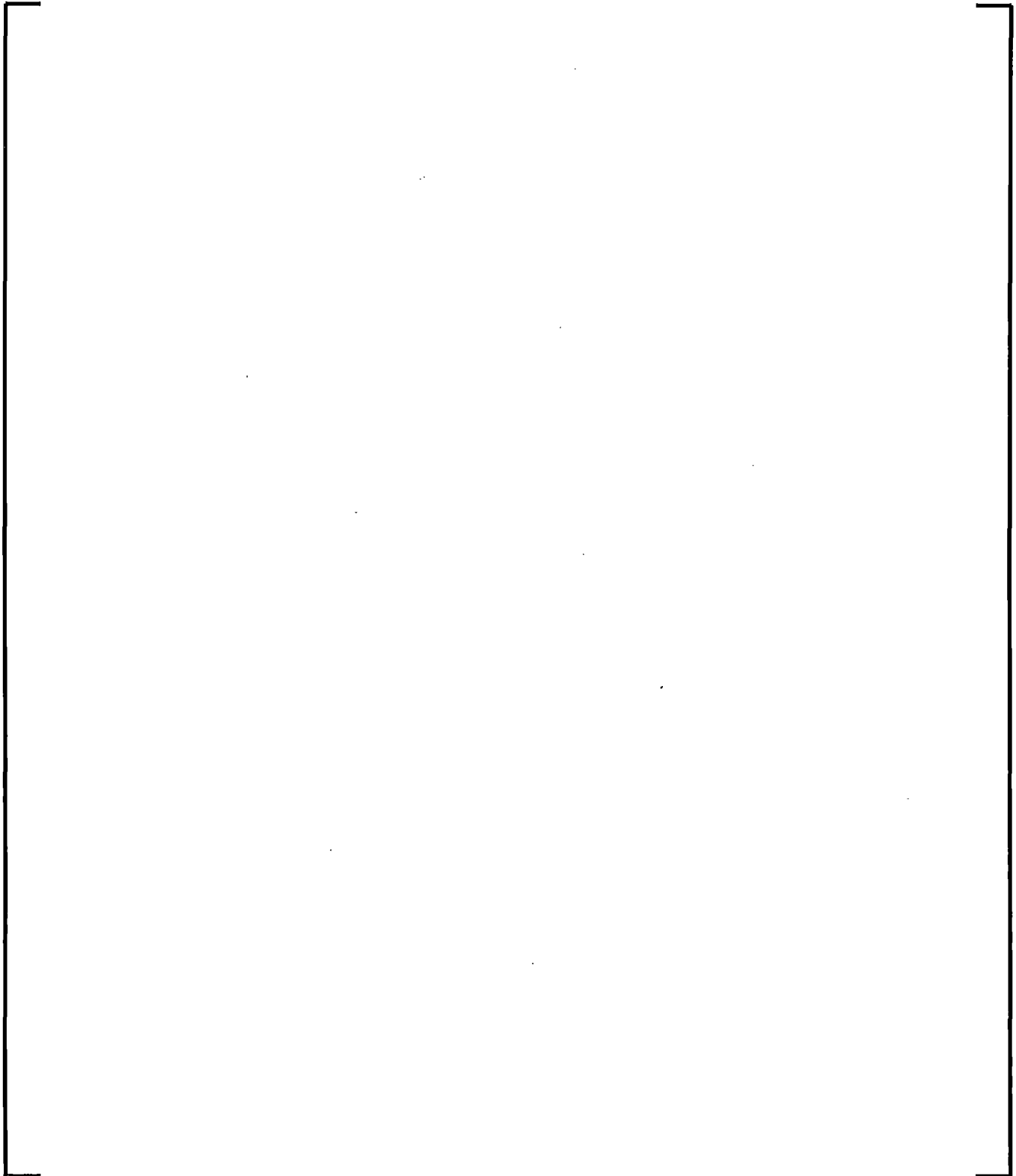
$$\Psi(\mathbf{r}) = \Psi(x, y, z) = \Psi_{i,j,k}$$

[

]

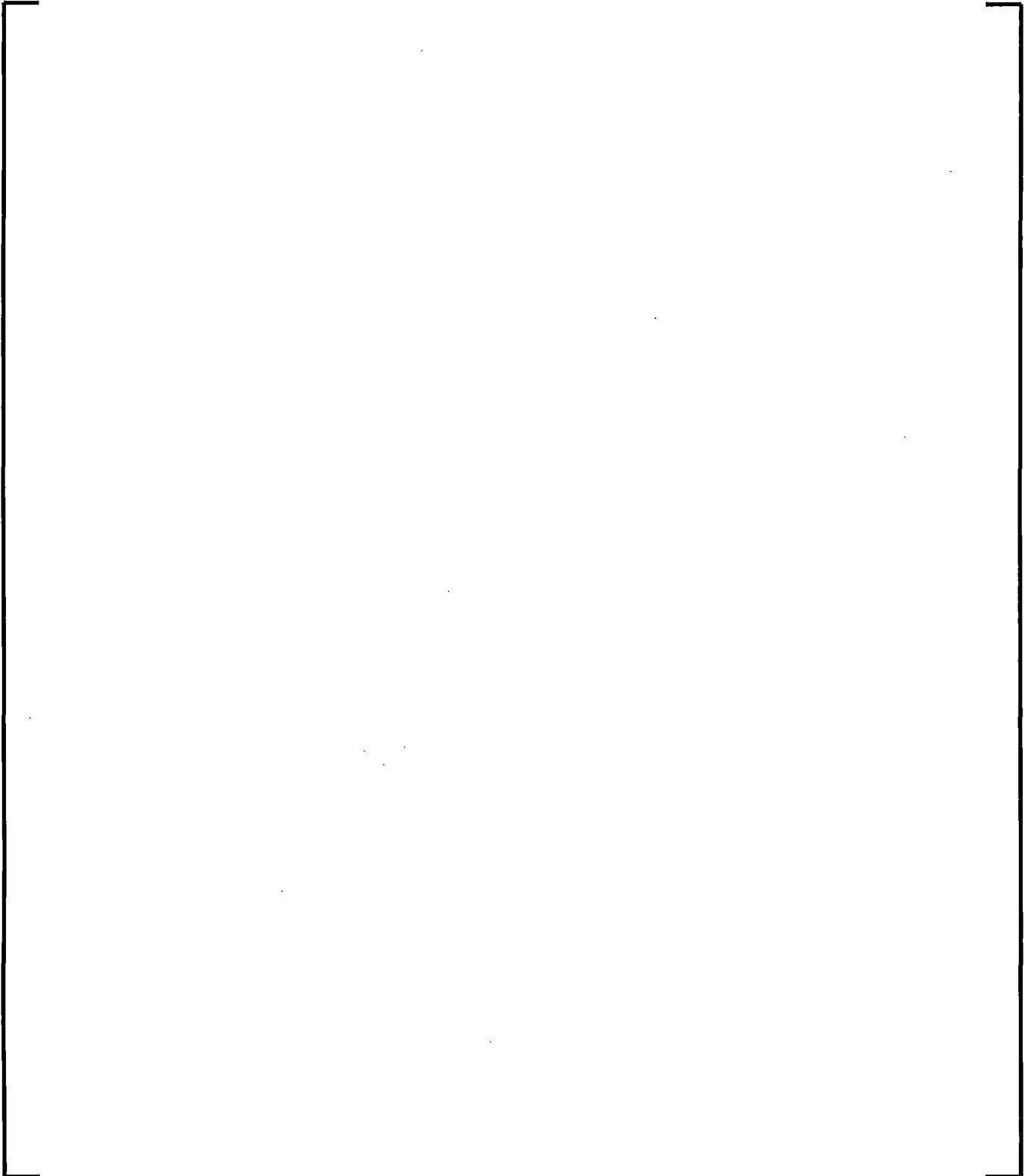
5.1.2.1 Interfacial Diffusion Coefficient Approximation

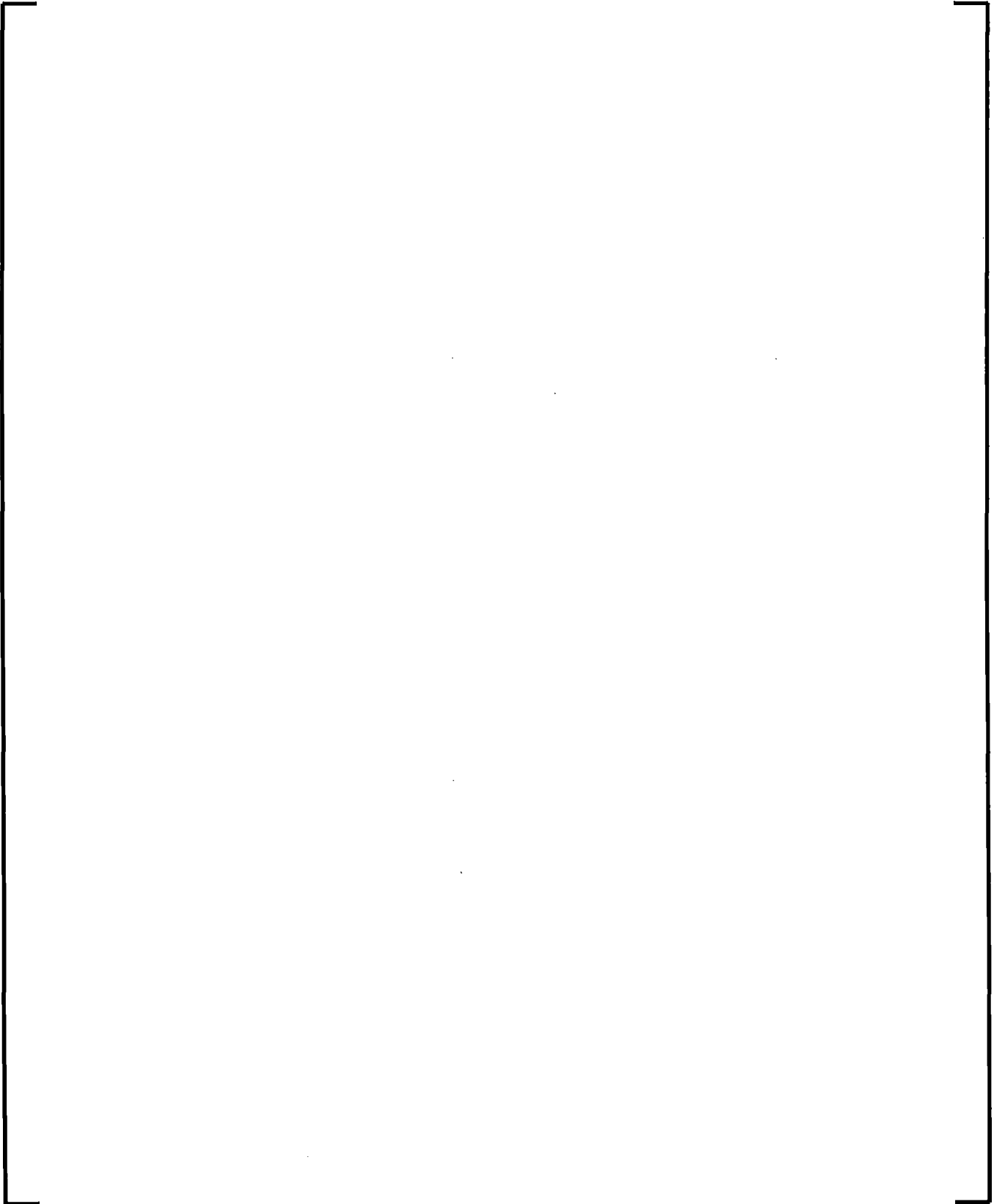


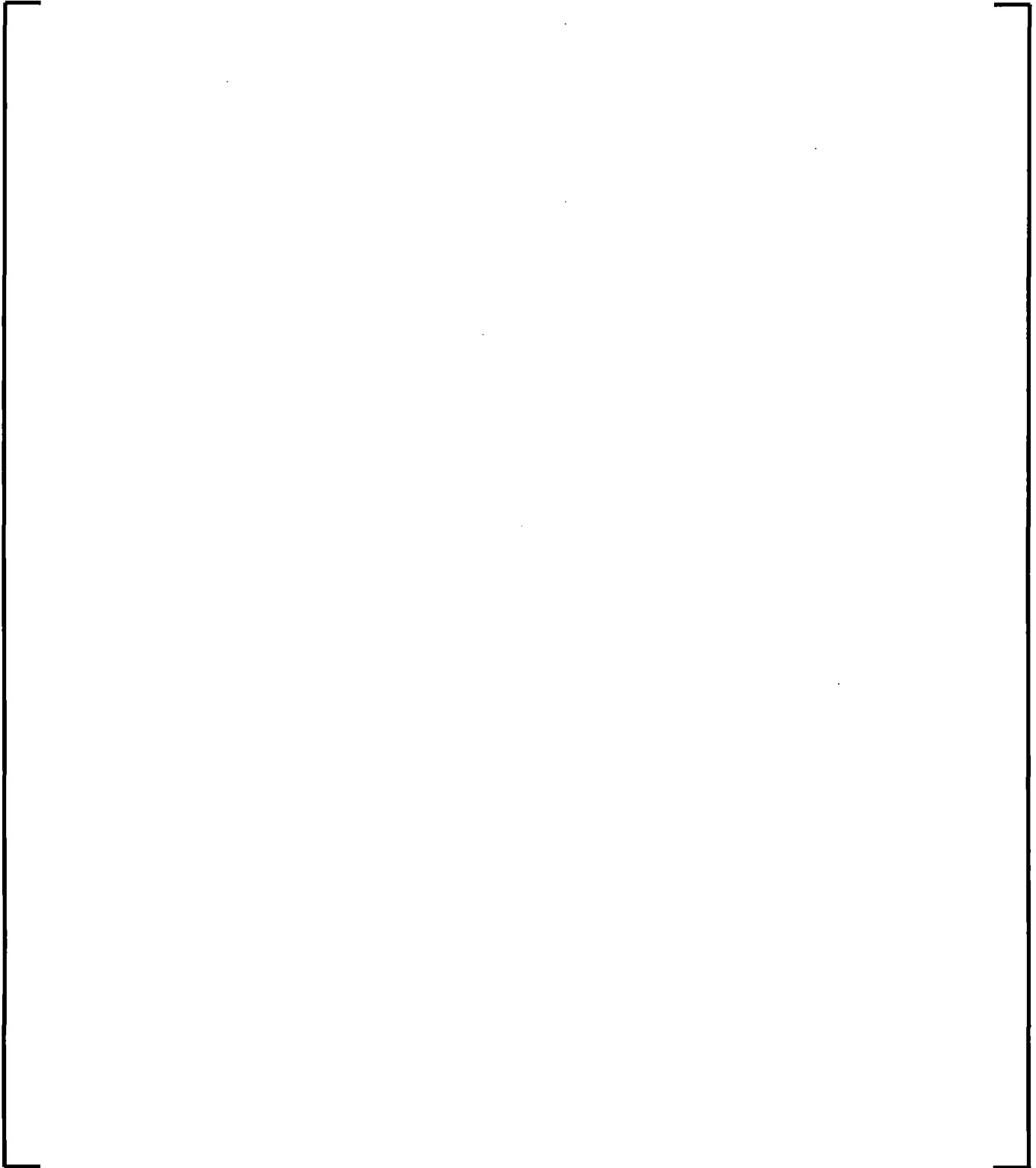


5.1.2.2 Steady State and Initialization

5.1.2.3 Time Integration Procedure







5.1.3 Cross Section Representation

5.1.4 Power Generation

The thermal-hydraulic calculations in RAMONA5-FA require the heat generation or power density in each computational cell. The power density at any point is the sum of two components, namely:

- Prompt fission heat: the amount of energy released promptly in the fission process, which is proportional to the fission rate.
- Decay heat: the amount of energy released by the decay fission products. It is delayed relative to the prompt fission heat and, hence, depends on the fission rate history.

The power density can be written as

$$q(\mathbf{r}, t) = q_P(\mathbf{r}, t) + q_D(\mathbf{r}, t) \quad (5.66)$$

where

q total heat generation rate,
 q_P prompt component,
 q_D delayed component,
 t time,
 \mathbf{r} spatial coordinate.

5.1.4.1 Prompt Fission Heat

5.1.4.2 Decay Heat

The amount of delayed energy released by the decay of the fission products following the shutdown of a reactor is fitted with a series of decay heat groups. Thus, the model is similar to the handling of delayed neutrons. The concentration of decay heat precursors in a decay group can be expressed in each neutronic node by the following differential equation

$$\frac{dD_i}{dt} = \alpha_i (\kappa \Sigma_{f1} \Phi_1 + \kappa \Sigma_{f2} \Phi_2) - \lambda_i D_i = \alpha_i \kappa F(\mathbf{r}, t) - \lambda_i D_i \quad (5.69)$$

where

- D_i concentration of decay heat precursors
- α_i fraction of the total energy appearing as decay heat in decay group
- λ_i decay constant [1/sec]
- i decay group number

The decay heat model is based on the American National Standard for Decay Heat Power in Light Water Reactors [Reference 23]. This standard uses 23 groups to fit the decay heat power t seconds after a fission pulse from a fissionable nuclide with a series of exponential terms. Each group is characterized by the fraction of the total fission energy appearing as decay heat in the group, α_i , and by a decay constant, λ_i .

The decay heat component can be written for RAMONA5-FA as:

$$q_D(\mathbf{r}, t) = \sum_{i=1}^{23} \lambda_i D_{H,i} \quad (5.70)$$

The concentration of the decay heat precursors, $D_{H,i}$, for the group i is given by the following differential equation, which is very similar to (5.69)

$$\frac{\partial D_{H,i}}{\partial t} = \gamma_i \kappa F(\mathbf{r}, t) - \varepsilon_i D_{H,i} \quad (5.71)$$

If we assume that $F(r, t)$ is a pulse at time zero, then the solution of (5.71) is given by

$$D_{H,i} = \gamma_i \kappa \exp(-\varepsilon_i t) \quad (5.72)$$

However, the ANS Standard gives the expression and the values of the coefficients for the function $f(t)$ which represents the decay heat power t seconds after a fission pulse,

$$f(t) = \sum_{i=1}^{23} \alpha_i \exp(-\lambda_i t) \quad (5.73)$$

Combining Equation (5.72) with (5.70), we obtain for a fission pulse

$$q_D(r, t) = \sum_{i=1}^{23} \gamma_i \varepsilon_i \kappa \exp(-\varepsilon_i t) \quad (5.74)$$

Comparing Equations (5.73) and (5.74), expressions for the coefficient set (γ, ε) are obtained in terms of the coefficients of the ANS standard (α, λ) . Thus,

$$\begin{aligned} \varepsilon_i &= \lambda_i \\ \gamma_i &= \frac{\alpha_i}{\kappa \lambda_i} \end{aligned} \quad (5.75)$$

The coefficients γ_i must be corrected to take into account two effects. First, if the fuel has been irradiated for a finite period of time, T , the coefficients are redefined as

$$\gamma_i = \frac{\alpha_i}{\kappa \lambda_i} [1 - \exp(-\lambda_i T)] \quad (5.76)$$

The second correction takes into account for the fact [

1.

The total fraction of fission energy appearing as decay heat is obtained from

$$\gamma_T = \sum_{i=1}^{23} \gamma_i \quad (5.77)$$

which is used in the prompt power density calculation in Equation (5.67).

5.1.5 Power Deposition

RAMONA5-FA takes into account the fact that the fission energy is deposited as thermal energy both inside the fuel pellet, where the fission takes place, and outside the pellet due to neutron slowing down and gamma attenuation. [

]

5.2 ***Fuel Thermodynamics***

In this section, the modeling of heat conduction in the heating elements is presented. The transient heat conduction serves as a link between the energy deposition from nuclear fission and the dynamics of the fluid flow in the fuel assemblies. The heat conduction in fuel rods consisting of pellet and cladding and pellet-clad gap is needed for the dynamic modeling of the reactor core, while modeling of heat conduction in electrically heated pins is needed for performing benchmarking calculations for comparison with test loop data. For either fuel or heater rods, the models for heat transfer between the rod surface and the coolant covering different heat transfer regimes are presented. For the analysis of fuel rods, [

]

[
].

5.2.1 ATWS-I Fuel Pin Heat Conduction

Heat conduction in the fuel pin is assumed to be azimuthally symmetric with no axial component. The transient heat conduction equation is thus

$$\rho C \frac{\partial T}{\partial t} = \frac{1}{r} \frac{\partial}{\partial r} \left(k r \frac{\partial T}{\partial r} \right) + q''' \quad (5.82)$$

where

r radial coordinate from the fuel pin center
 t time
 $T(r, t)$ temperature
 $q'''(r, t)$ volumetric heat generation rate
 ρ density
 C specific heat at constant pressure
 k thermal conductivity

The fuel rod is made of 3 components, fuel pellet, clad and pellet-clad gap. [

]

The boundary condition at the pellet center is

$$\frac{\partial T}{\partial r} = 0 \quad \text{at} \quad r = 0 \quad (5.83)$$

The boundary condition at the outer clad surface is obtained as heat flux continuity, thus

$$-k_c \frac{\partial T}{\partial r} \bigg|_{r=R} = h(T_{wall} - T_{ref}) \quad (5.84)$$

where

T_{ref}	heat sink (coolant) temperature
R	outer clad radius
T_{wall}	outer clad surface temperature
h	heat transfer coefficient
k_c	clad thermal conductivity

The pellet-clad gap is modeled as a thin layer with no thermal inertia but finite thermal resistance. Thus the inner clad radius is approximated as equal to the outer pellet radius, R_f . The heat flux across the gap is obtained from

$$-k_c \frac{\partial T}{\partial r} \bigg|_{r=R_f+} = -k_f \frac{\partial T}{\partial r} \bigg|_{r=R_f-} = h_{gap} (T_f - T_{ci}) \quad (5.85)$$

where

h_{gap}	gap heat conductance
T_f	temperature at fuel pellet outer radius
T_{ci}	temperature at clad inner radius
k_c	clad thermal conductivity
k_f	pellet thermal conductivity
R_f	pellet outer radius (R_{f-} and R_{f+} refer to the pellet and clad sides of the gap respectively)

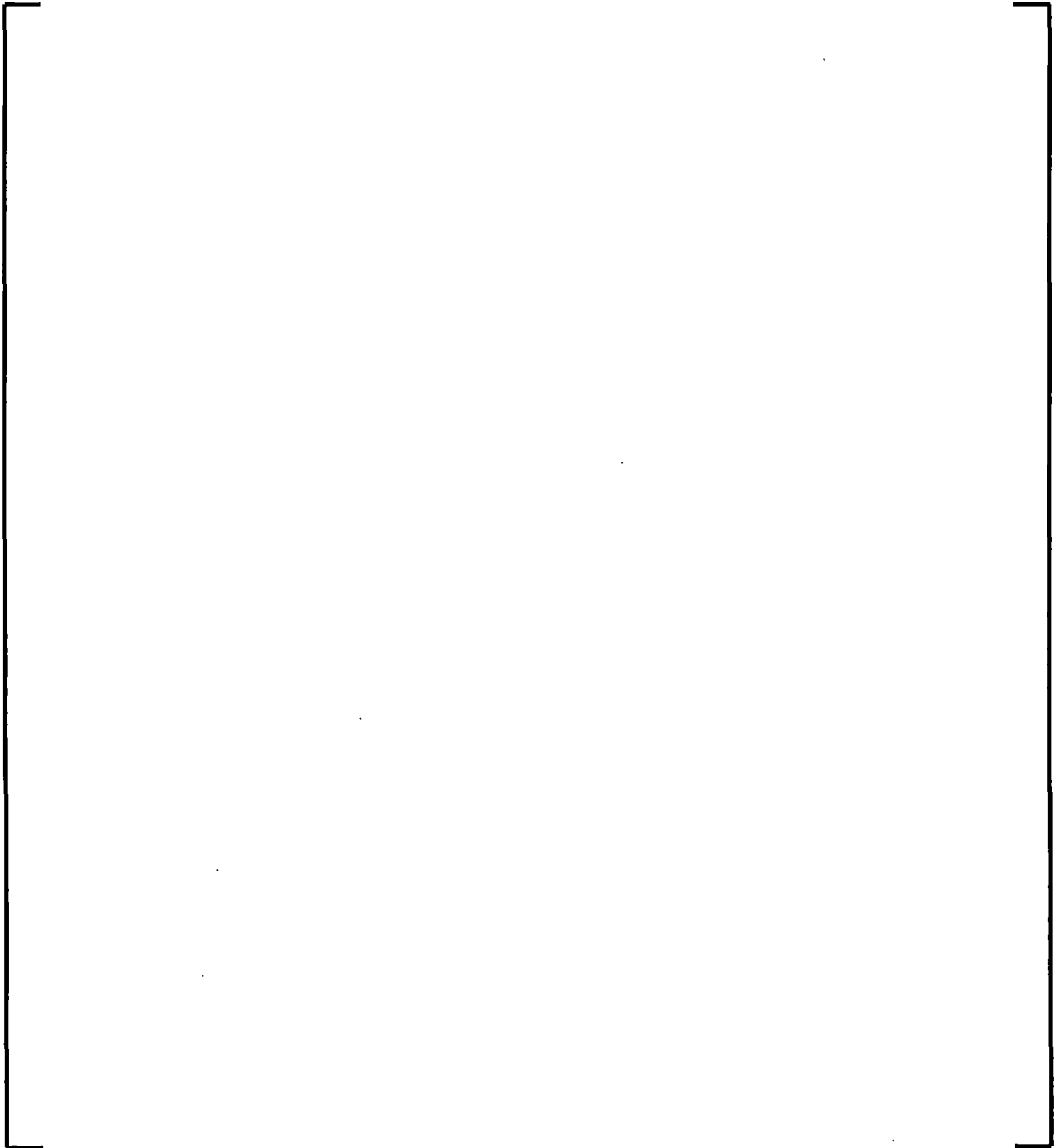
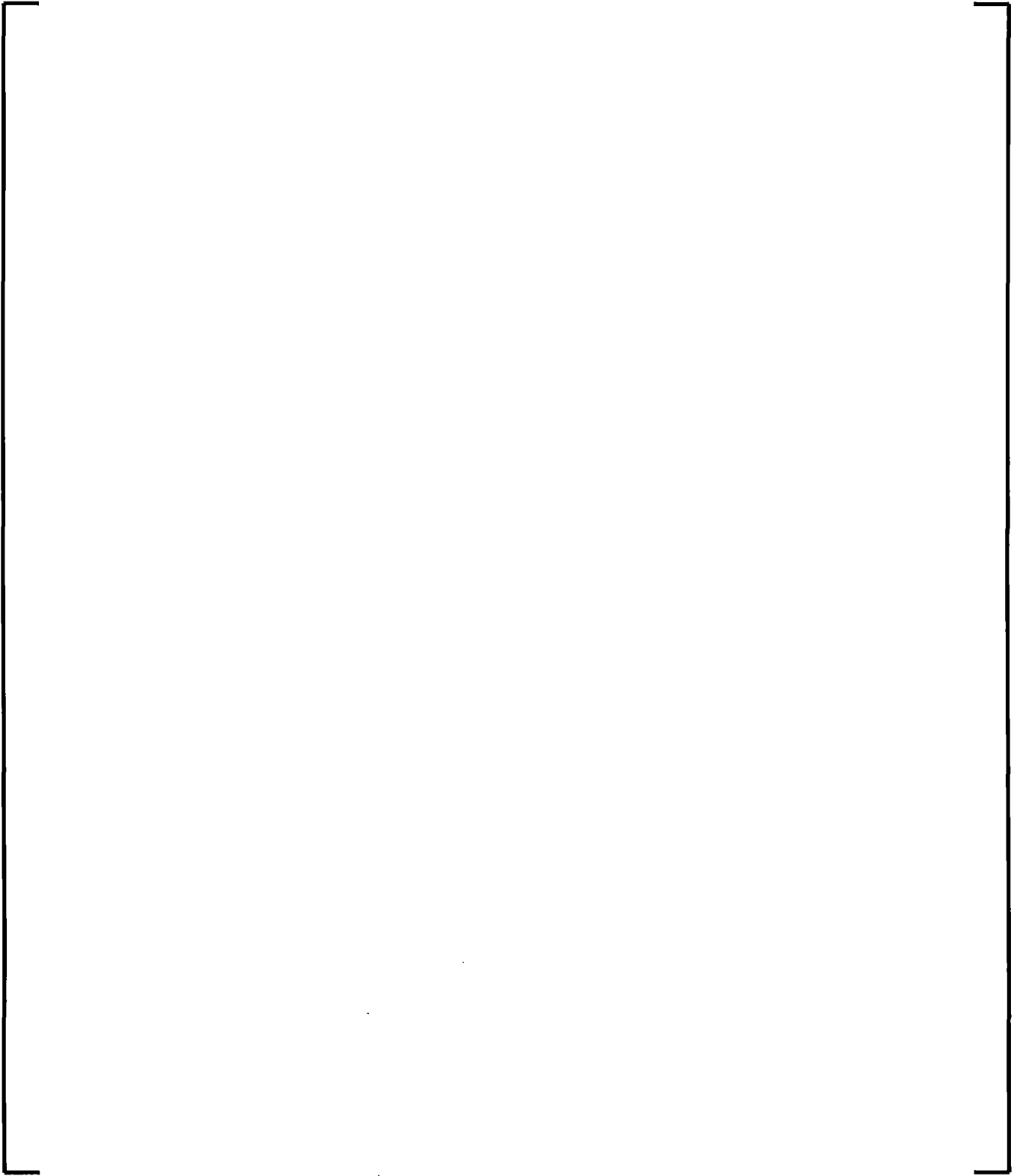
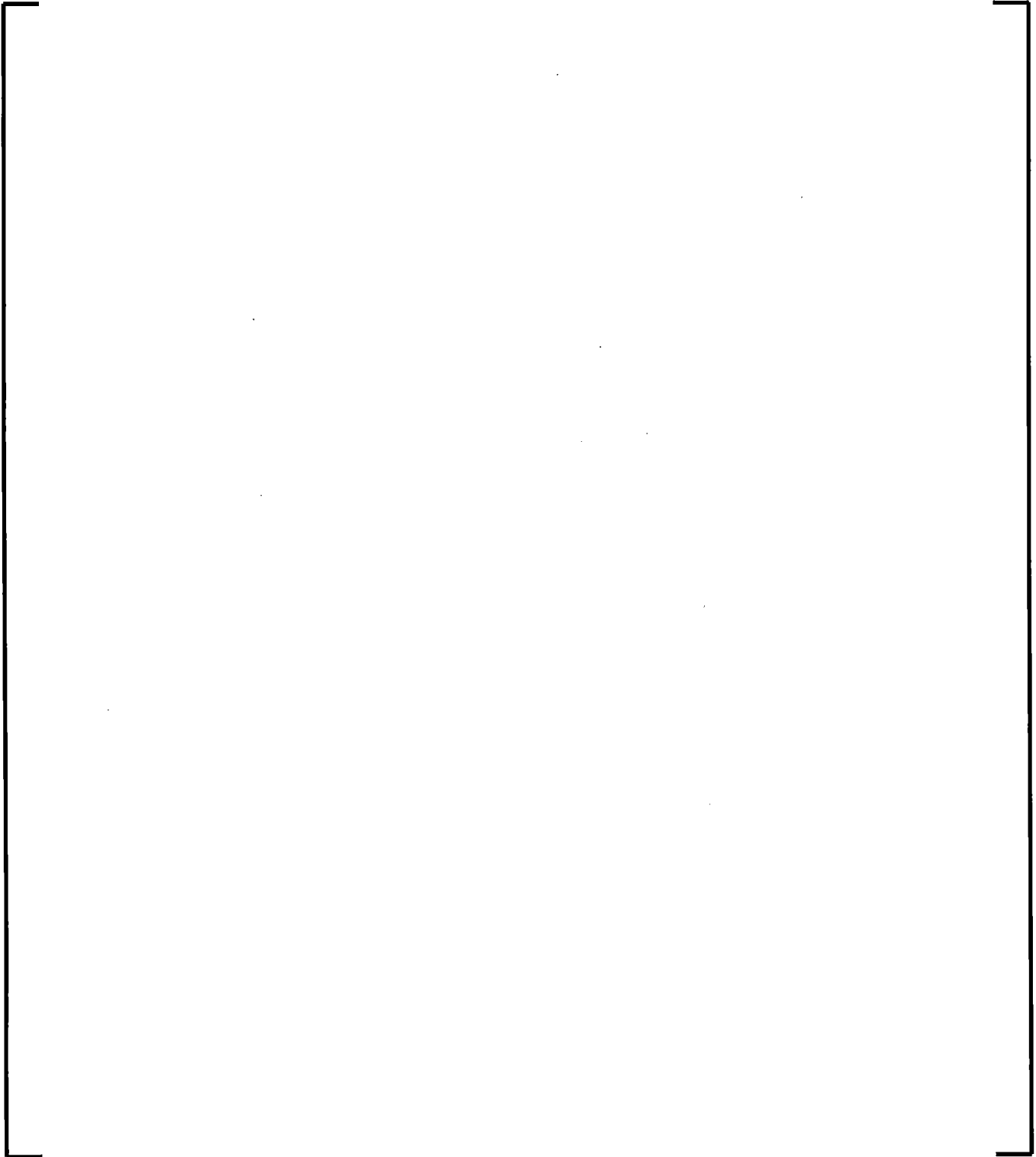
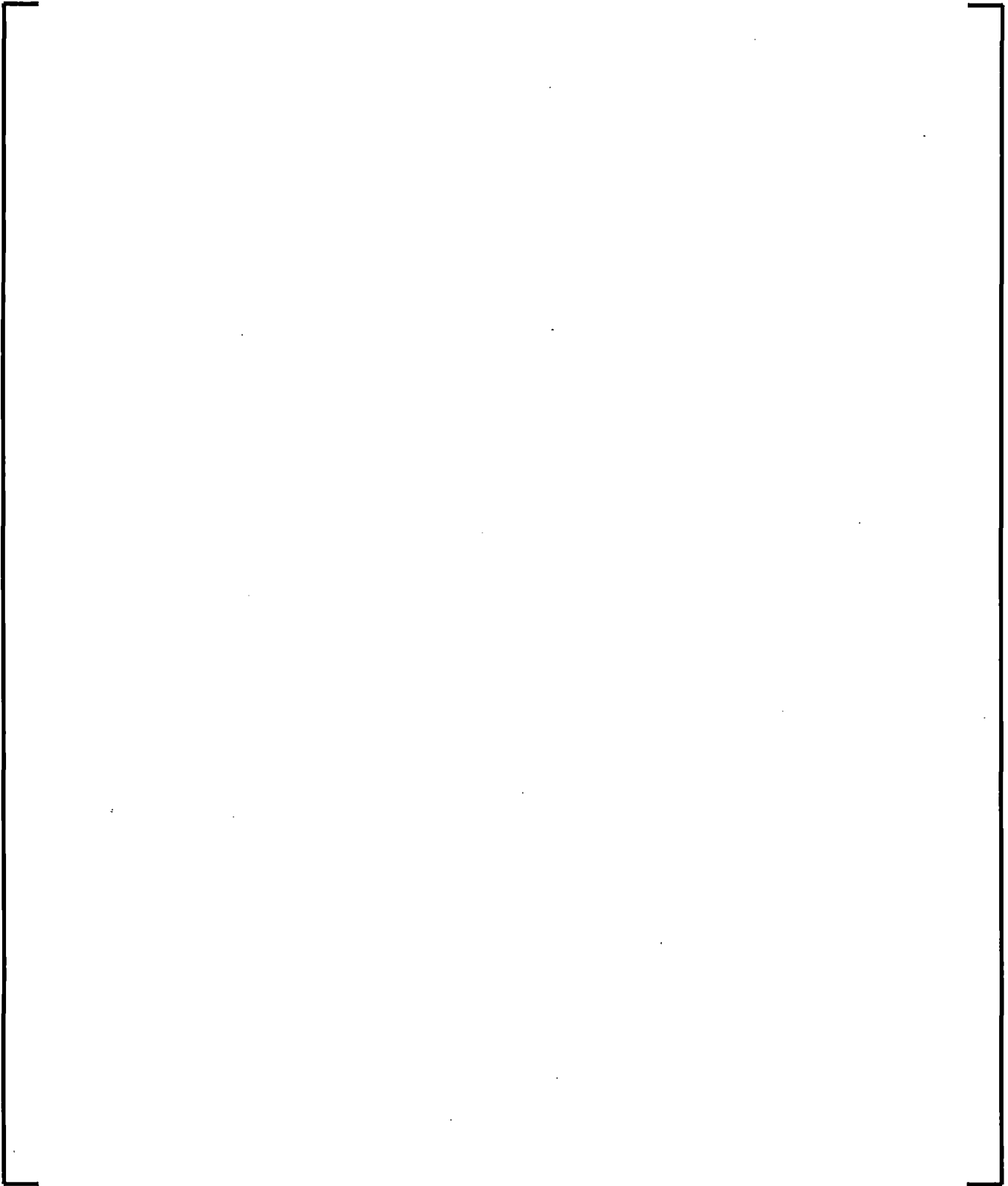
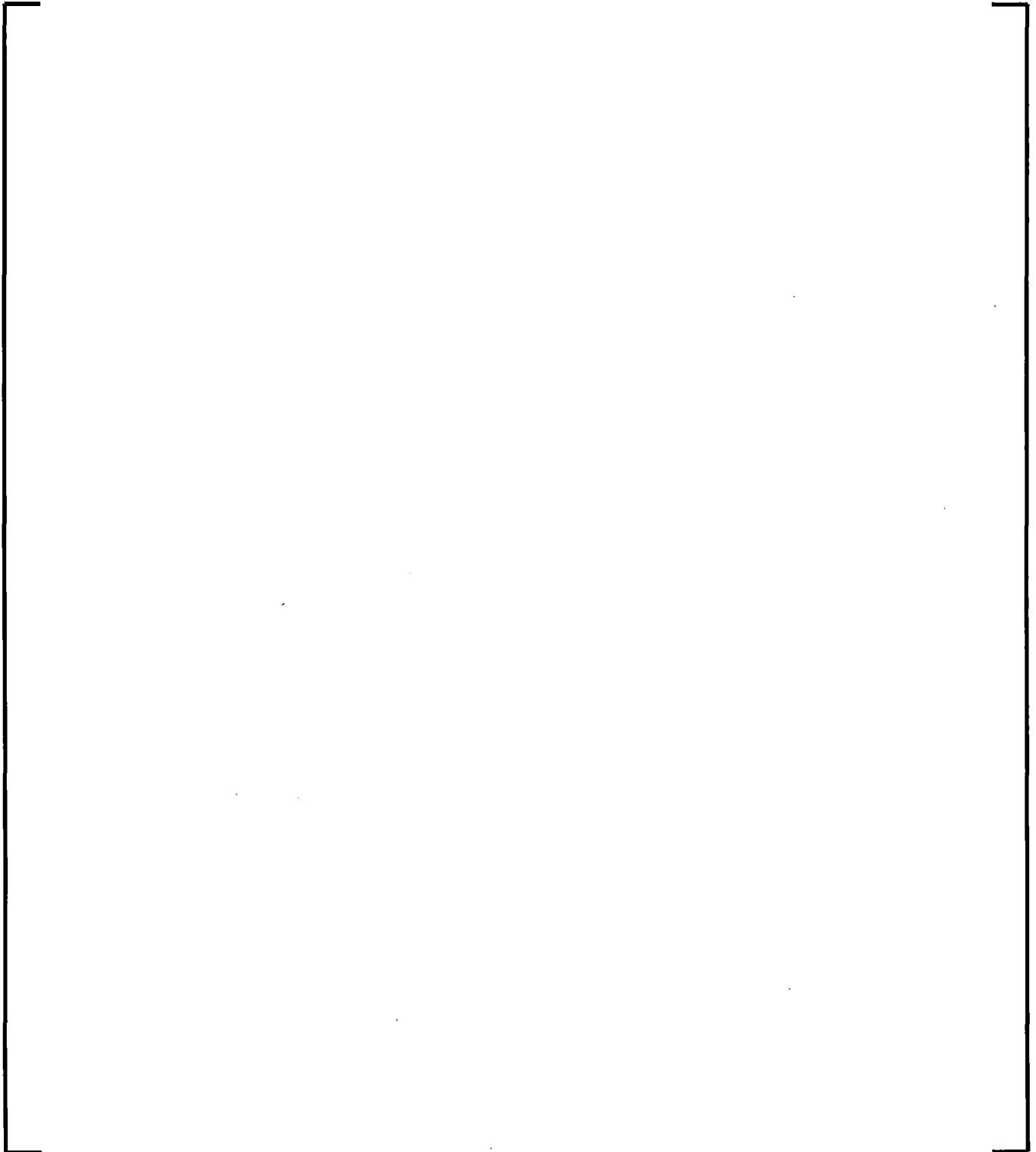


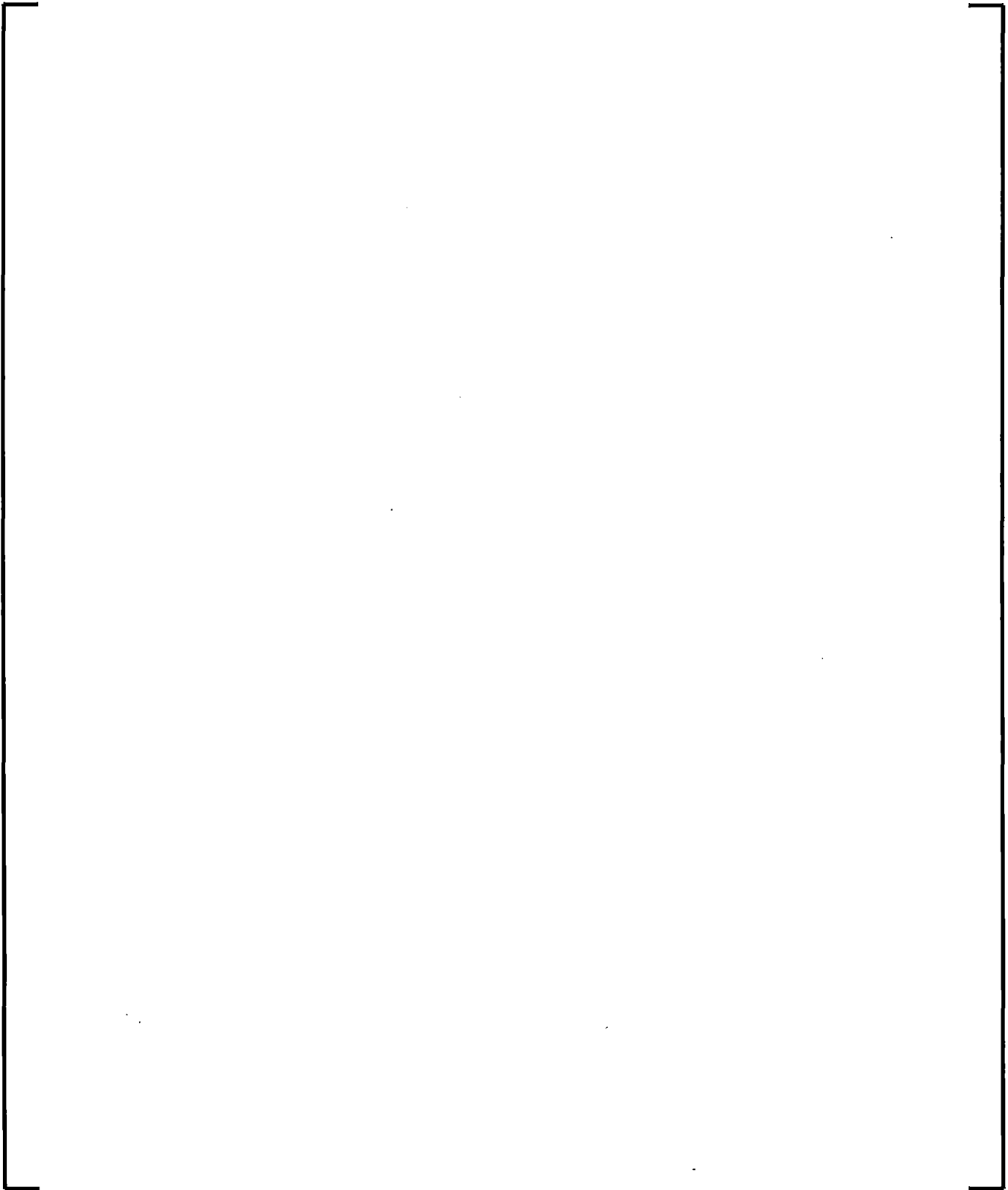
Figure 5-1: Fuel rod discretization











5.2.2 ATWS-I Heater Rod Heat Conduction

In order to properly model the KATHY test facility, [

]. The transient heat

conduction equation in the radial direction is written as

$$\rho C \frac{\partial T}{\partial t} = \frac{1}{r} \frac{\partial}{\partial r} \left(r k \frac{\partial T}{\partial r} \right) + q''' \quad (5.121)$$

The different variables used in Equation (5.121) are defined below

ρ	Heater rod material density (kg/m ³)
C	Heater rod material heat capacity (J/kg.K)
k	Heater rod material thermal conductivity (W/m.K)
q'''	Time-dependent Ohmic heat source deposited in the heater per unit volume (W/m ³)
T	Time- and space-dependent temperature in the rod wall (C)
t	Time (s)
r	Radial distance (m)



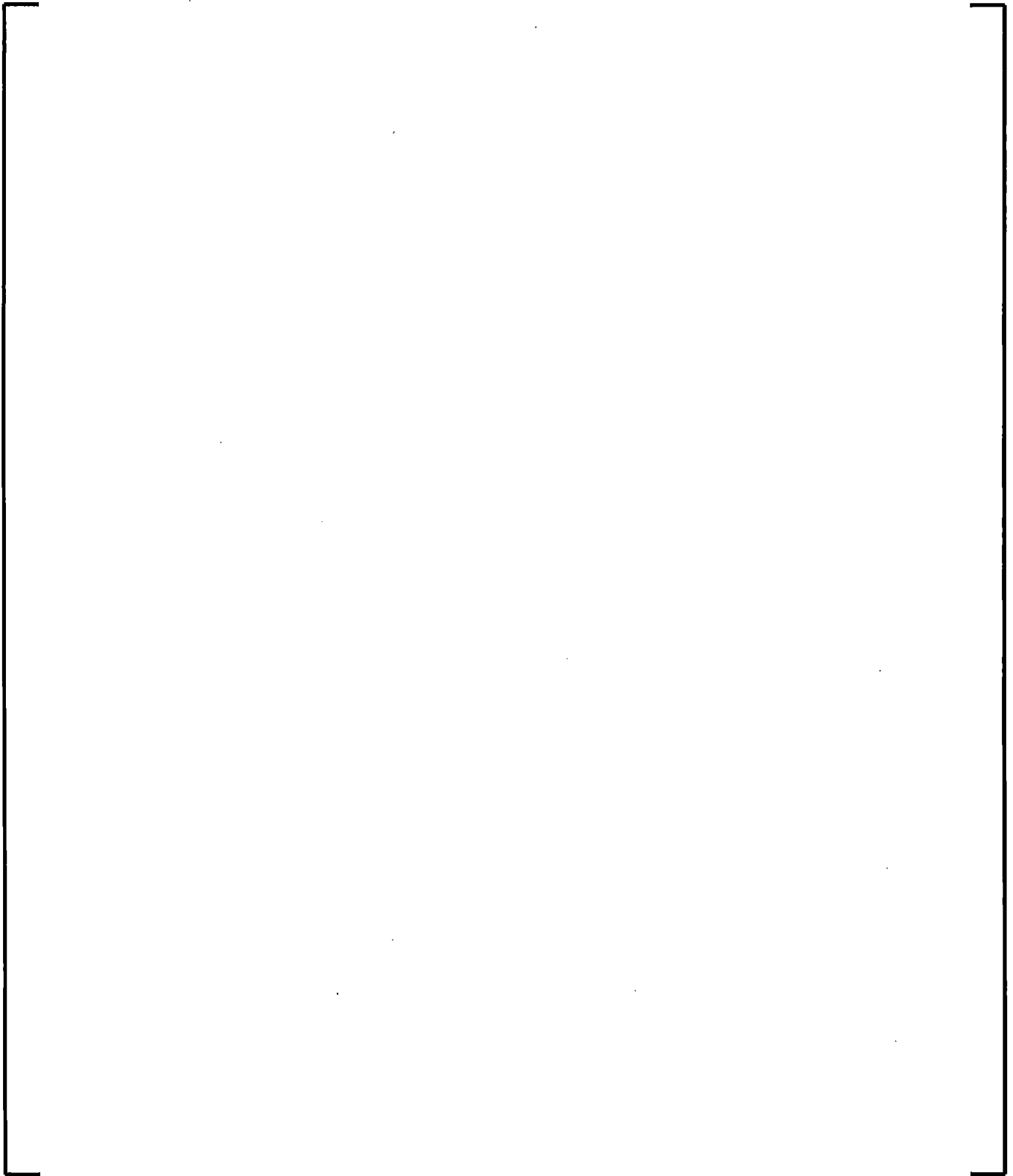


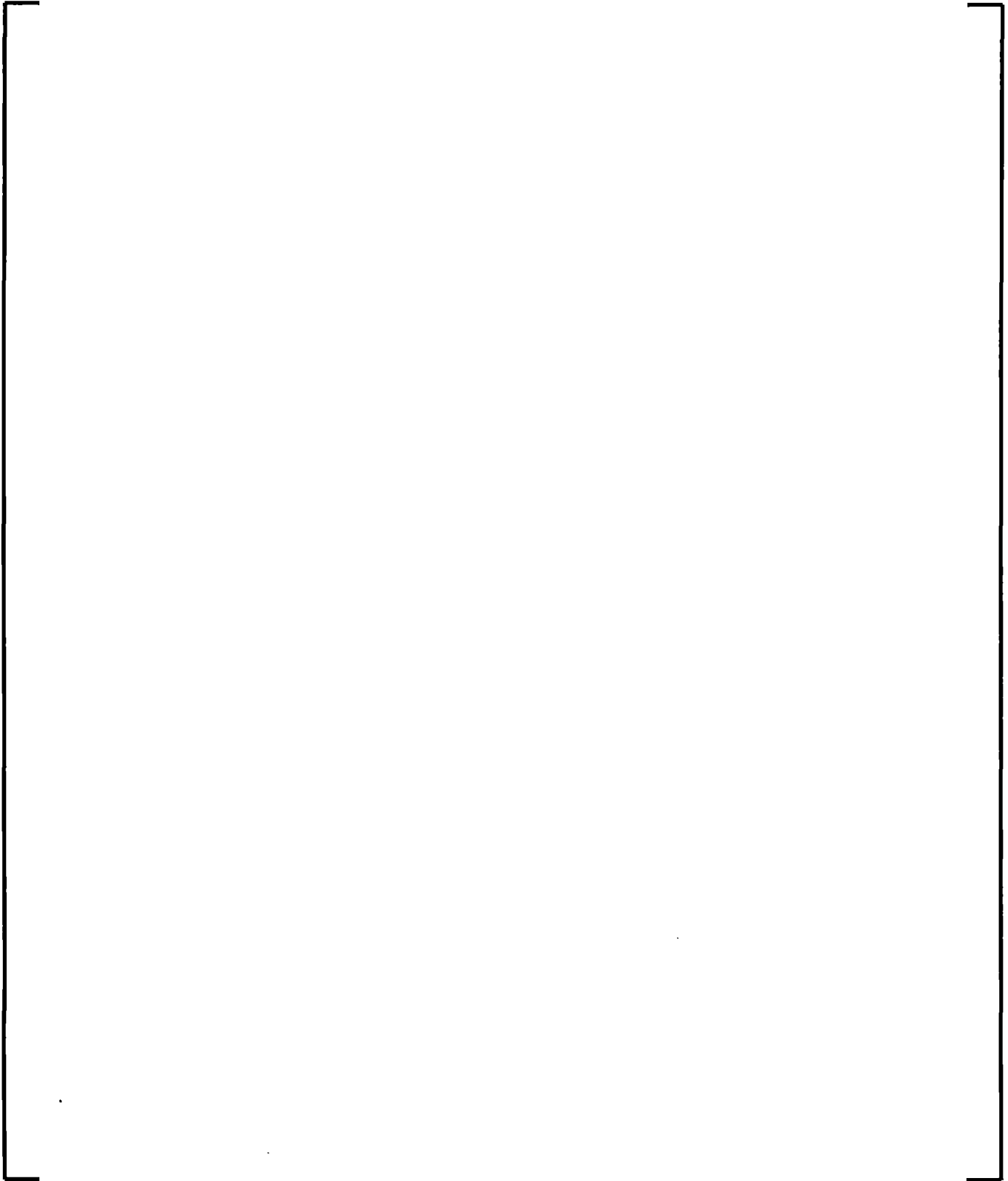
Figure 5-2: Heater rod discretization

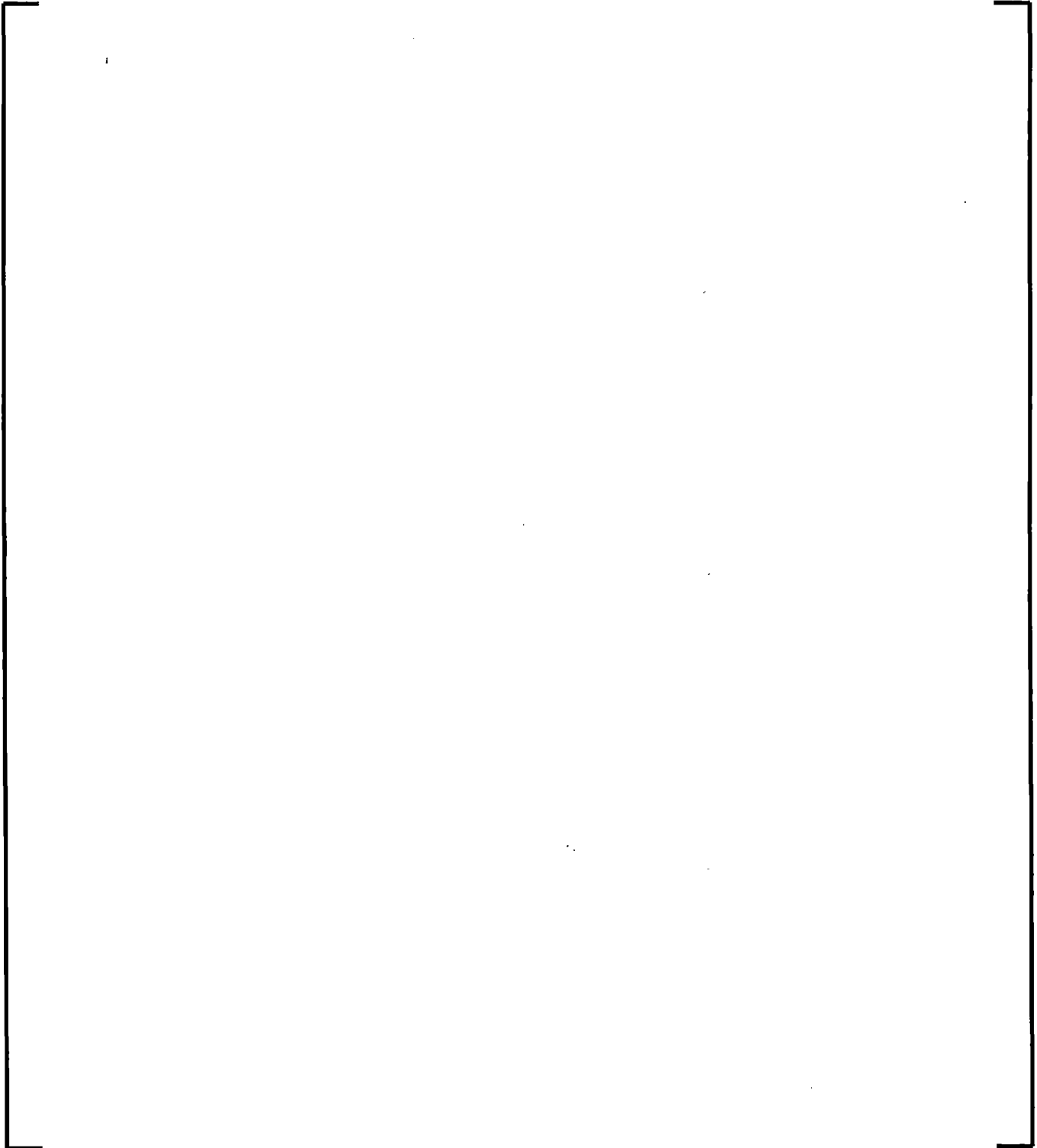
The steady state solution is obtained by setting the time derivative on the left hand side of Equation (5.121) to zero to get

$$\frac{1}{r} \frac{d}{dr} \left(r k \frac{dT}{dr} \right) = -q''' \quad (5.123)$$







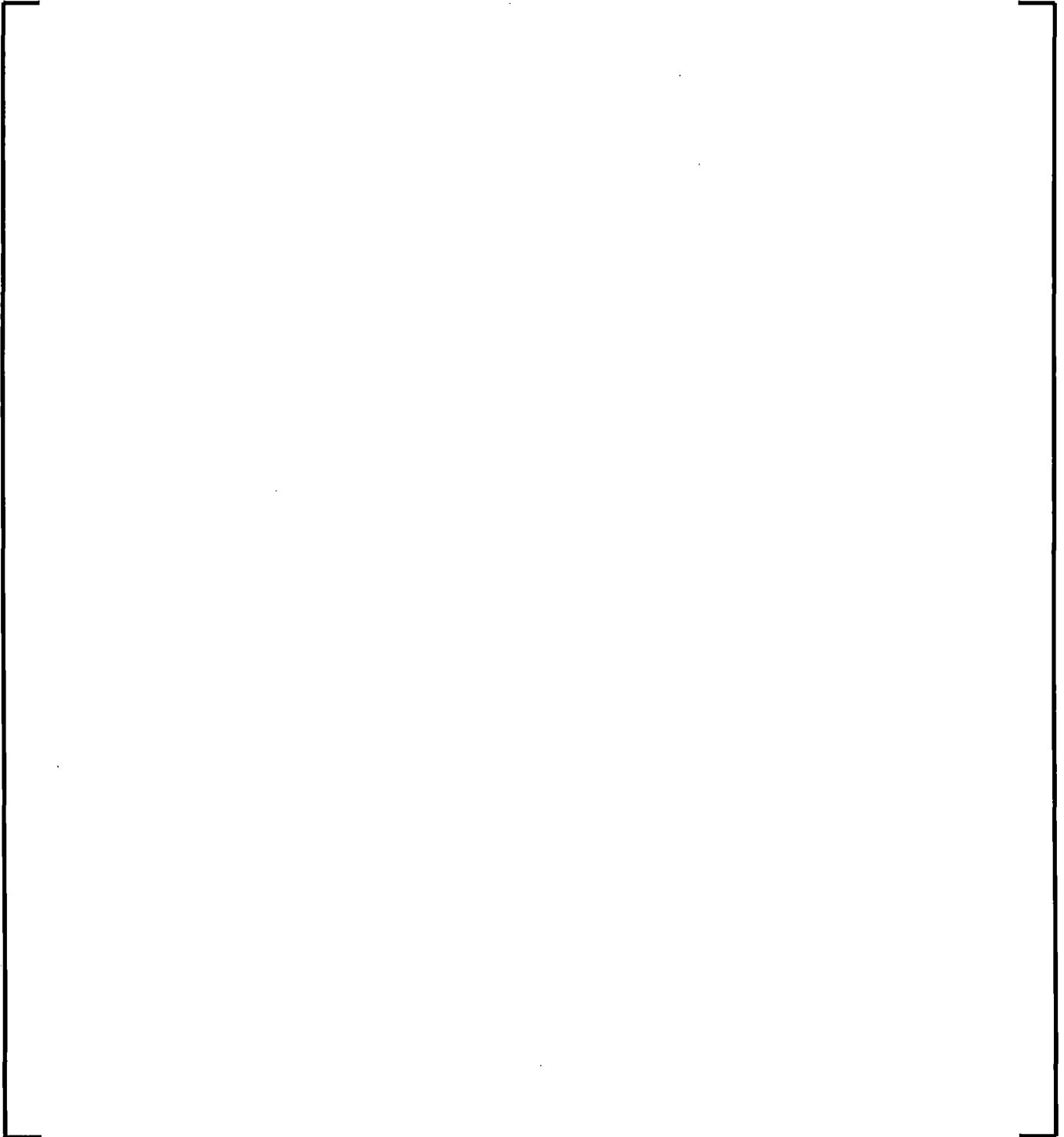


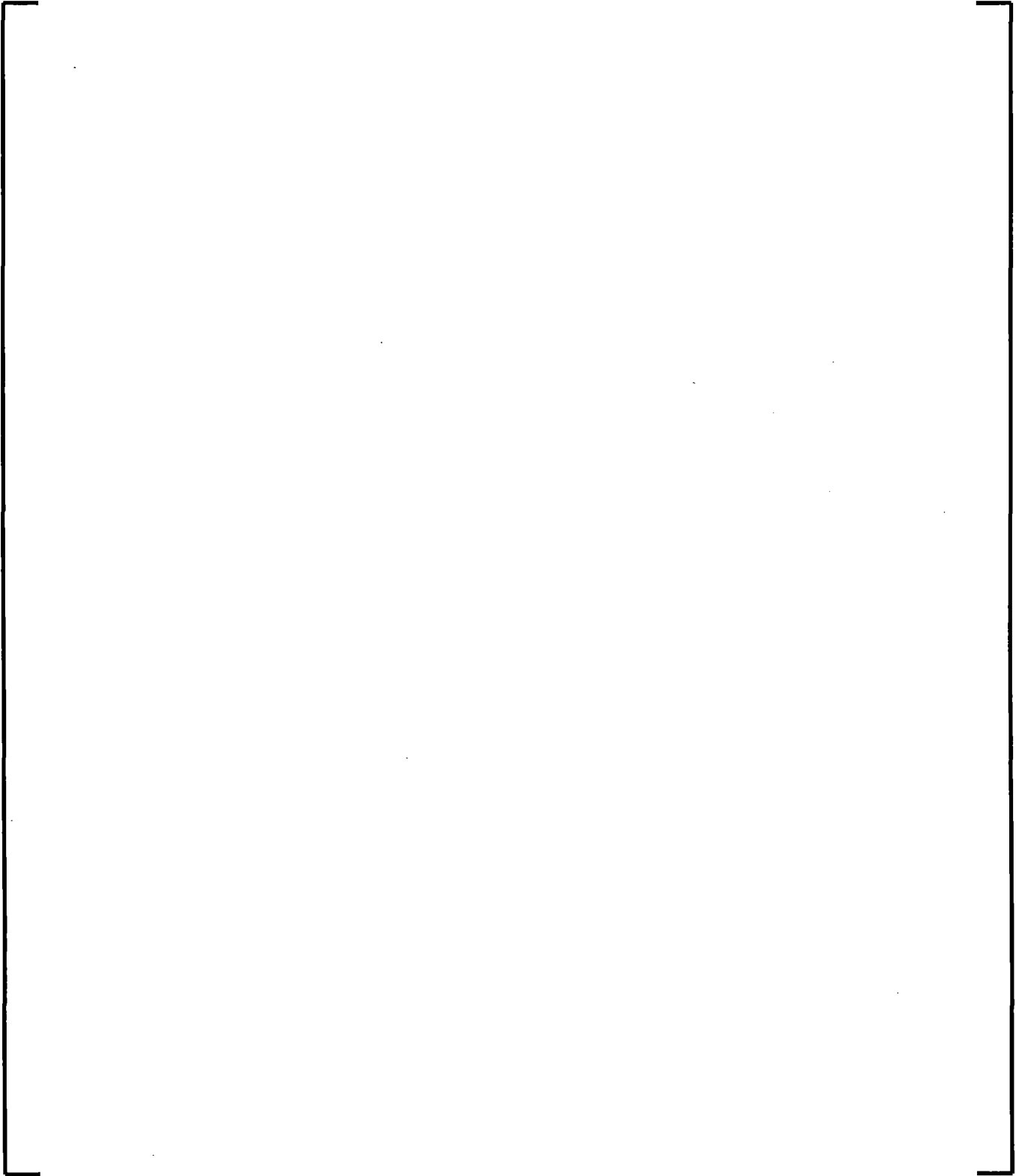
5.2.3 Heat Transfer Coefficient

The heat transfer coefficient calculations include wetted conditions under single- or two-phase flow, partially or fully dry conditions, and the transitions between these different regimes. With possible heat transfer from pin surface to liquid and/or vapor [

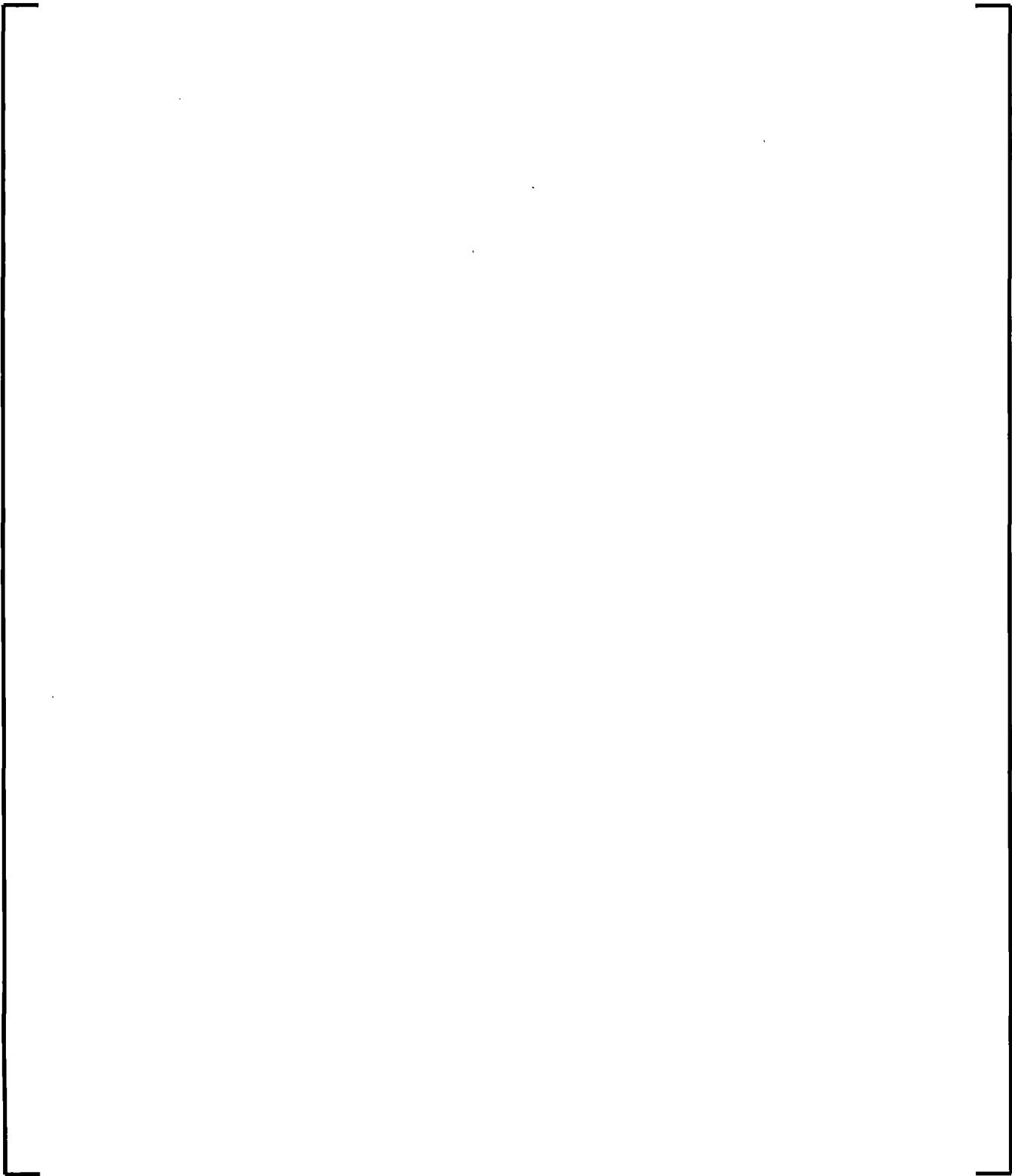
]

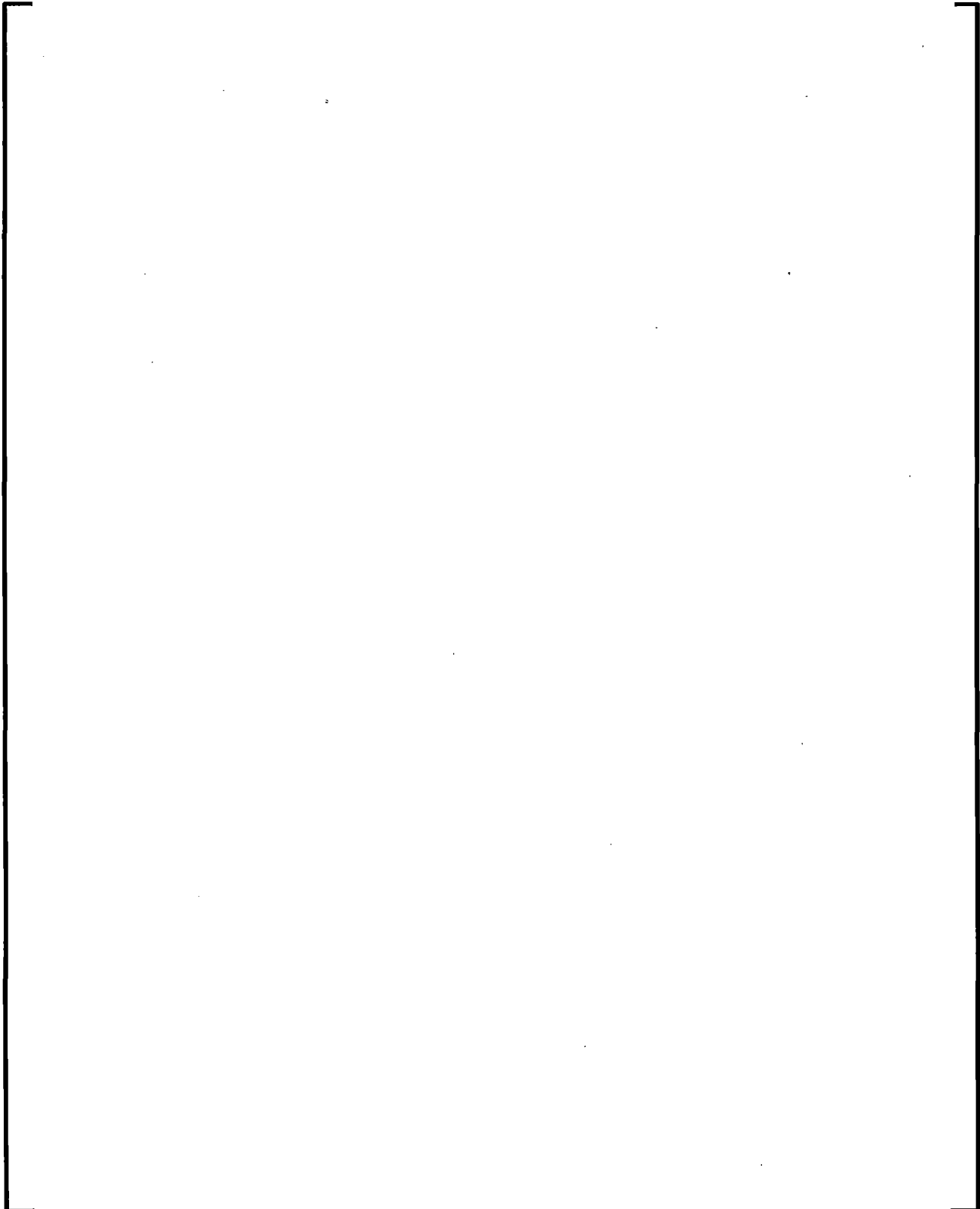
Wet heat transfer coefficient





Dry heat transfer coefficient

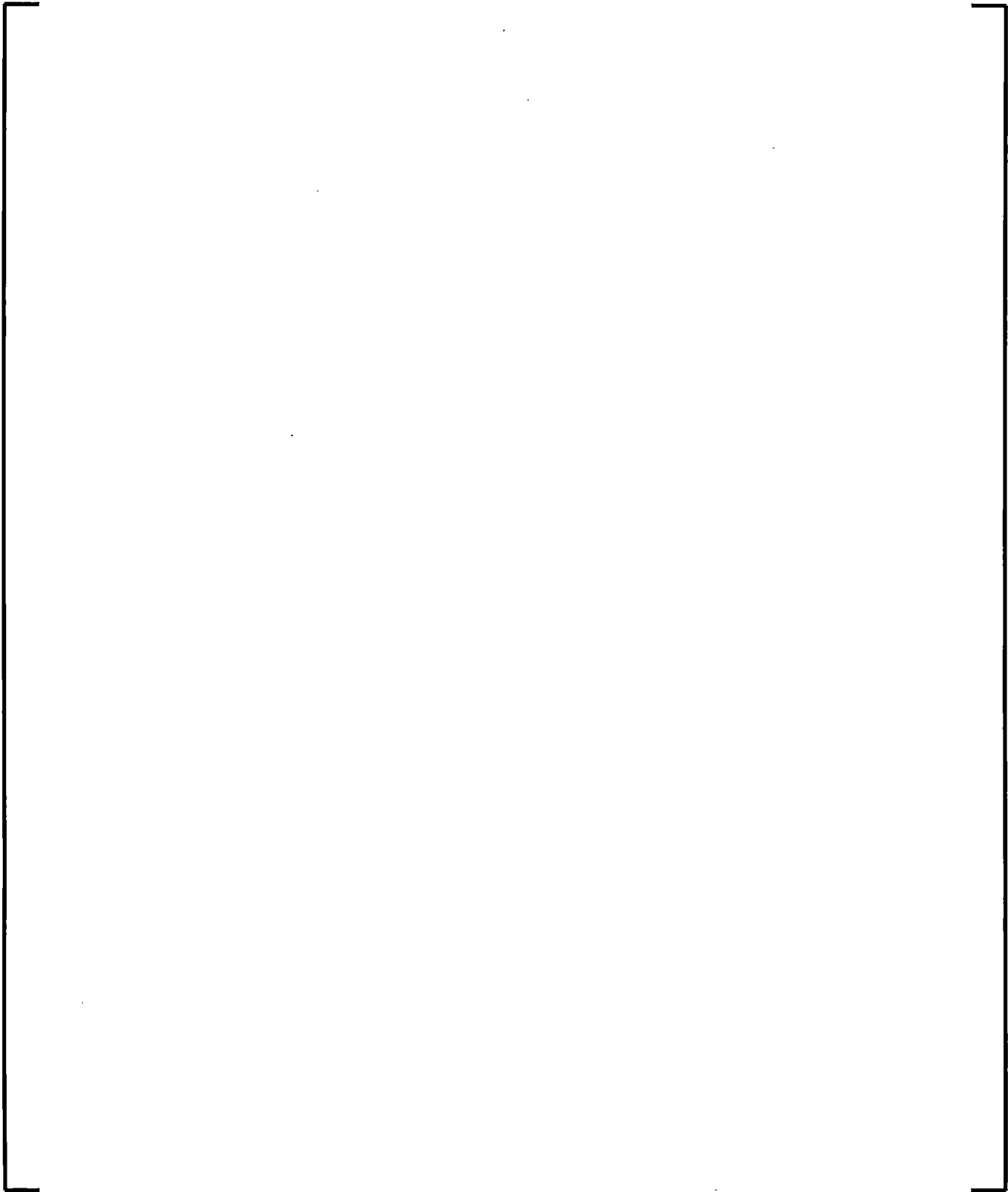




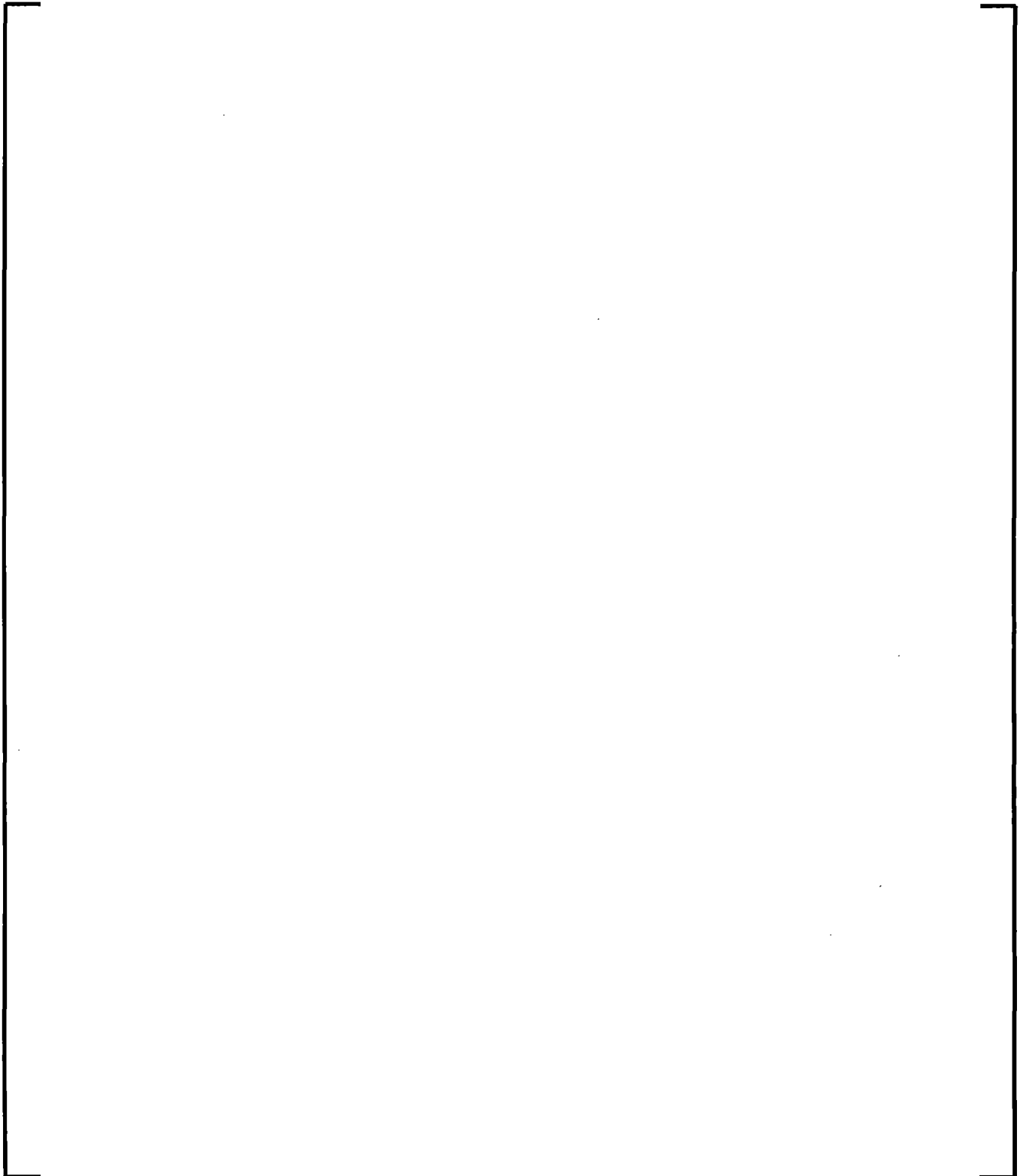
5.2.4 Hot Fuel Pin Model

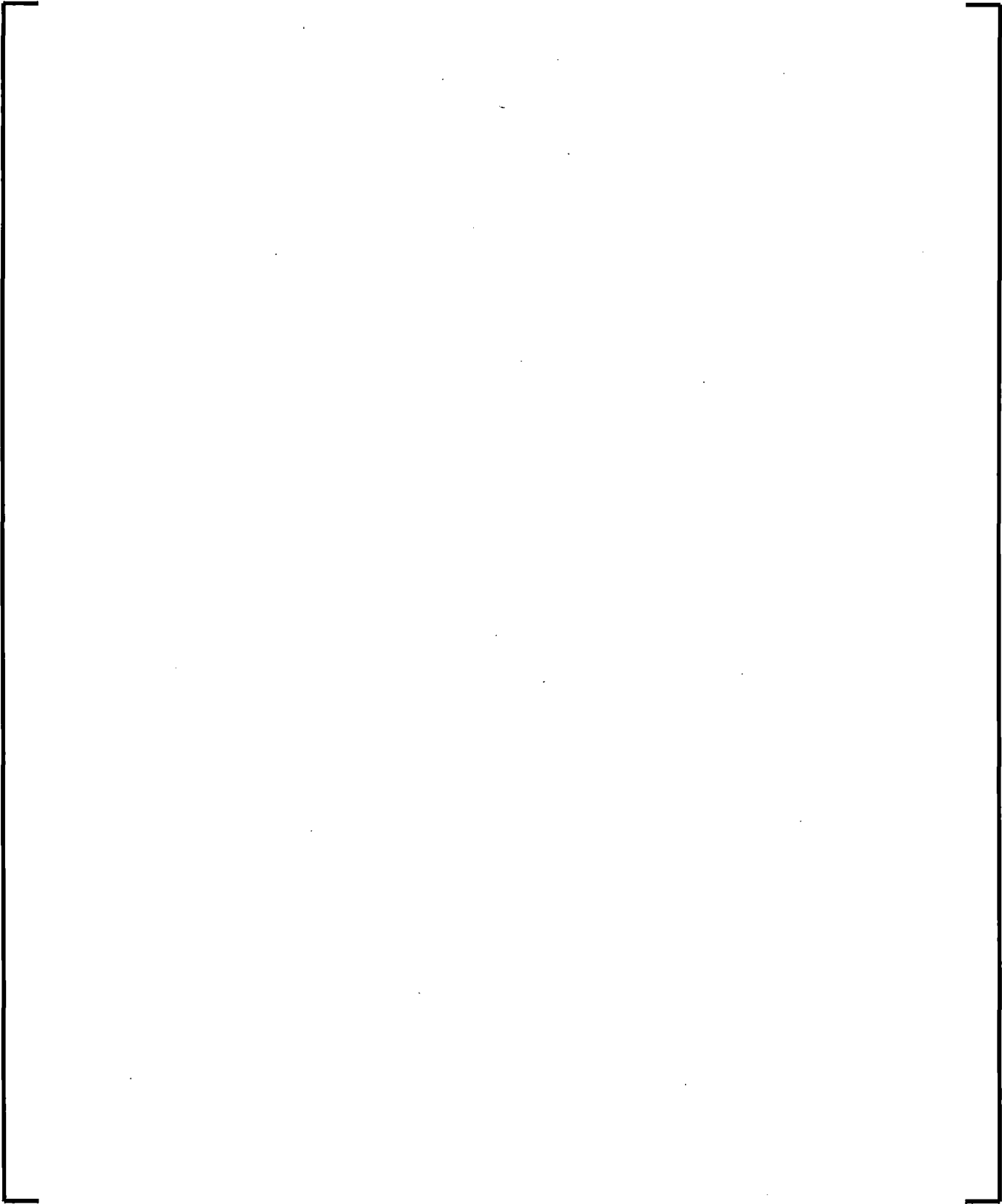
The following assumptions are made to model the hot pin in addition to the ones described in the previous section:

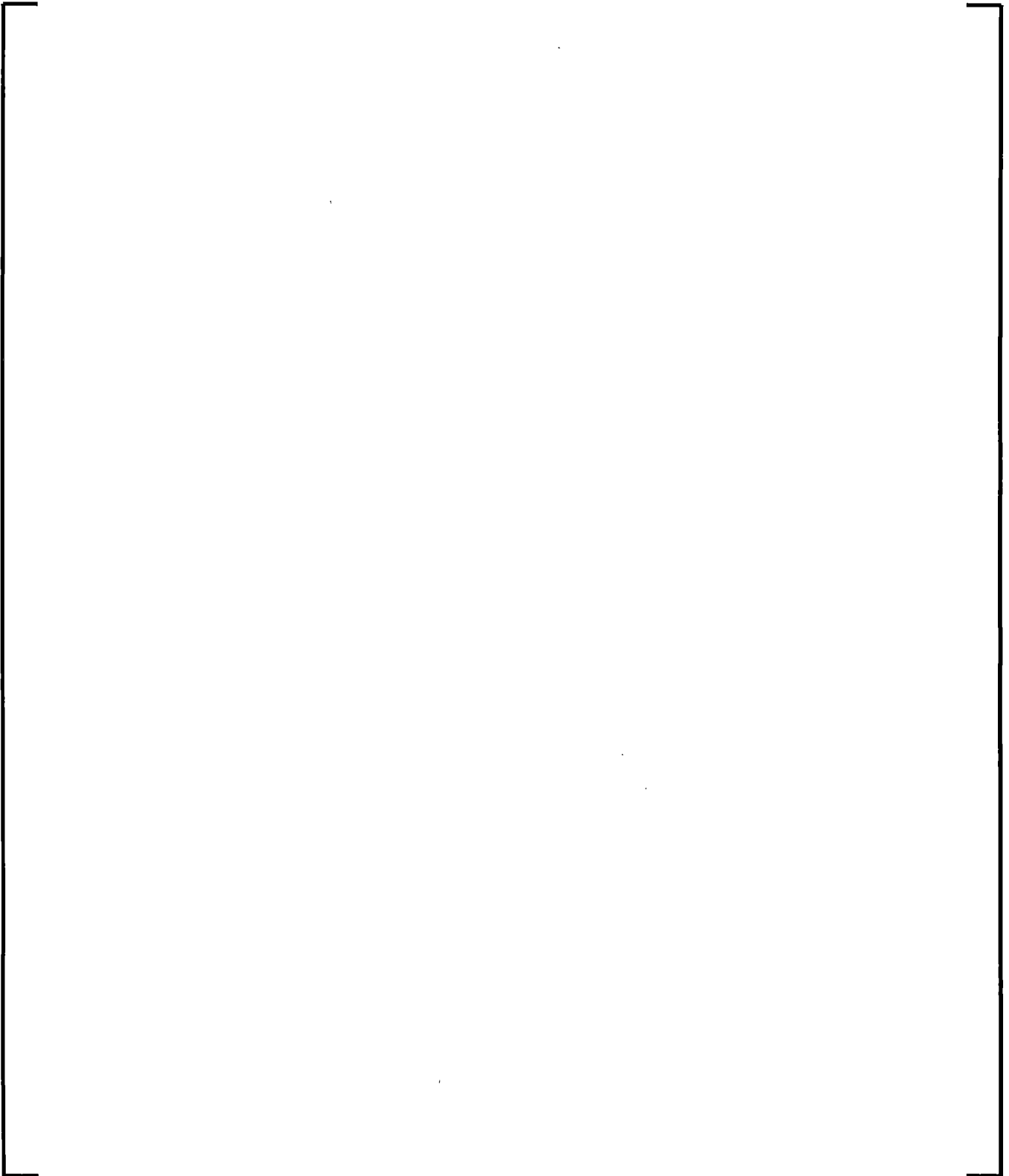
5.2.5 Material Properties

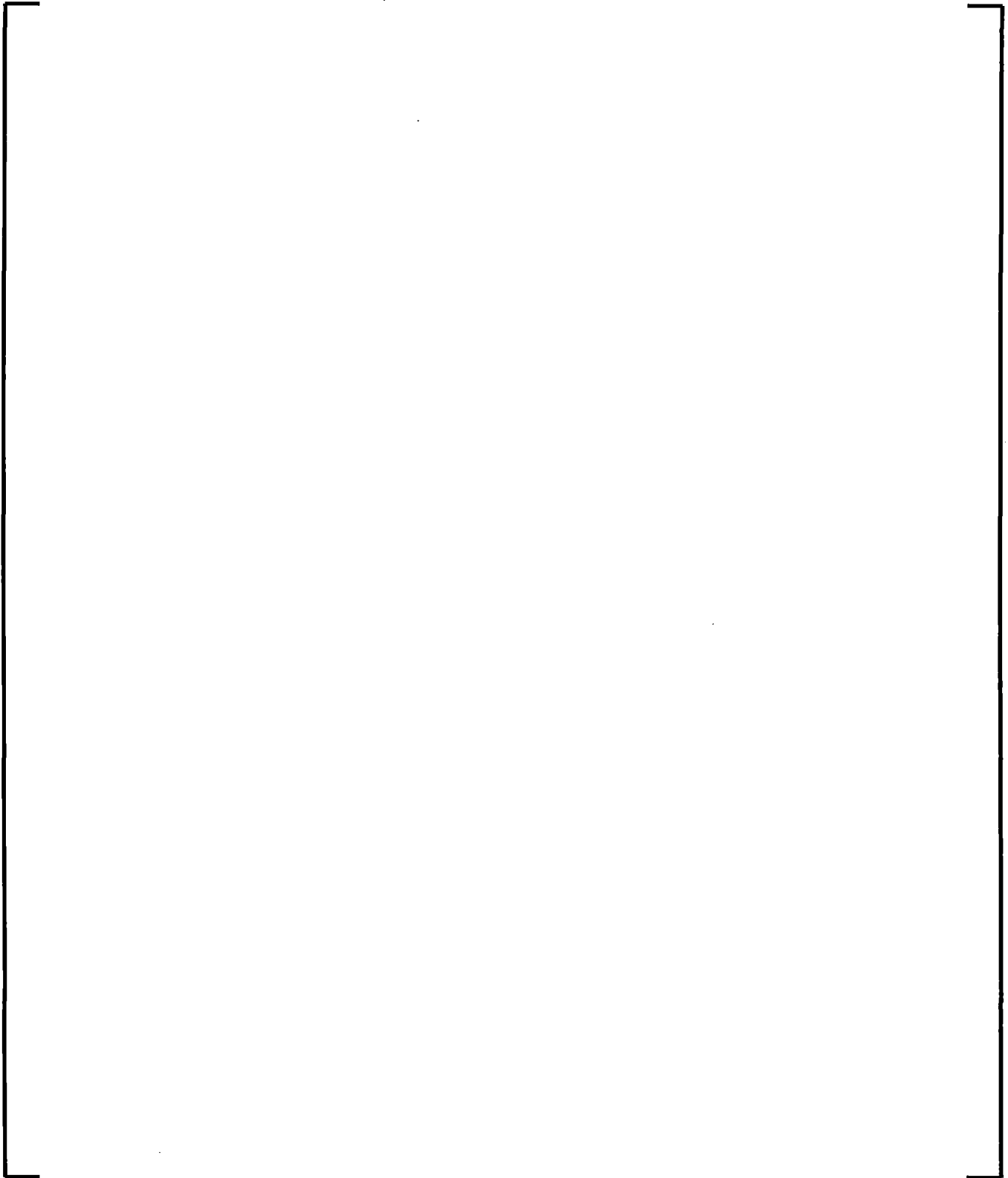


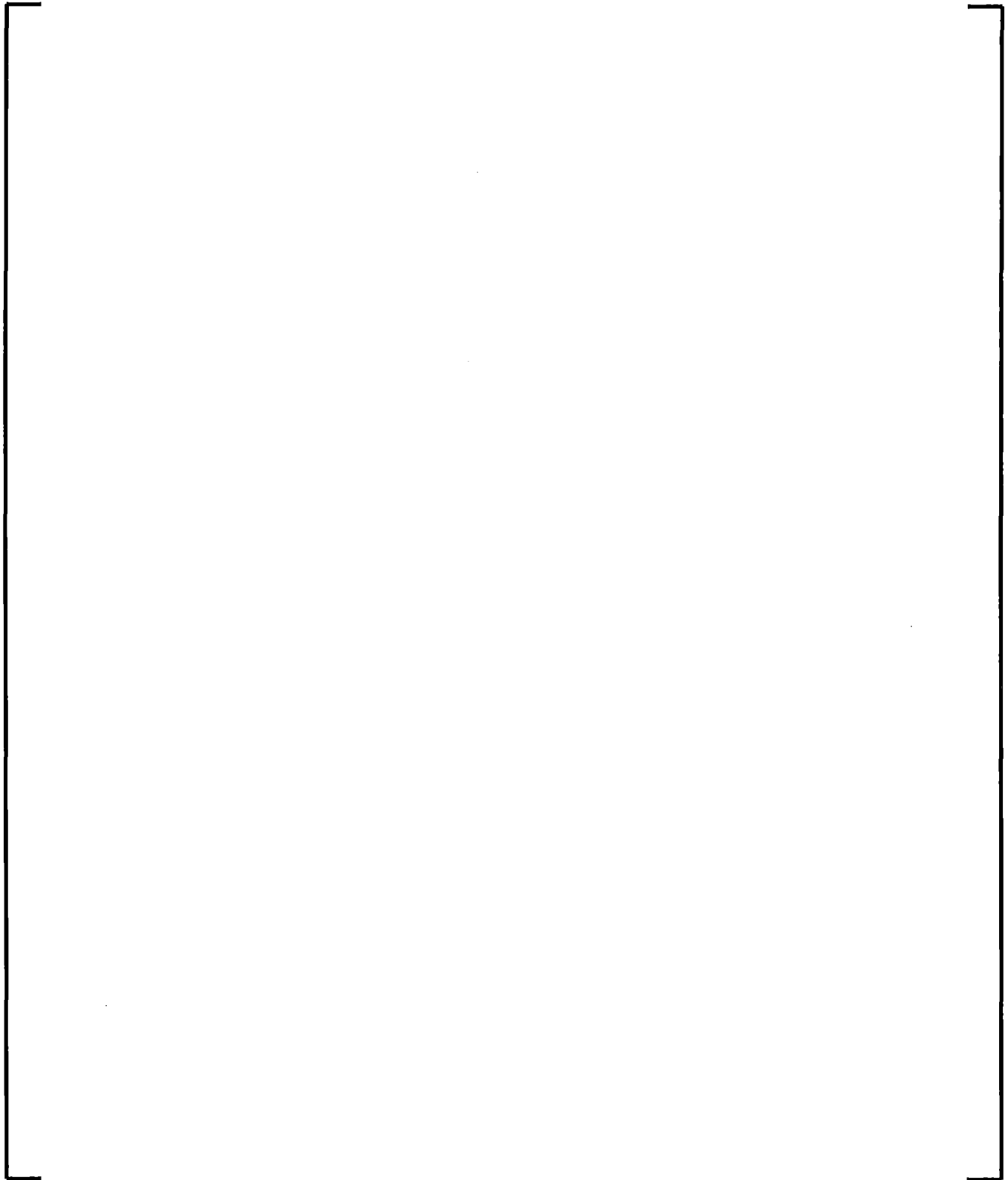
5.2.6 Pellet-Clad Gap Heat Transfer Coefficient











5.2.7 Radial Power Deposition Distributions in Fuel Pellets

5.3 *Thermal-hydraulic Model*

The RAMONA5-FA ATWS-I thermal-hydraulics model is a [] equation, non-homogeneous, non-equilibrium, one-dimensional two-phase flow model with constitutive equations for thermodynamic state variables, as well as heat transfer and vapor generation/condensation. Thermal non-equilibrium between the phases is accounted for by allowing the liquid in a two-phase mixture to depart from saturated conditions. Similarly, [

]. A description of the hydraulics is given in this section.

The channel is divided into N nodes, which are control volumes [

]. The flow area and hydraulic diameter for each node is allowed to vary in order to account for specific bundle design features such as part-length fuel rods. The 1-D formulation

[

]

[

] These equations are written directly for control volumes which directly correspond to the as programmed model. The control volume formulation is straightforward, and there is no need to follow the customary style of first writing the partial differential equation set and applying finite differencing over the control volume as approximations.

It is important to note that a volume conservation equation is not an independent equation with physical significance like the mass, momentum, and energy equations. However, the fact that the volume of the fluid species in a node sum up to the volume of that node, is useful in arranging the information content of the physical balance equations.

5.3.1 General Description of the System Considered

The hydraulic loop is divided into nine main parts as shown in Figure 5-3, namely:

Downcomer 1
 Downcomer 2, with NDC2 parallel paths
 Lower Plenum 1
 Lower Plenum 2
 Core, with NPC parallel paths
 Core Upper Plenum
 Standpipes
 Steam Separators
 Steam Dome

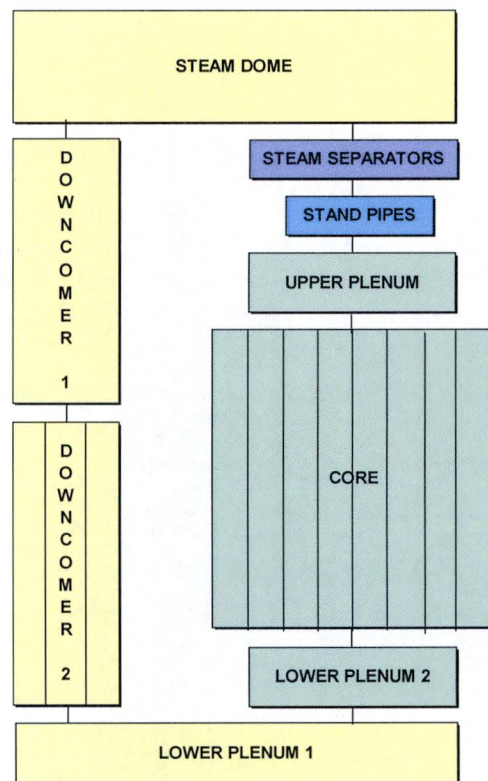


Figure 5-3: Loop Parts in the Vessel Hydraulics Model

All the loop parts are vertical except for Lower Plenum 1, which is horizontal. As indicated in Figure 5-3, Downcomer 2 is divided into NDC2 parallel paths, and the core is divided into NPC parallel channels consisting of NCC coolant channels and one moderator or bypass channel. The bypass channel accounts for the inter-channel flow as well as the internal water structures in the assemblies.

The parallel paths of Downcomer 2 (DC2) are hydraulically coupled at the Downcomer 1 (DC1) and at the Lower Plenum 1 (LP1). The core channels are also hydraulically coupled at the Lower Plenum 2 (LP2) and core Upper Plenum (UP). The Upper Plenum

(UP), Standpipes (SP), and Steam Separators (SS) can be modeled separately or lumped into one volume (riser component).

[

]

The position of the feedwater inlet is limited to Downcomer 1 (DC1) and the pump may be anywhere in Downcomer 1 or Downcomer 2 (DC2). Systems with multiple pumps can be explicitly modeled.

[

]

Power is supplied to the loop in two different ways:

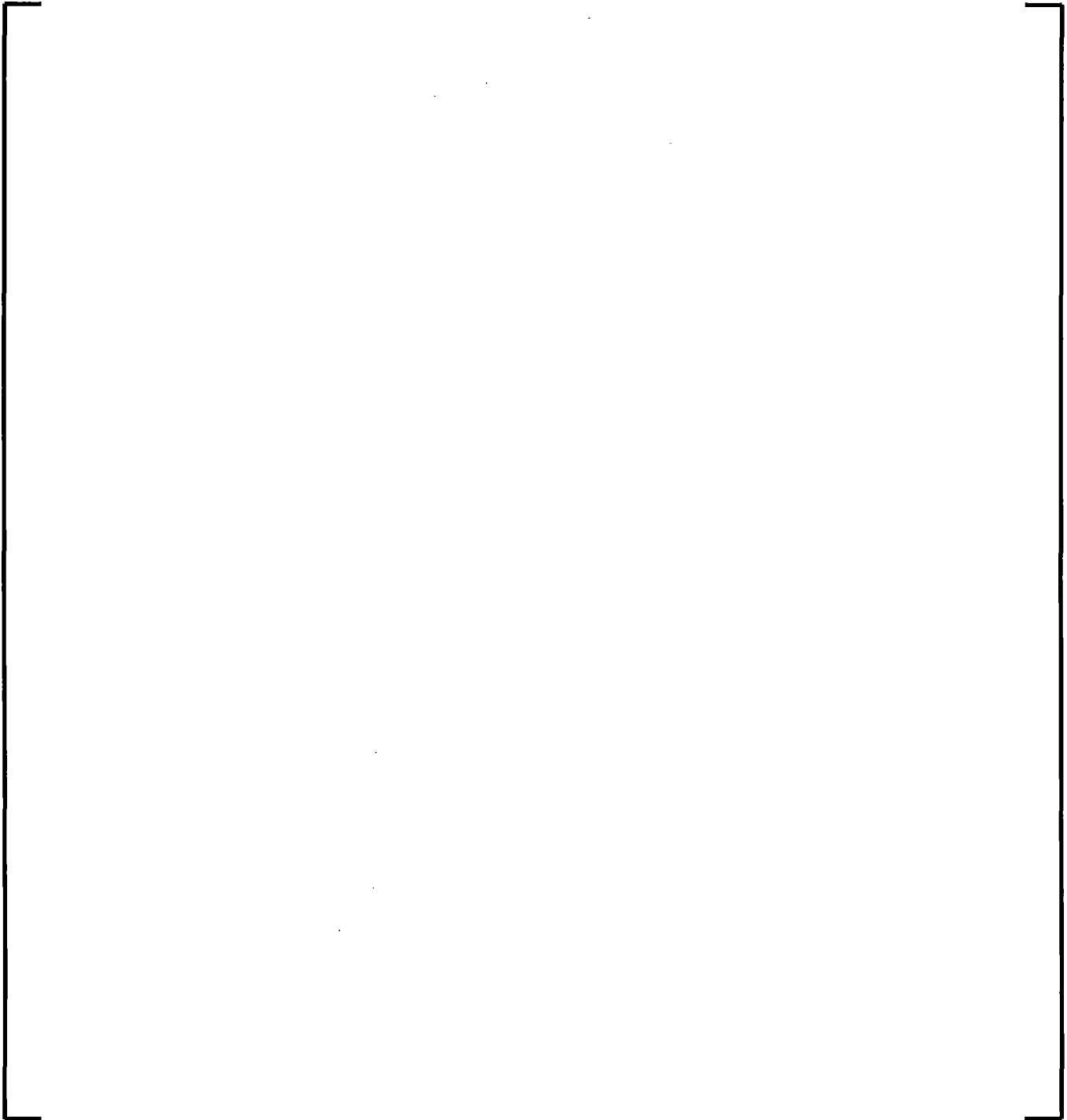
- Heat transfer from the surfaces of the fuel rods to the coolant (see Section 5.2.1)
- A fraction of the nuclear power is directly generated in the coolant and moderator (see Section 5.1.5 above)

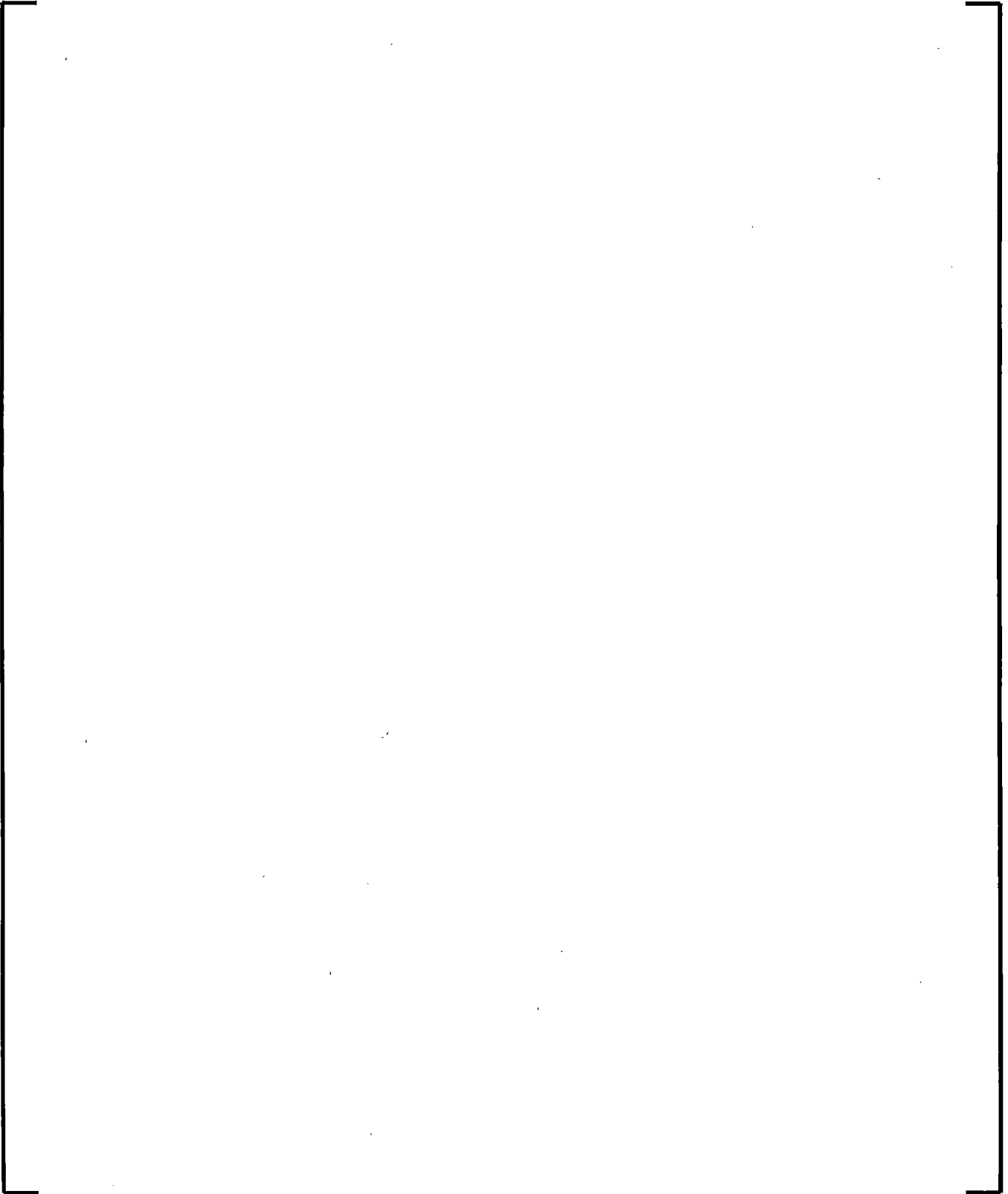
5.3.2

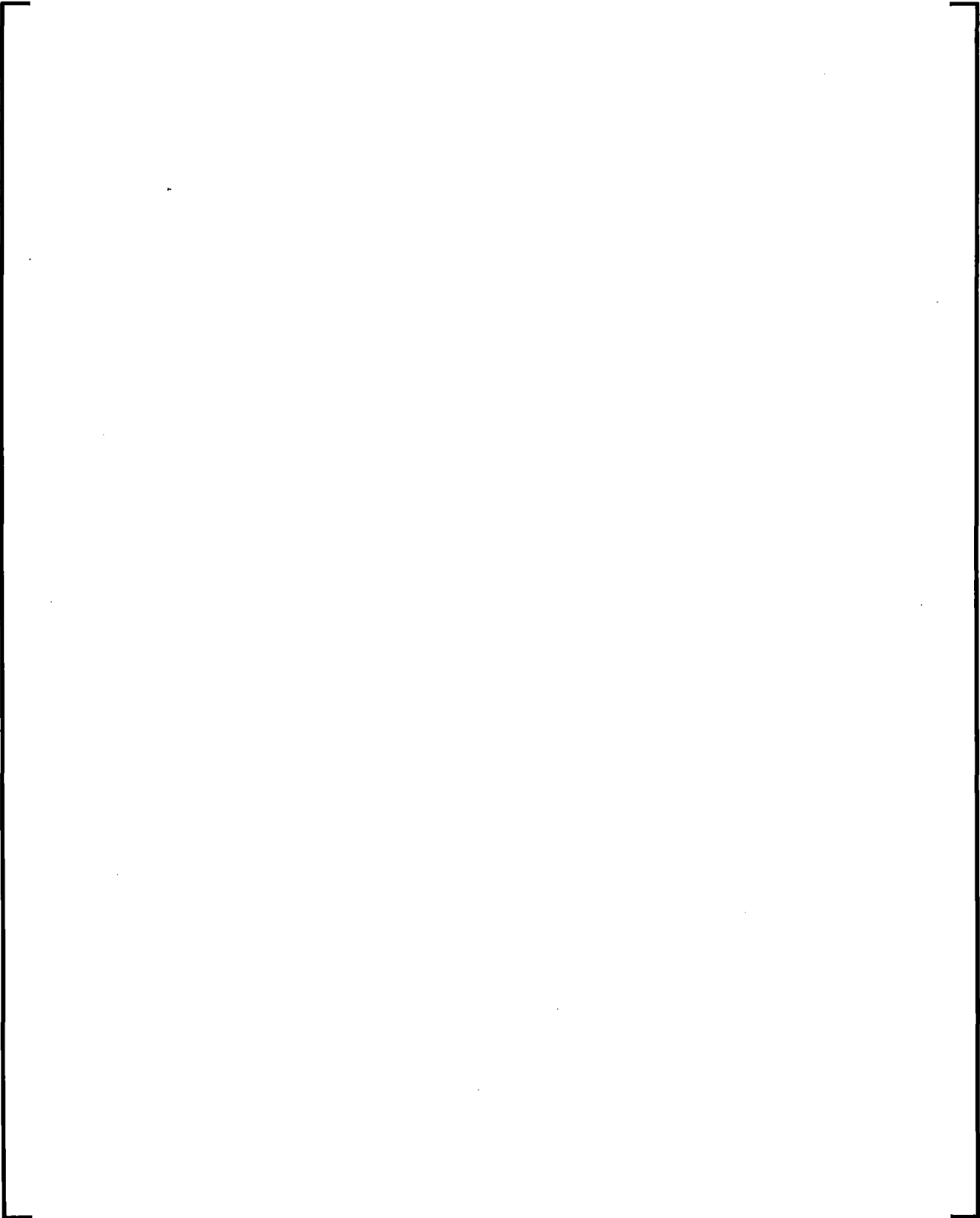
[

]

1







[

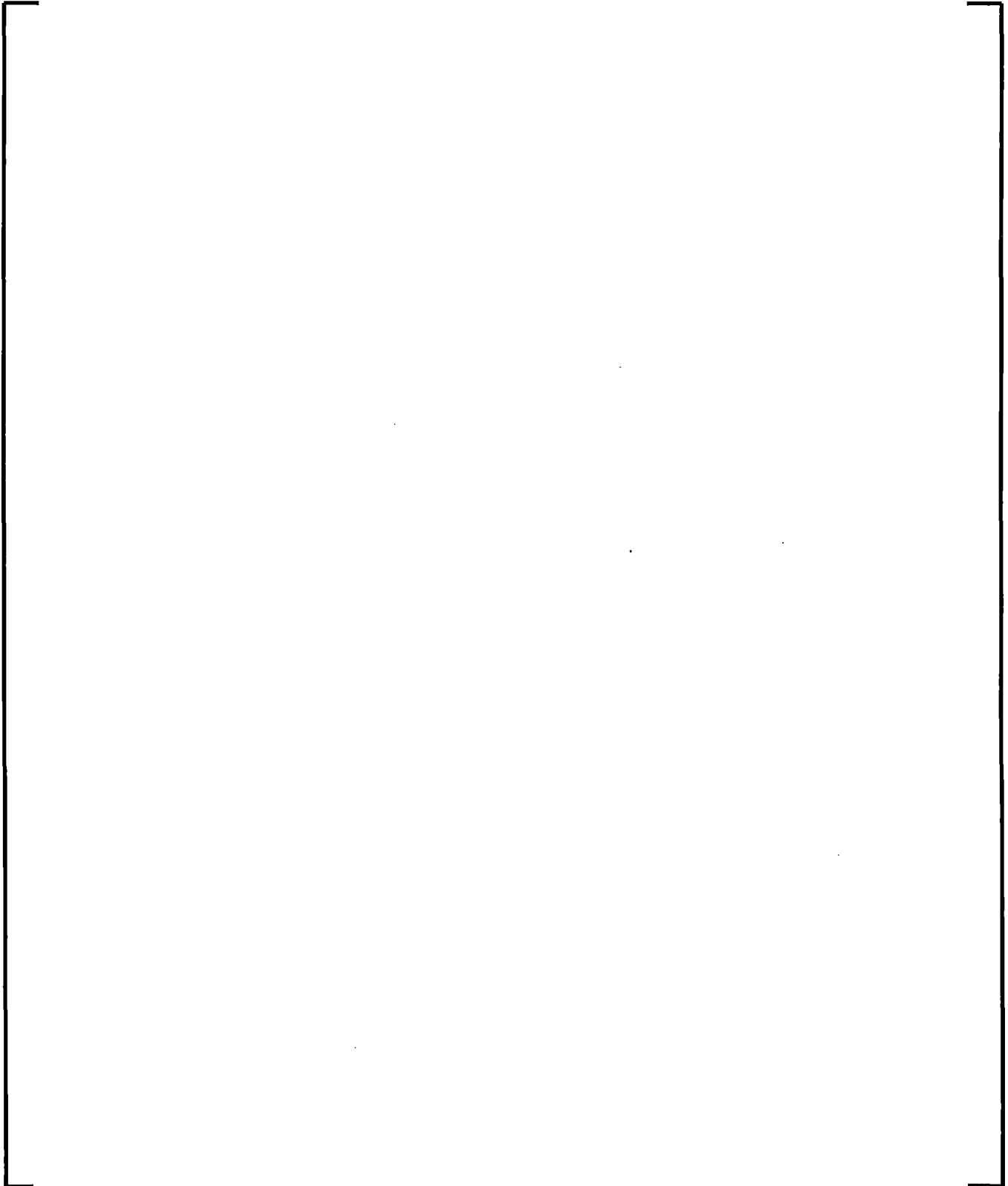
]

5.3.3 Vapor generation rate

The vapor generation rate is modeled [

1





5.3.4 Mass conservation

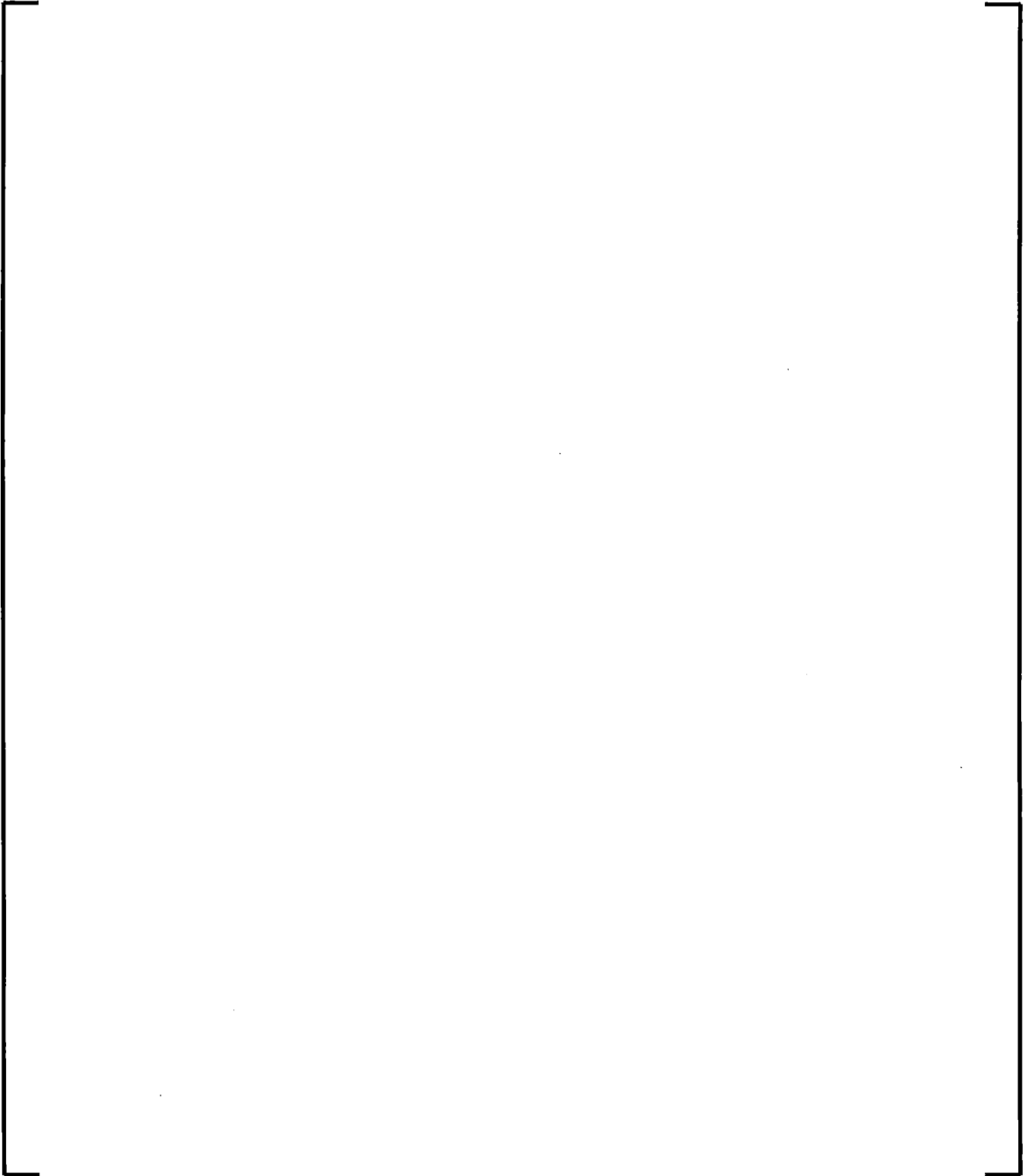
The mass conservation equation is solved for the liquid and vapor phases. [

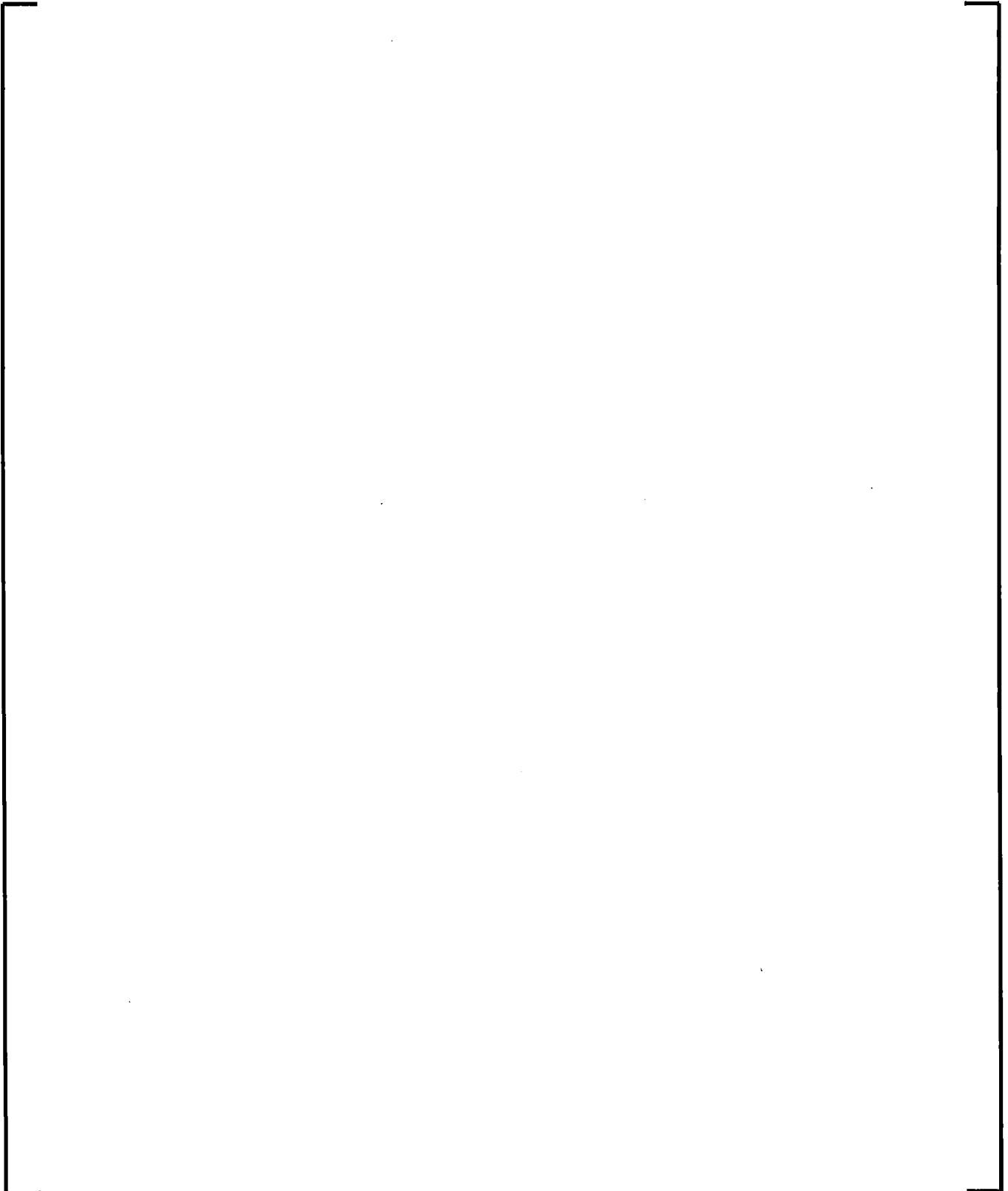
]

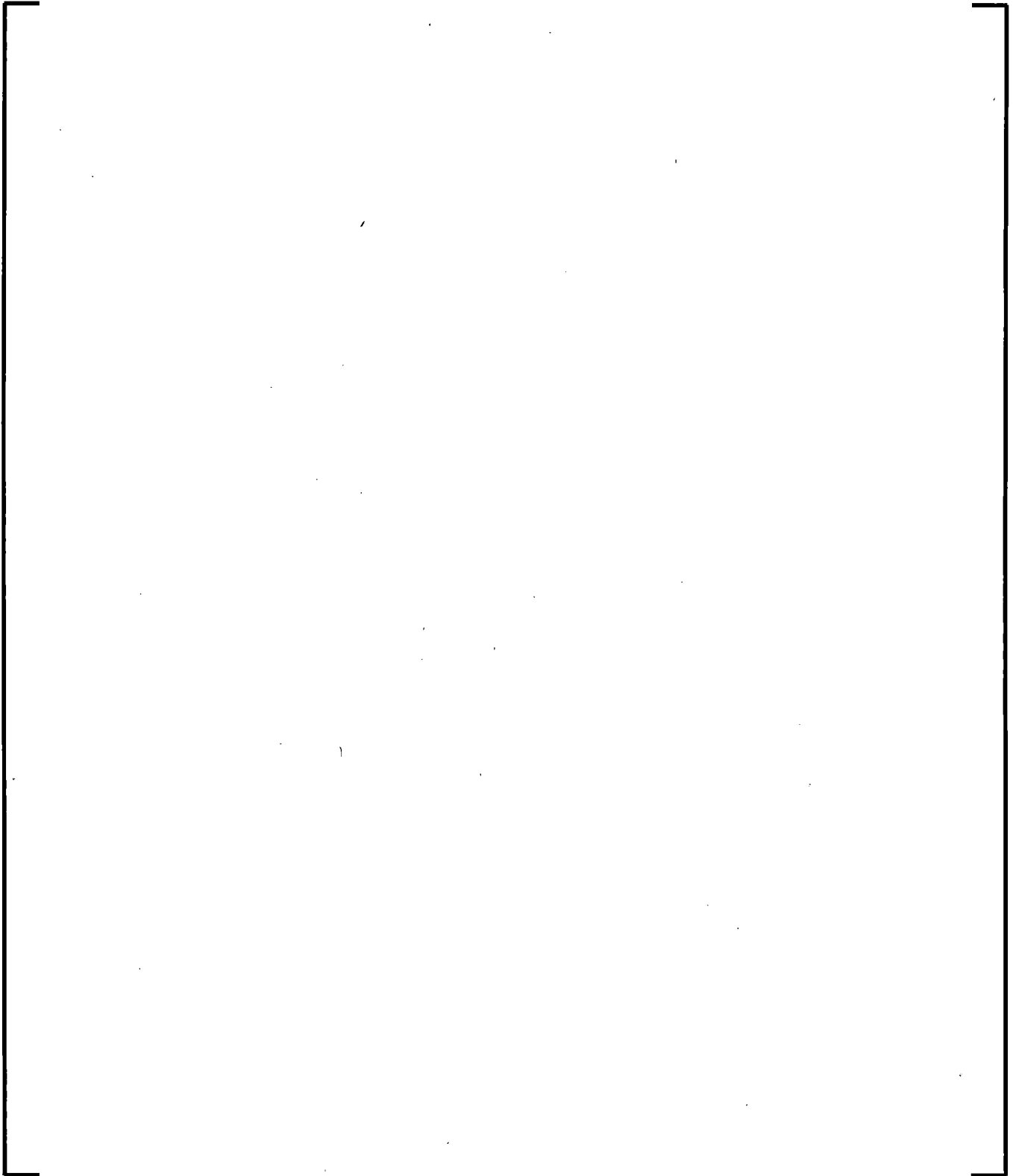
5.3.5 Energy Conservation

Energy conservation, in the ATWS-I formulation, requires solving [

]



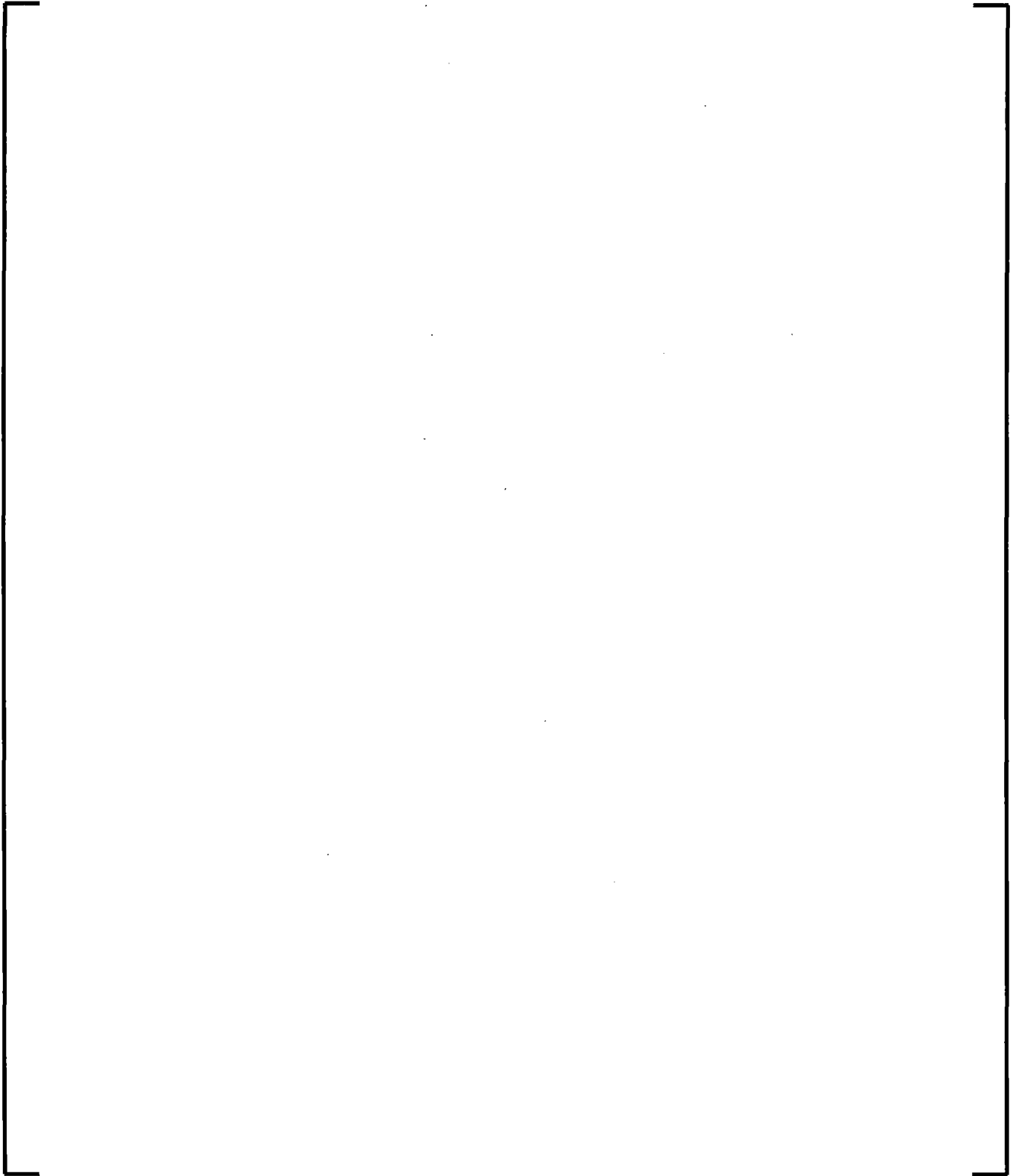




[]

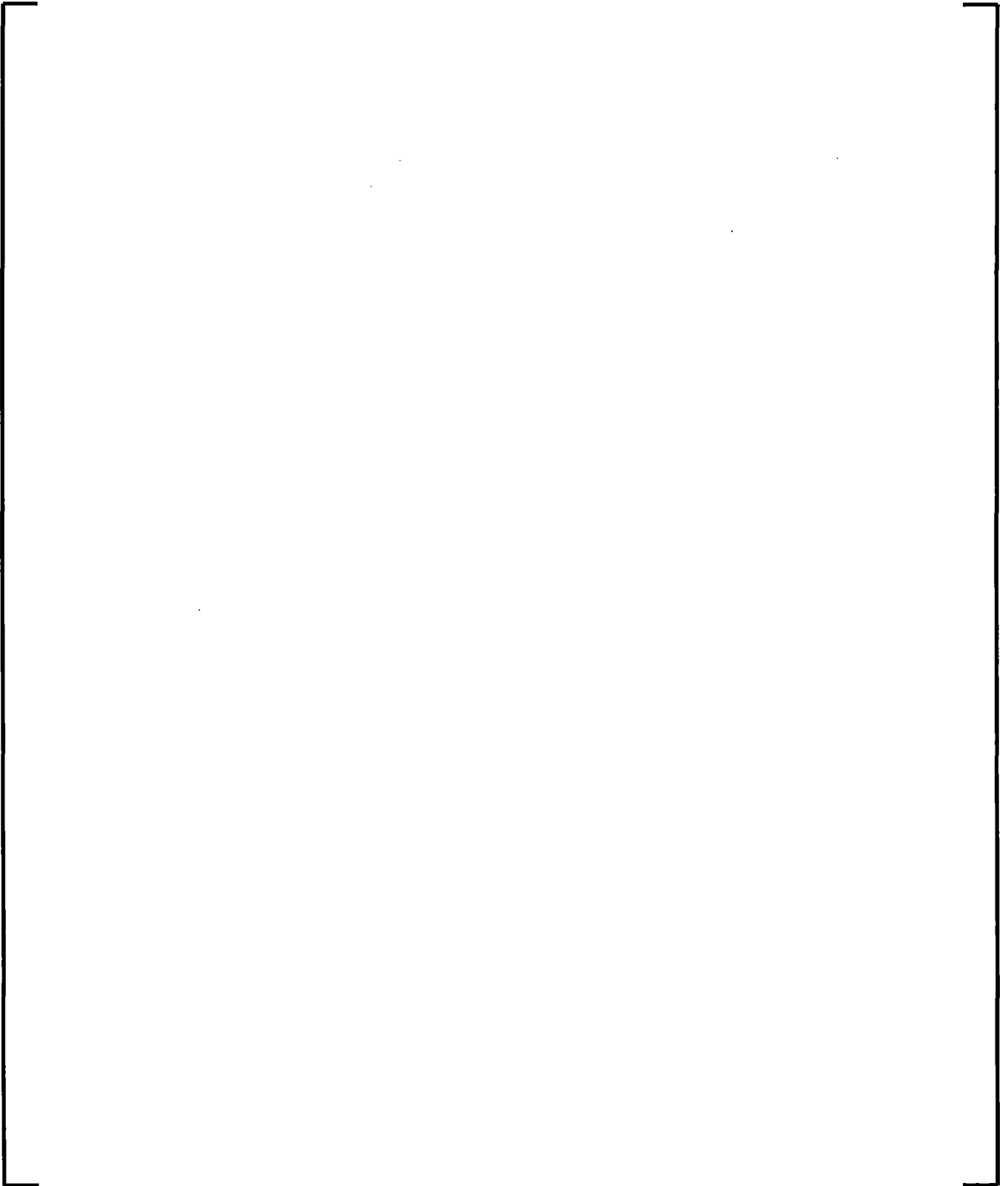
5.3.6 []

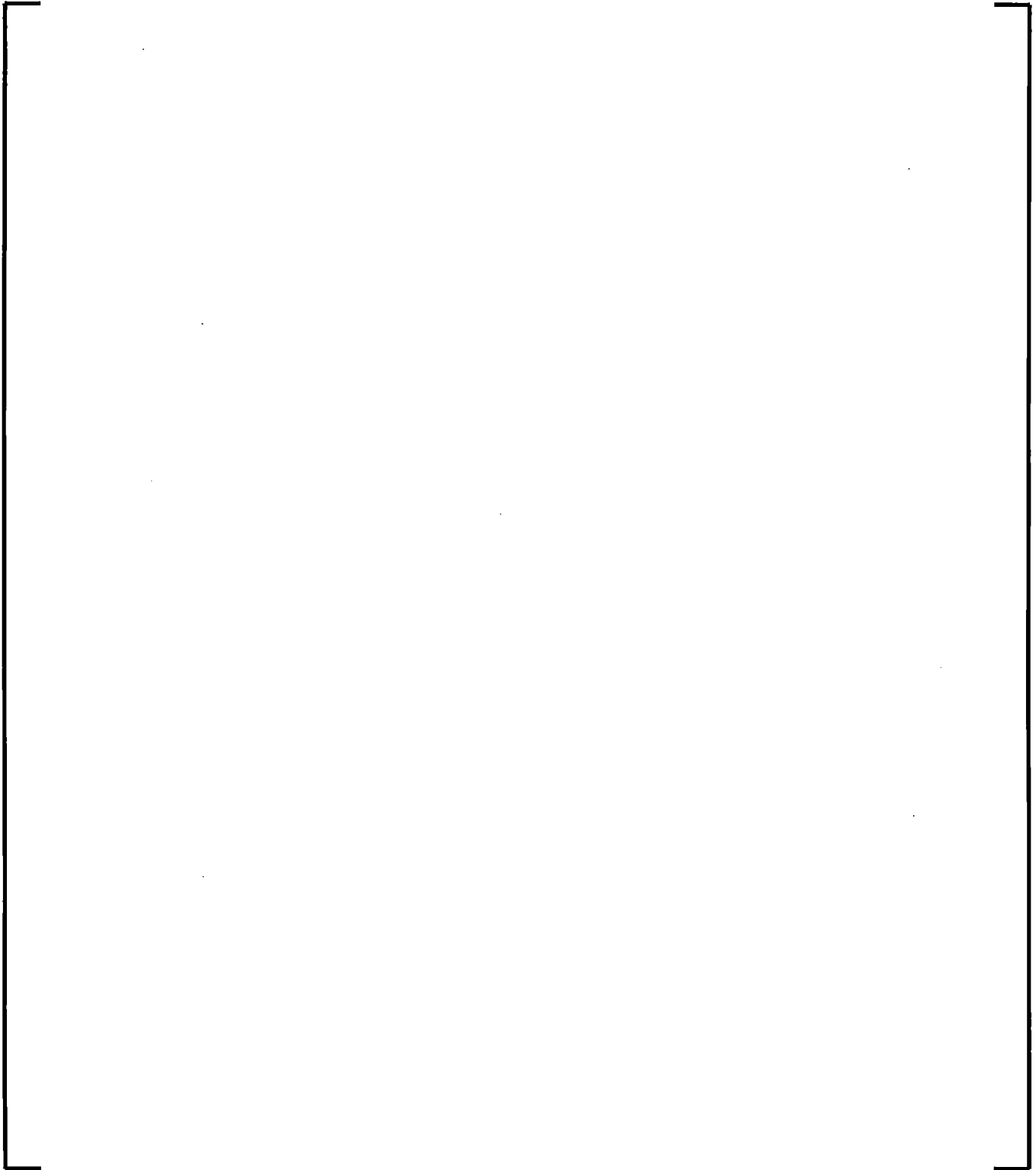
[]

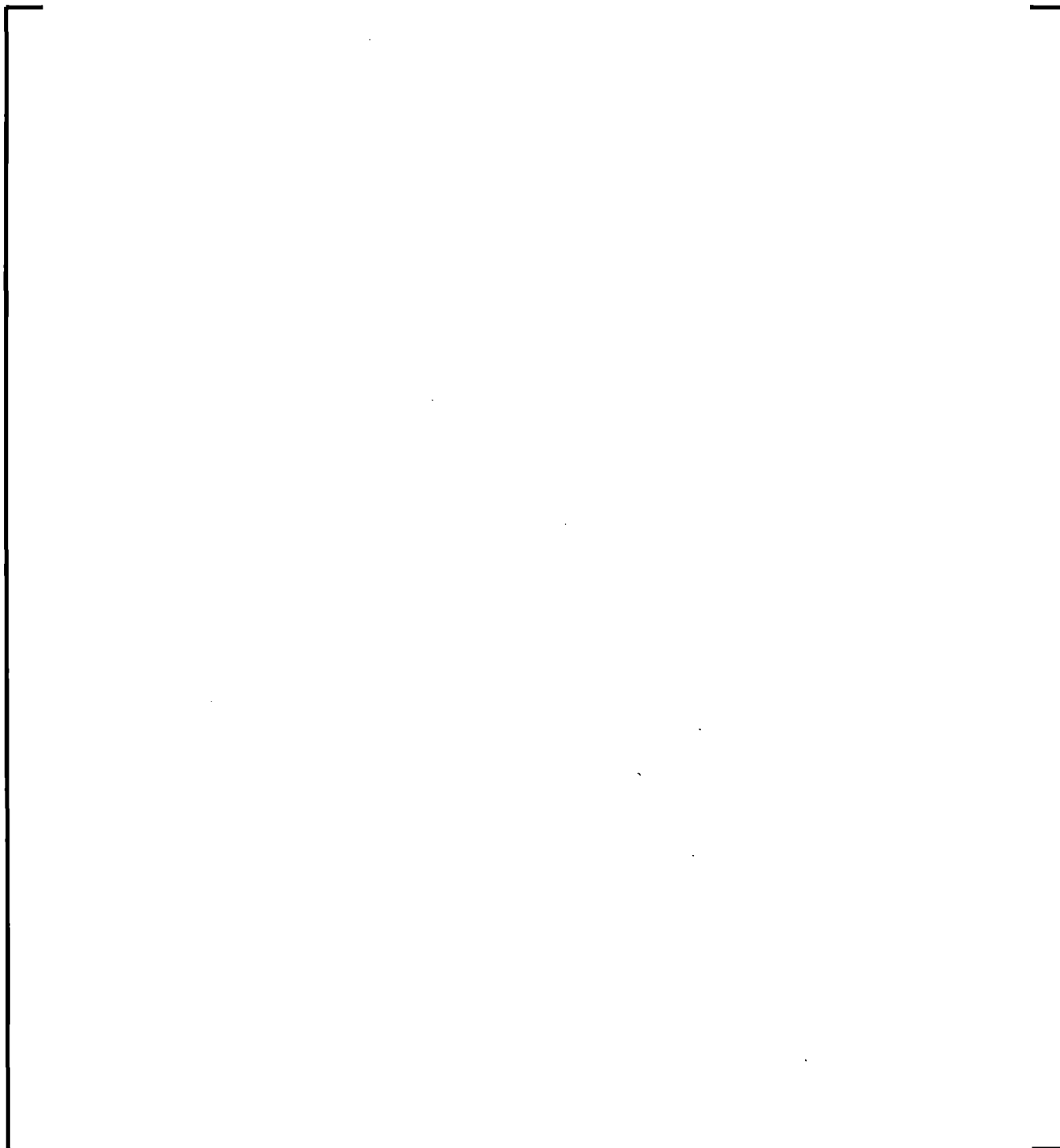


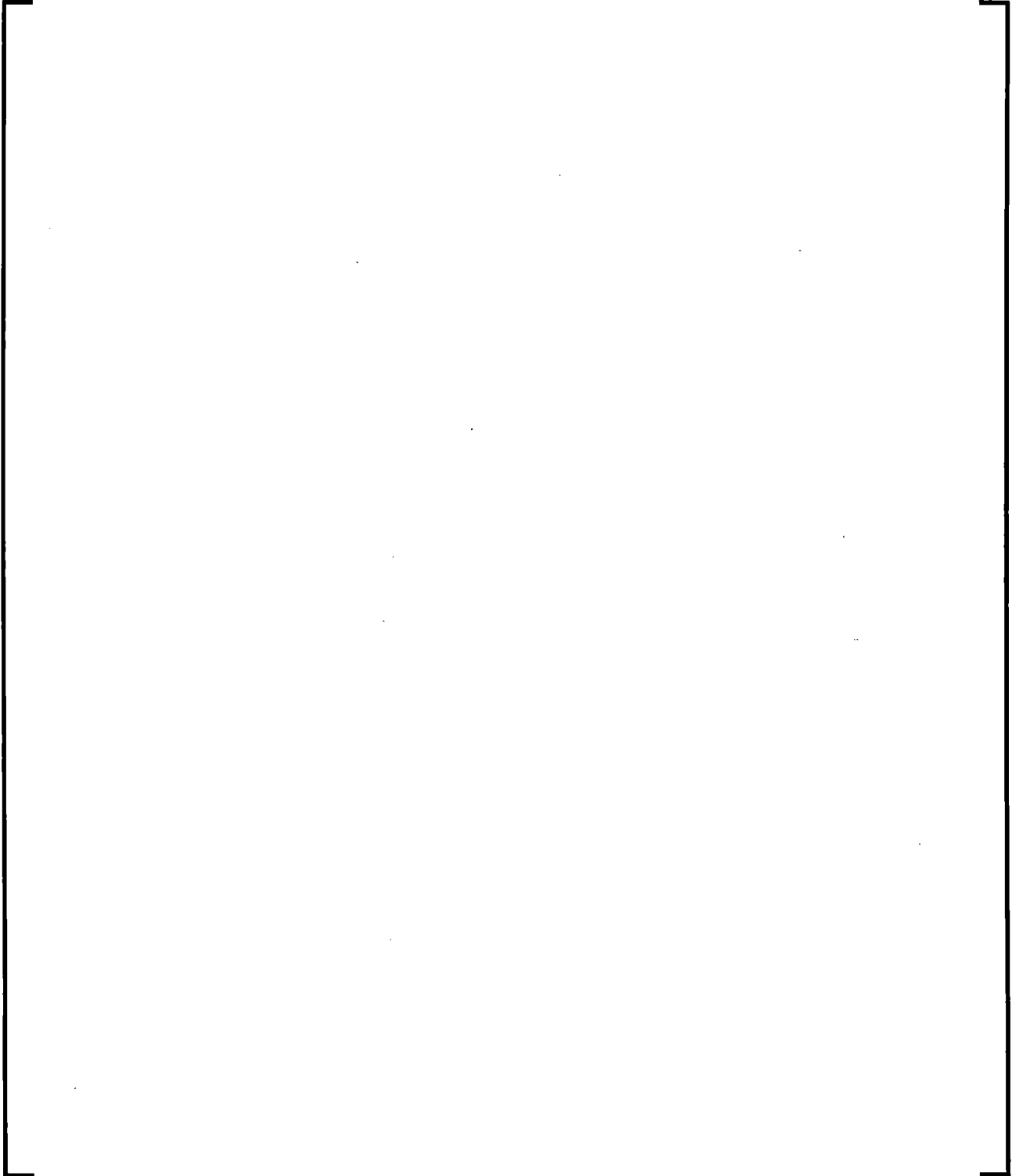
The wall surface temperature is obtained by solving the heat conduction equation for the fuel rod, which is presented in Section 5.2.4.

5.3.7 [] Momentum Conservation

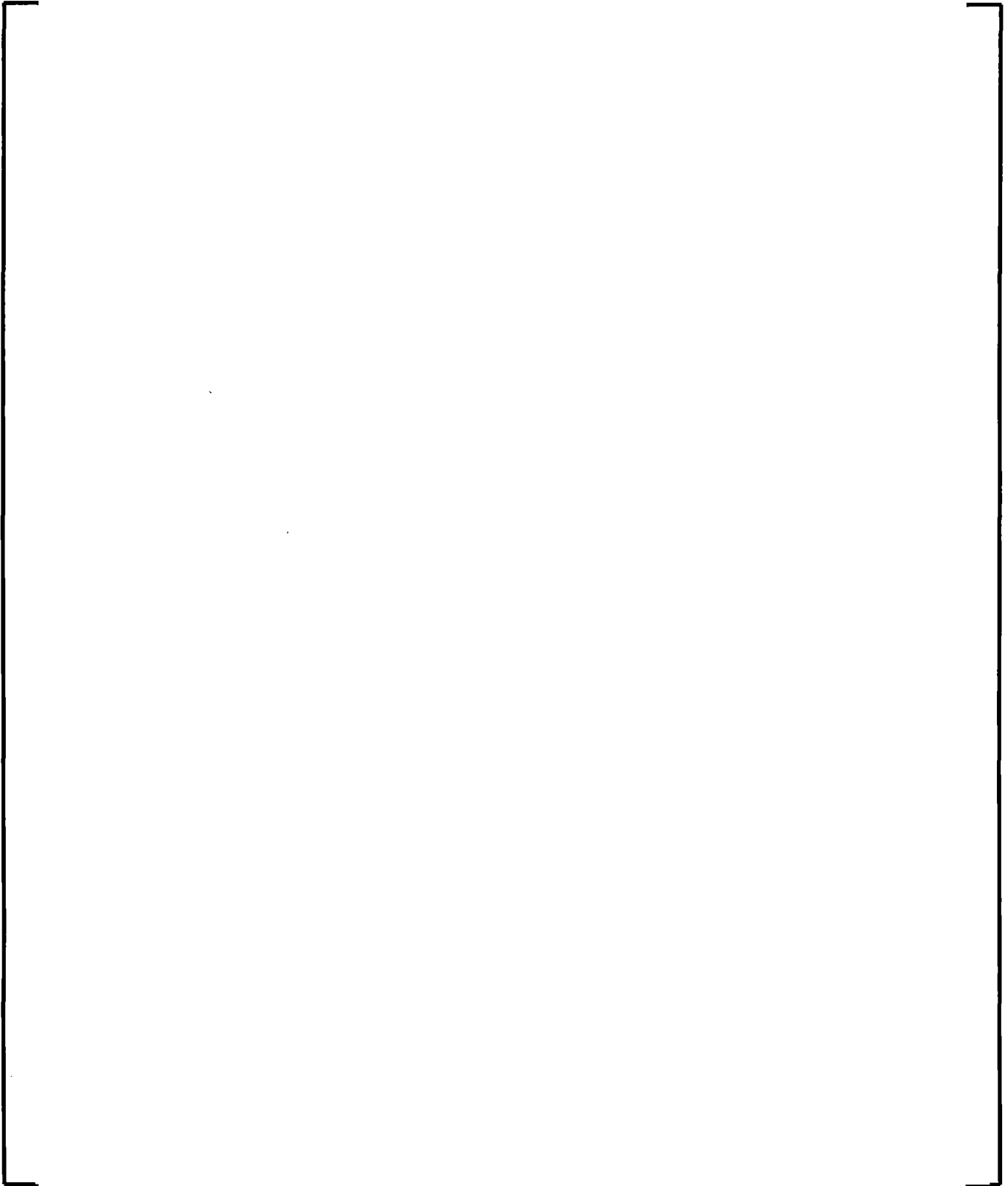




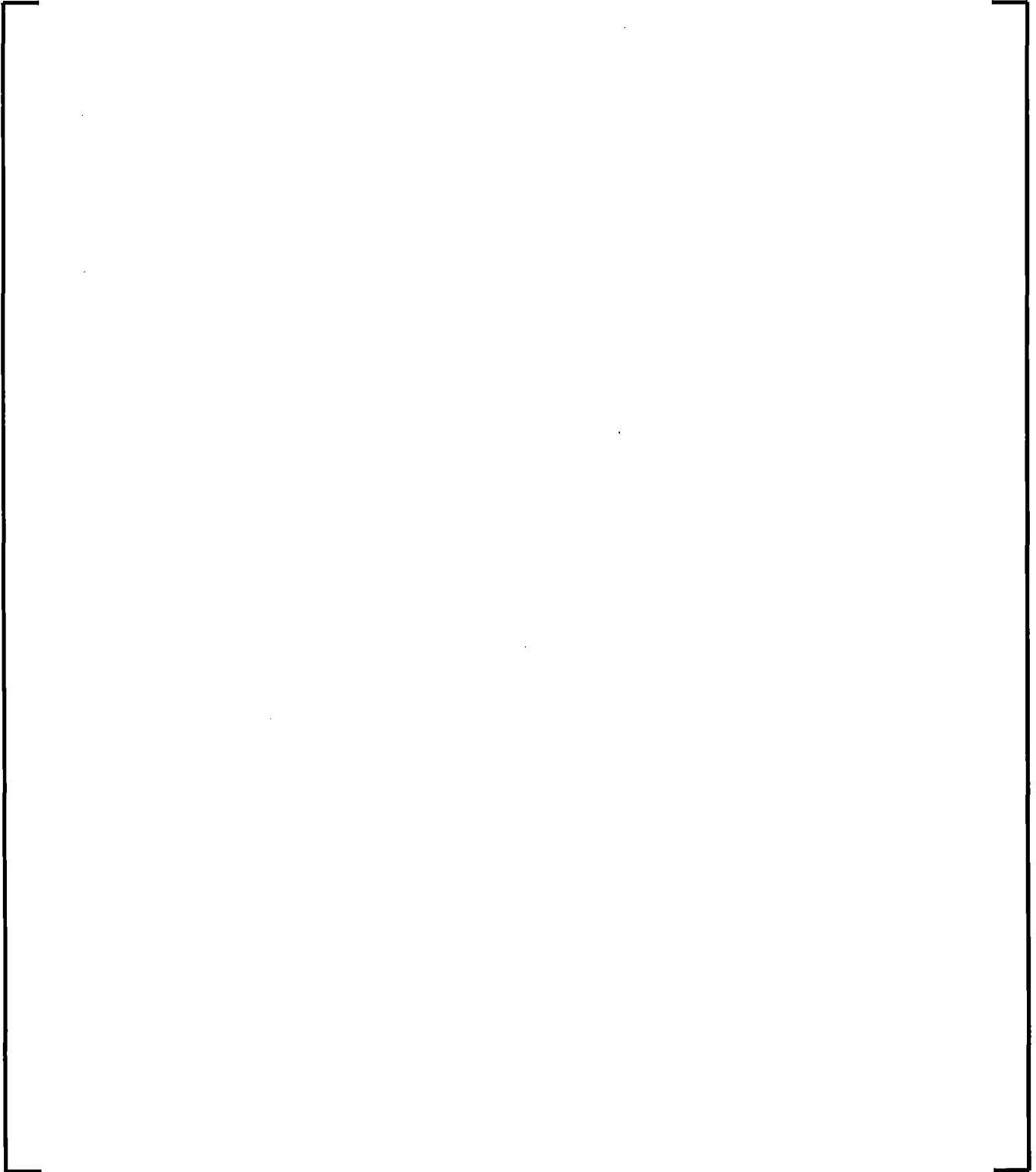




5.3.7.1 [] Formulation in the Vessel Components



5.3.7.2 [] Formulation in the Core



[

]

5.3.8 Pressure Calculation

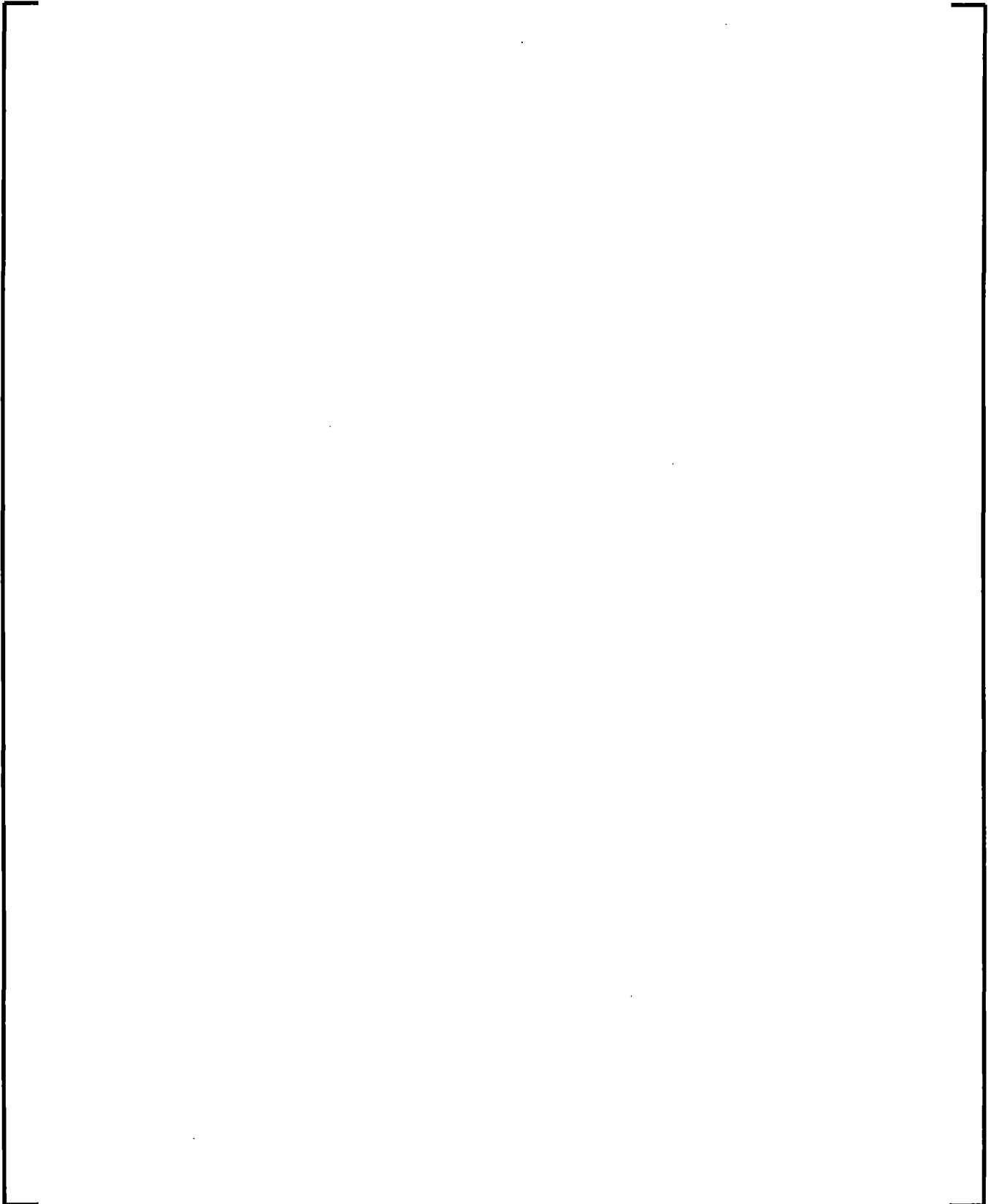
[

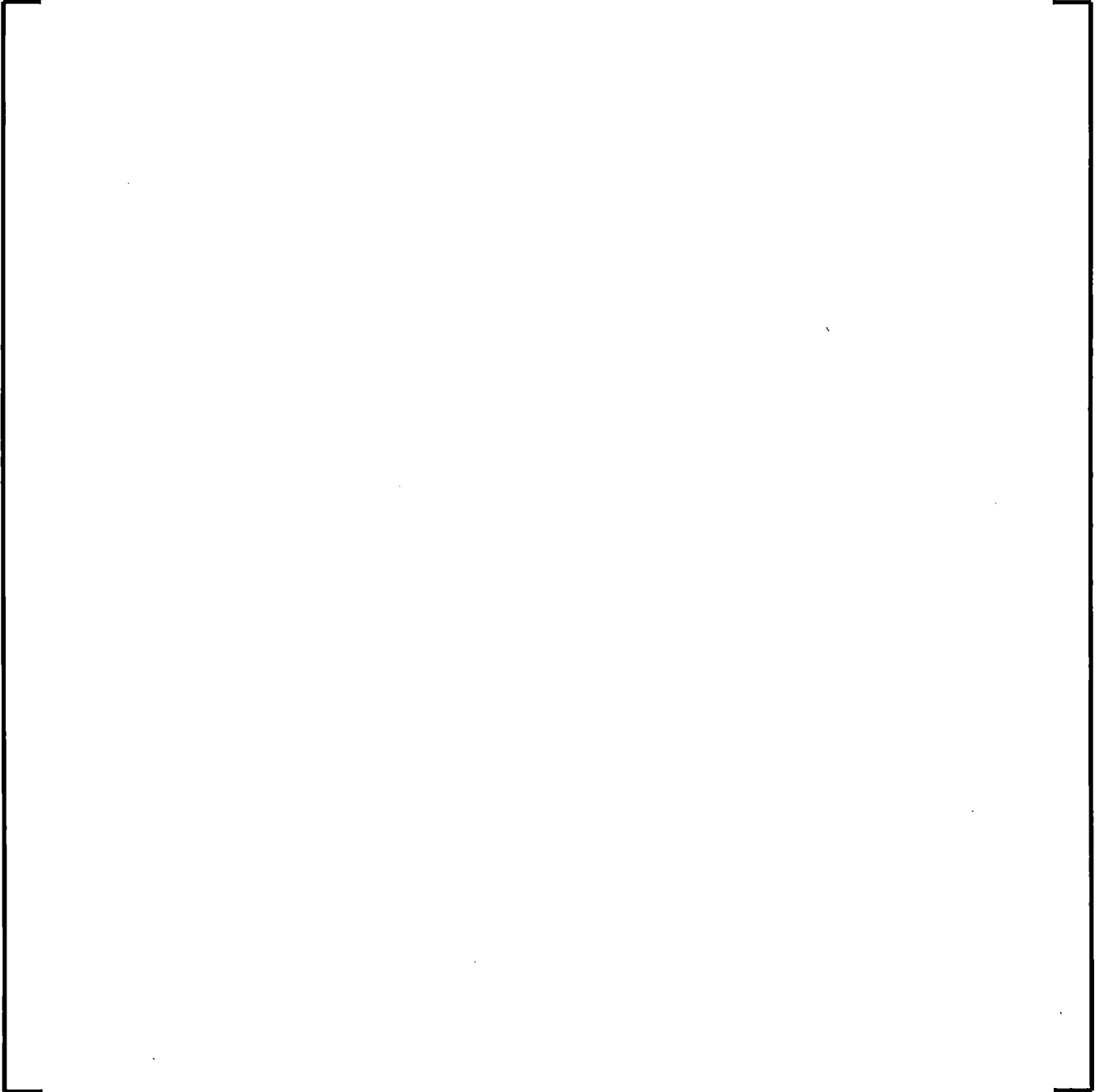
] The equations describing the transient pressure calculation are presented in this section.

The mass balance equations for the vapor and liquid phases respectively are

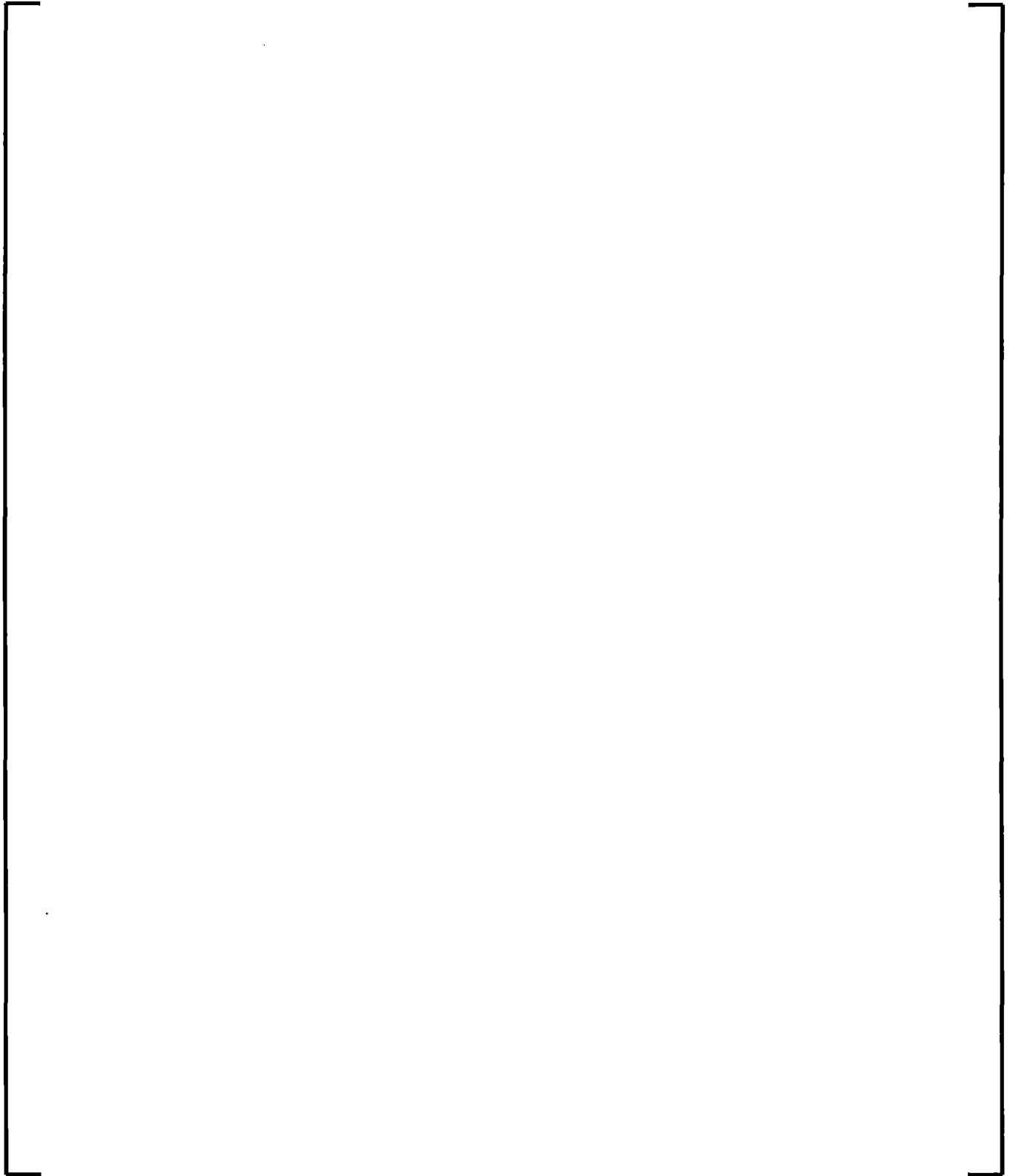
[

]





5.3.9 Steam Dome Equations



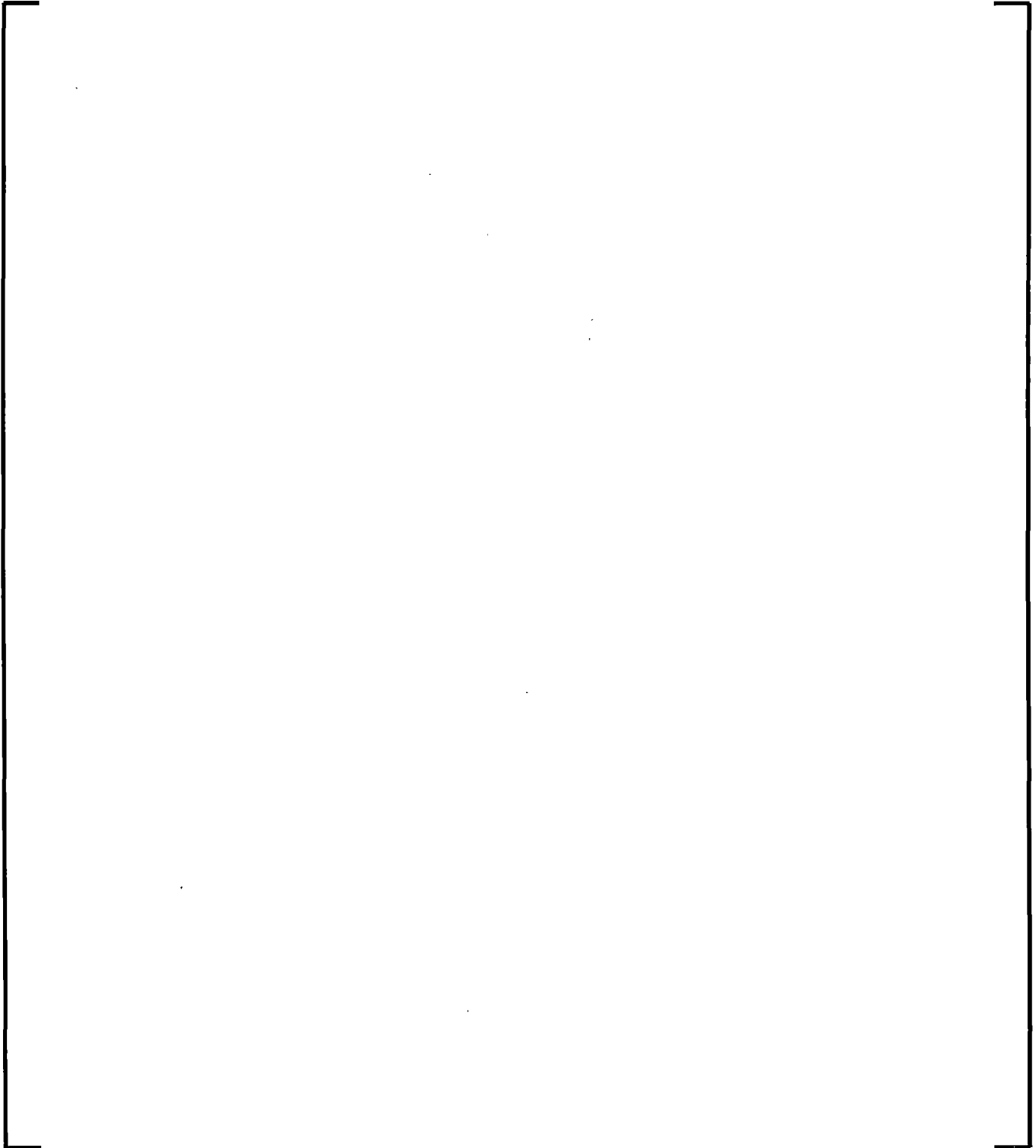
5.3.10 Recirculation Flow

The recirculation flow calculation is based on [

]



Figure 5-4: Recirculation Loop



5.3.11 Constitutive Equations

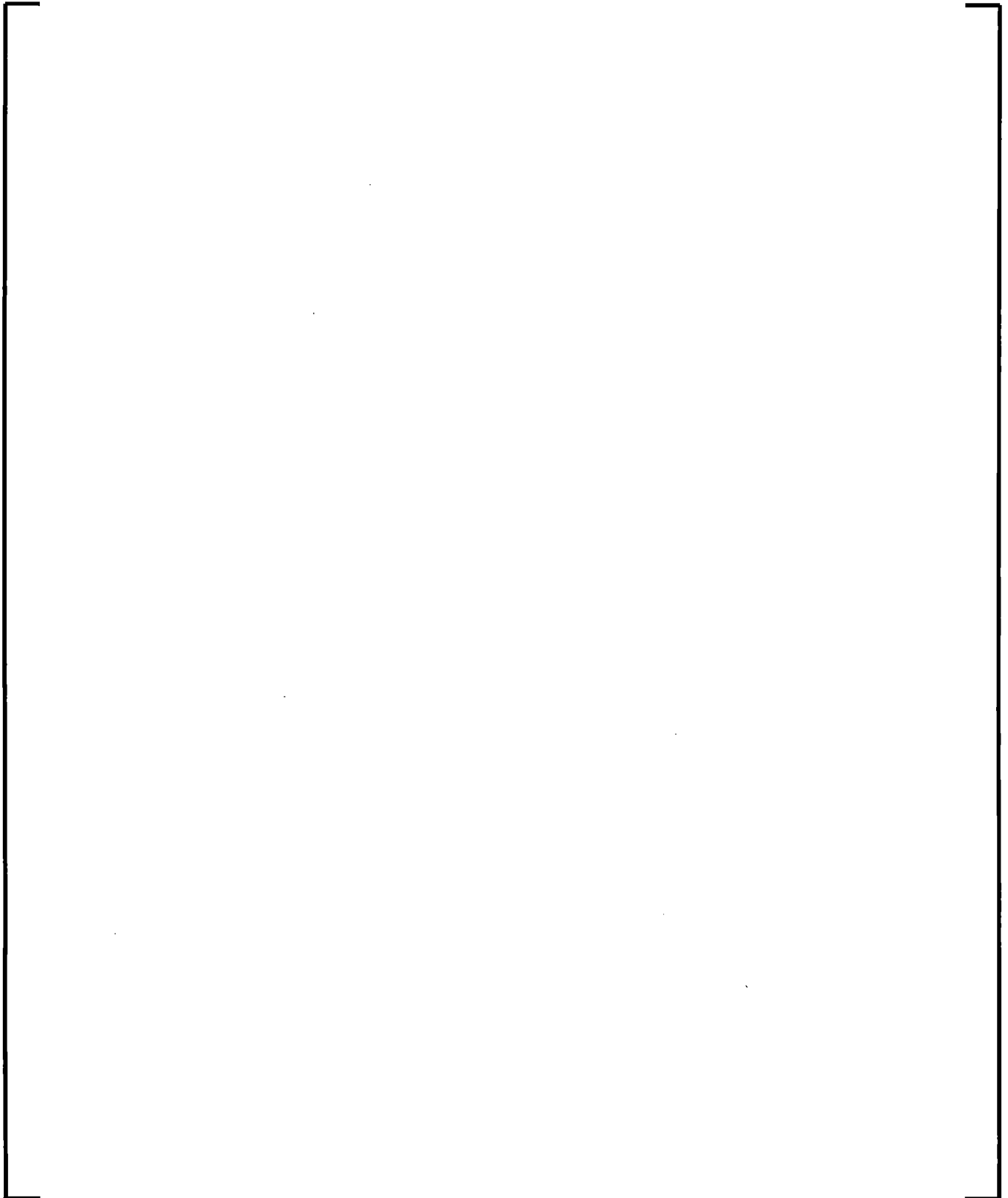
The most important constitutive equations used in the standard thermal-hydraulics are

- Friction and two phase friction multiplier
- Local pressure loss models
- Abrupt contraction/expansion pressure change models
- []
- Thermodynamic steam-water properties
- []
- Heat transfer correlations
- Evaporation rate correlation

5.3.11.1 Friction and Two Phase Friction Multiplier

Two options are available in RAMONA5-FA to specify the single-phase friction factor.

The first option is of the form:



5.3.11.2 Local Pressure Loss Models

Local pressure loss models are available in RAMONA5-FA to predict the local pressure loss effect of spacer grids, tie plates, etc. contained in the BWR core and vessel. Local pressure losses are captured in the Δp_{loc} term of Equation (5.244).

[

]

5.3.11.3 Abrupt Contraction/Expansion Pressure Change Model

In addition to pressure losses related to loss coefficients, the local pressure drop is affected by models for treating the pressure change resulting from abrupt contractions and expansions that occur at the inlet and outlet of core component hydraulic channels.

[

]

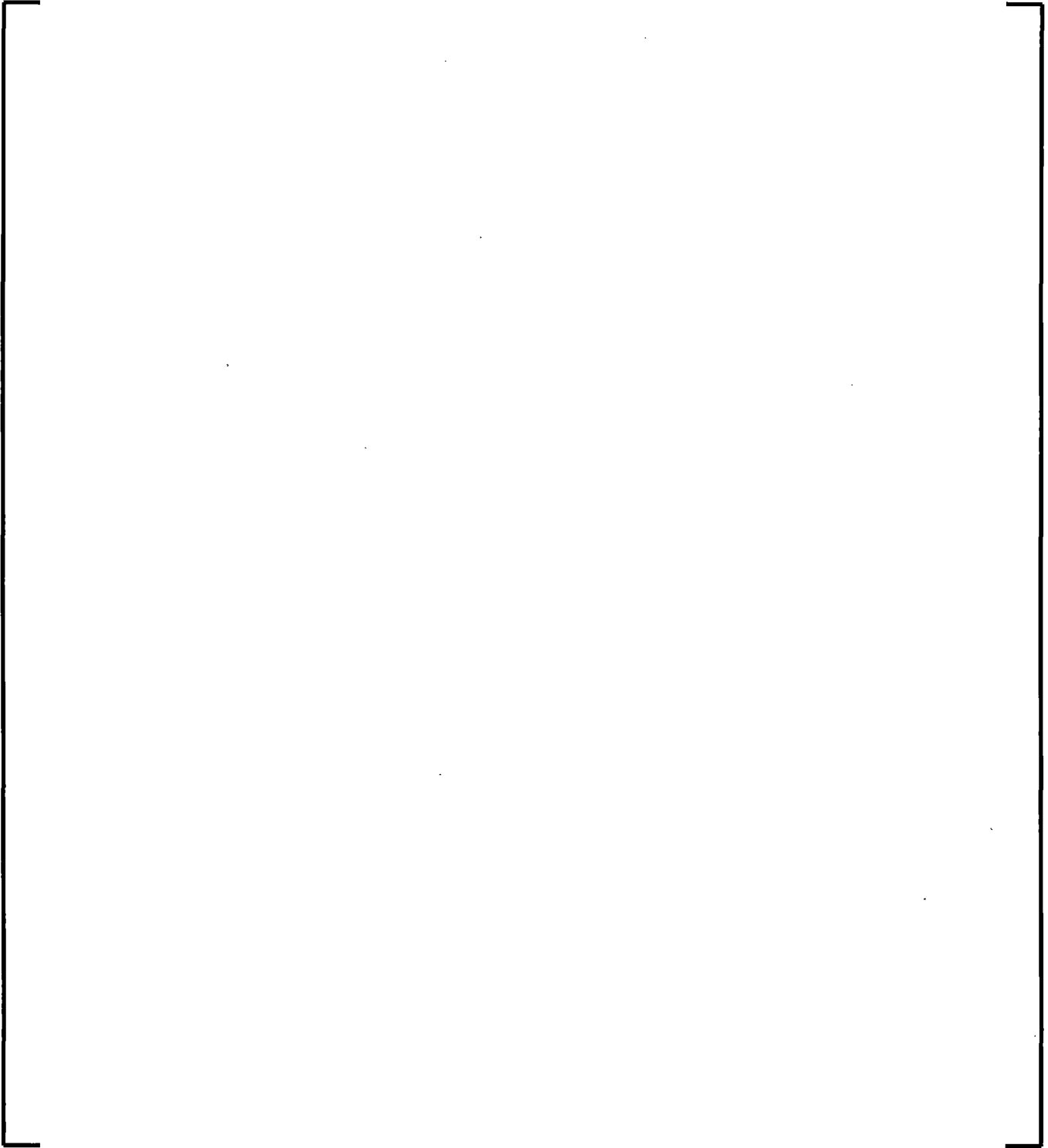
5.3.11.4 [

]

5.3.11.5 Thermodynamic Steam-Water Properties

Thermodynamic variables are determined corresponding to the system pressure and liquid or vapor enthalpy. The water properties in RAMONA5-FA utilize the new IF97 formulation [Reference 29].

5.3.11.6 []



5.3.12 Numerical Integration Techniques



Table 5-1: Summary of State Equations

5.4 *Steam Line Flow Dynamics*

RAMONA5-FA has a steam line model to make it capable of simulating acoustic effects in the steam line due to sudden valve closures or openings, leading to pressure waves traveling back and forth in the steam line. Strong pressure pulses in the steam line will in turn induce pressure pulses in the steam dome and core, thus causing a void collapse in the core and a sudden increase in reactivity.

As the time-scale of these phenomena is much shorter than the time scale of the dominating phenomena inside the reactor vessel, the need for a separate model to be able to resolve these effects is obvious.

[

]

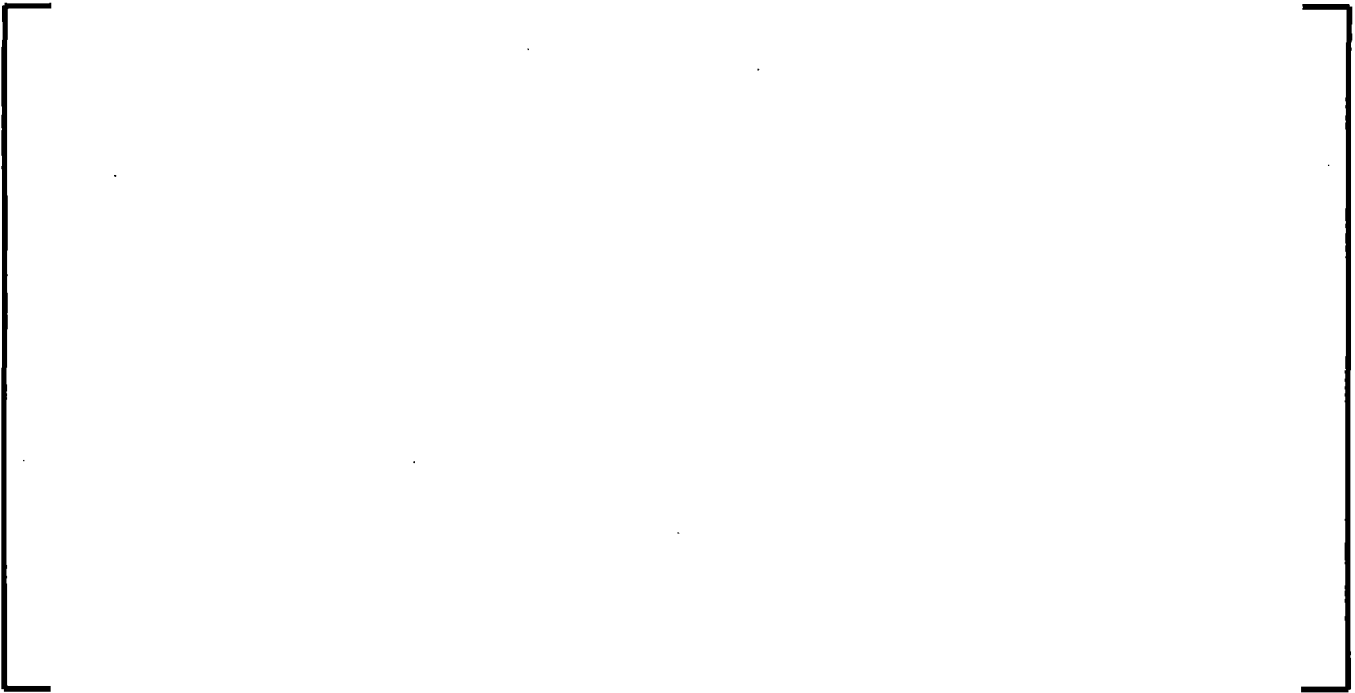
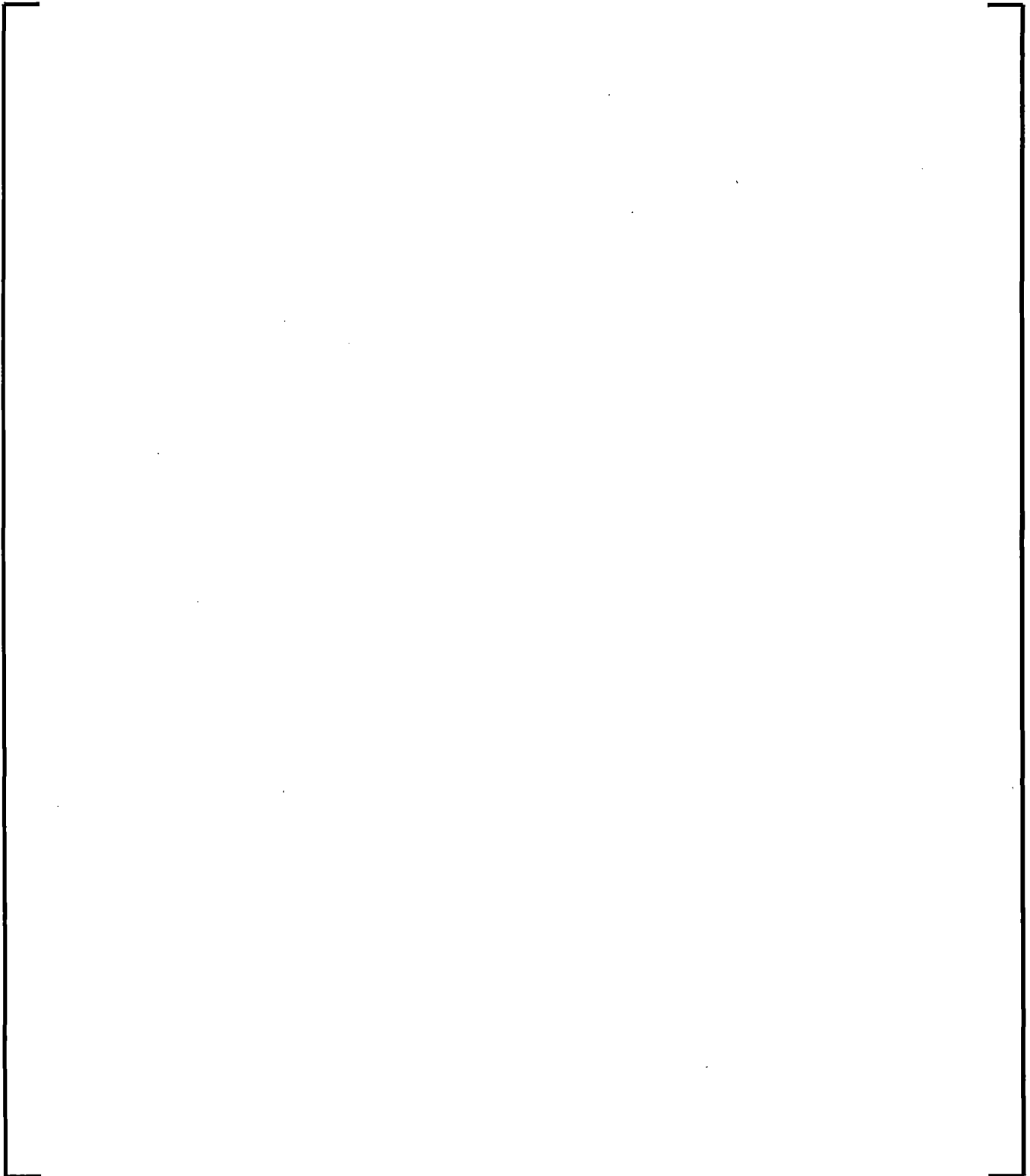


Figure 5-5: Steam Line Model





[

]

5.5 SPECIAL MODELS

Special models are included in RAMONA5-FA to simulate specific flow conditions.

They include at present:

- Recirculation flow pumps
- Jet pump model
- Feedwater sparger
- Steam separators
- Dryout/rewet model

5.5.1 Recirculation Pump Model

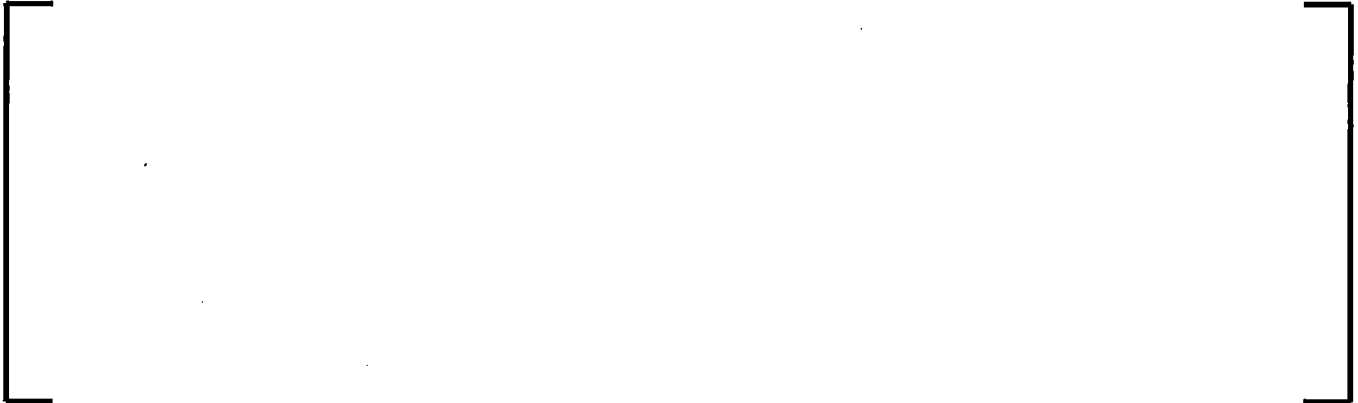
The recirculation pumps, one in each recirculation loop, drive the recirculation flow through the recirculation loops into the jet pumps or drive the core flow in the plants with internal pumps. The recirculation pumps are used to control the core flow, consequently the inlet subcooling temperature, the non-boiling heat and, thereby, the vapor void fraction, moderator density and fission power. The purpose of the recirculation pump model is to predict the pressure rise (Δp_{pump}) used in the drive force (Equation (5.242)). This pressure rise depends not only on the flow rate in the pump but also in the angular speed (N_{pump}) of the recirculation pump. The angular speed is computed from the equation of motion for the pump, the motion being governed by the balance between the electrical torque, the friction torque and the hydraulic torque.

There are three different recirculation pump types implemented in RAMONA5-FA.

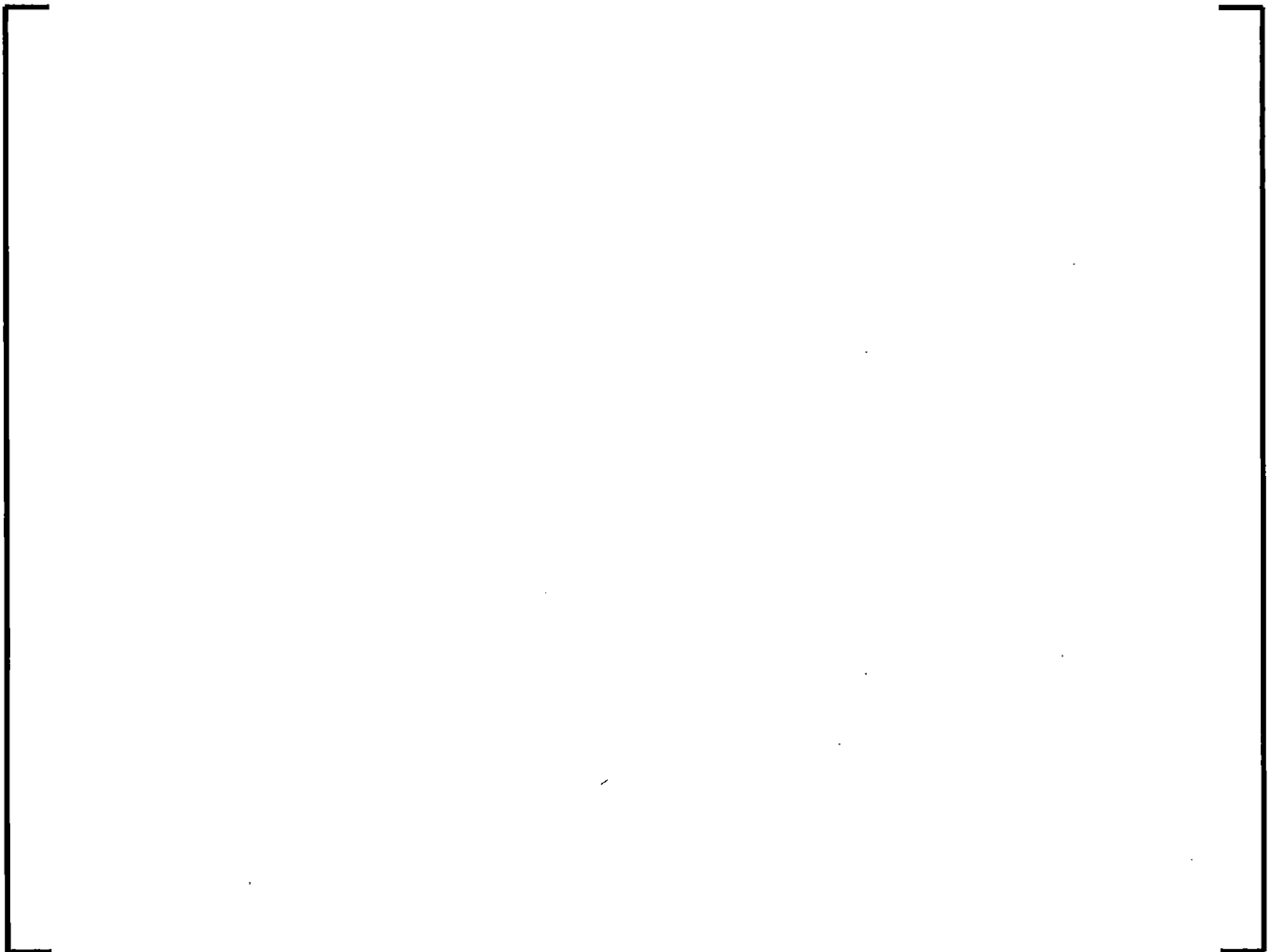
[

]

5.5.1.1 Pump Model 1



5.5.1.2 Pump Model 2



5.5.1.3 Pump Model 3

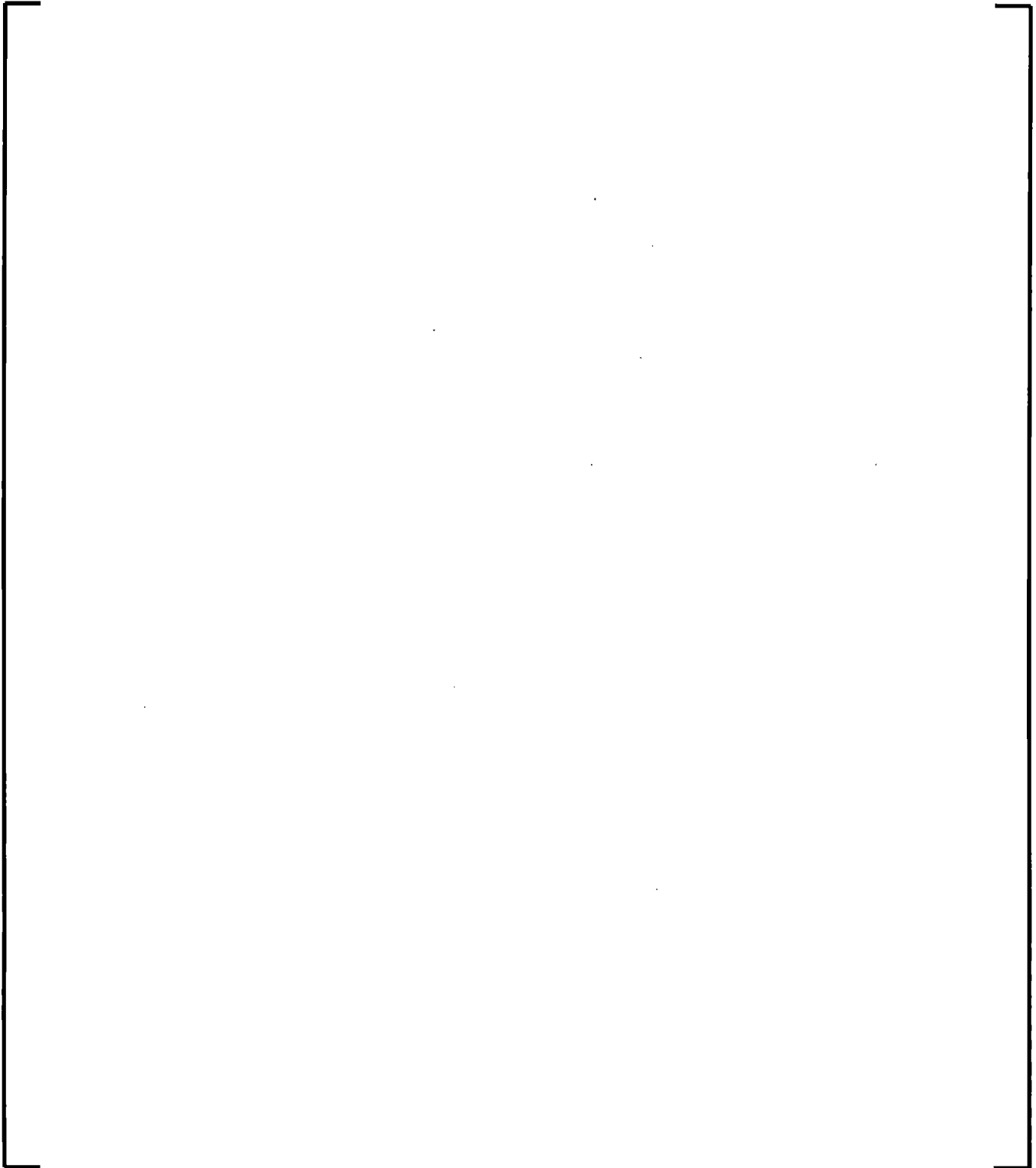
[

1

This image shows a single sheet of white paper with horizontal blue or grey ruling lines. A vertical margin line is present on the left side, creating a narrow left margin. The paper appears to be from a notebook or a standard ruled document. There are some very faint, small dark spots scattered across the surface, likely due to scanning artifacts or dust. The overall appearance is clean and professional.

The jet pump model calculates the pump head of the internal jet pumps. [

1



5.5.3 Steam Separator Model

When modeling the steam separators, there are two main effects which will be accounted for in this section:

- the flow inertia in the spiral path of the separators
- the volumetric flow of saturated vapor leaving the circulation loops and entering the steam dome above the coolant level (entrainment of vapor or carry under)

The effect of the form loss is taken into consideration in the same manner as other flow components.

5.5.3.1 Flow Inertia

5.5.3.2 Carry under Flow

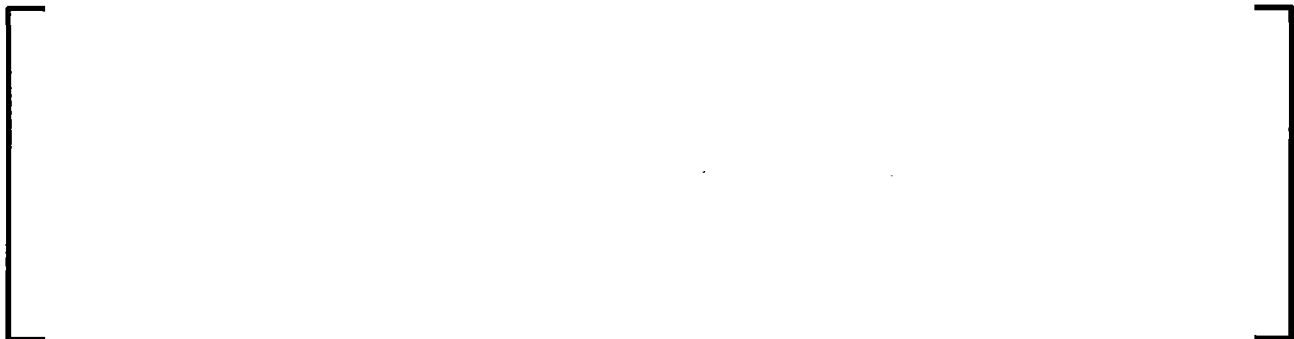
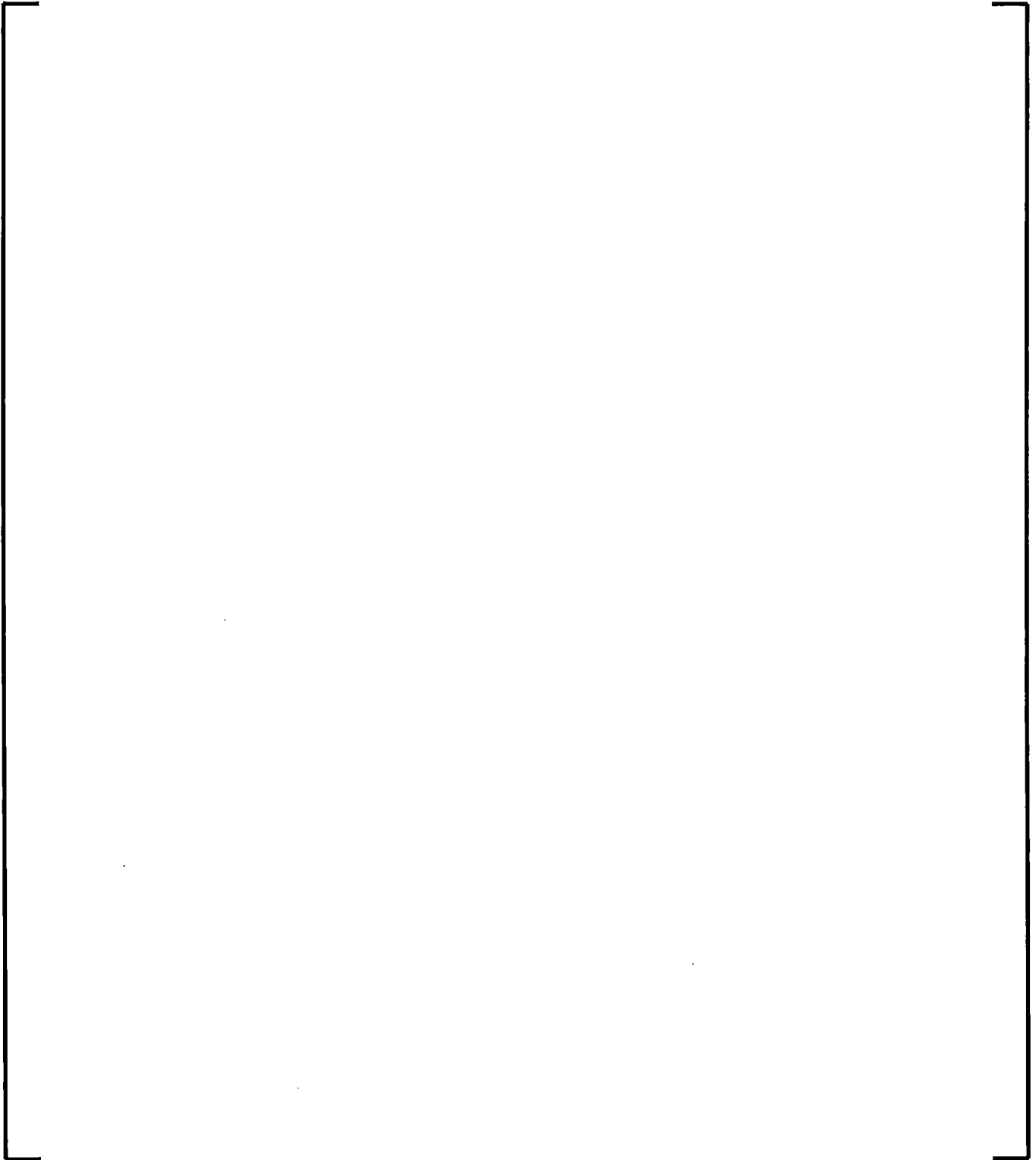




Figure 5-6: The Loop Parts of the Vessel Hydraulics



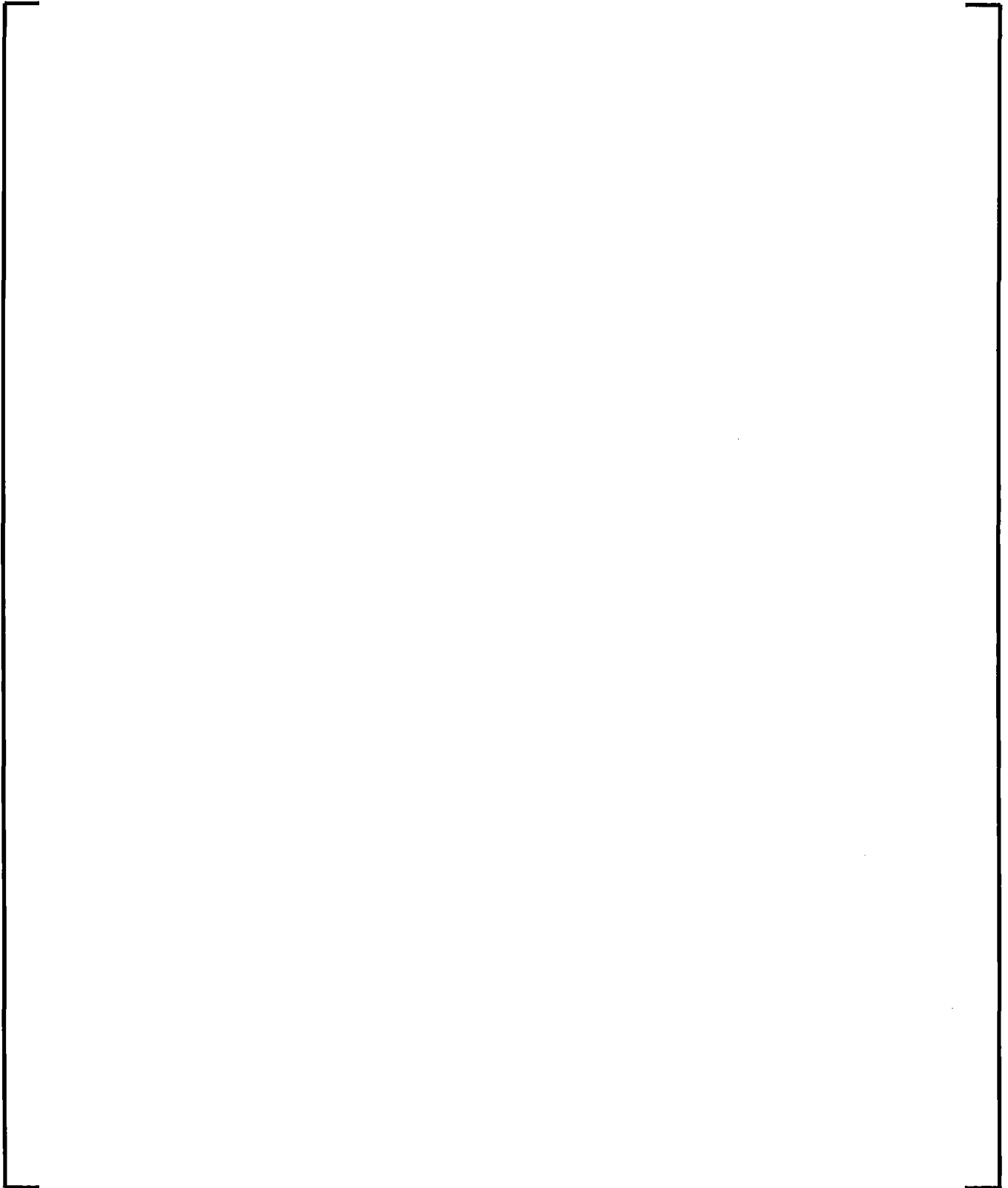
5.5.4 Feedwater Sparger Condensation Model

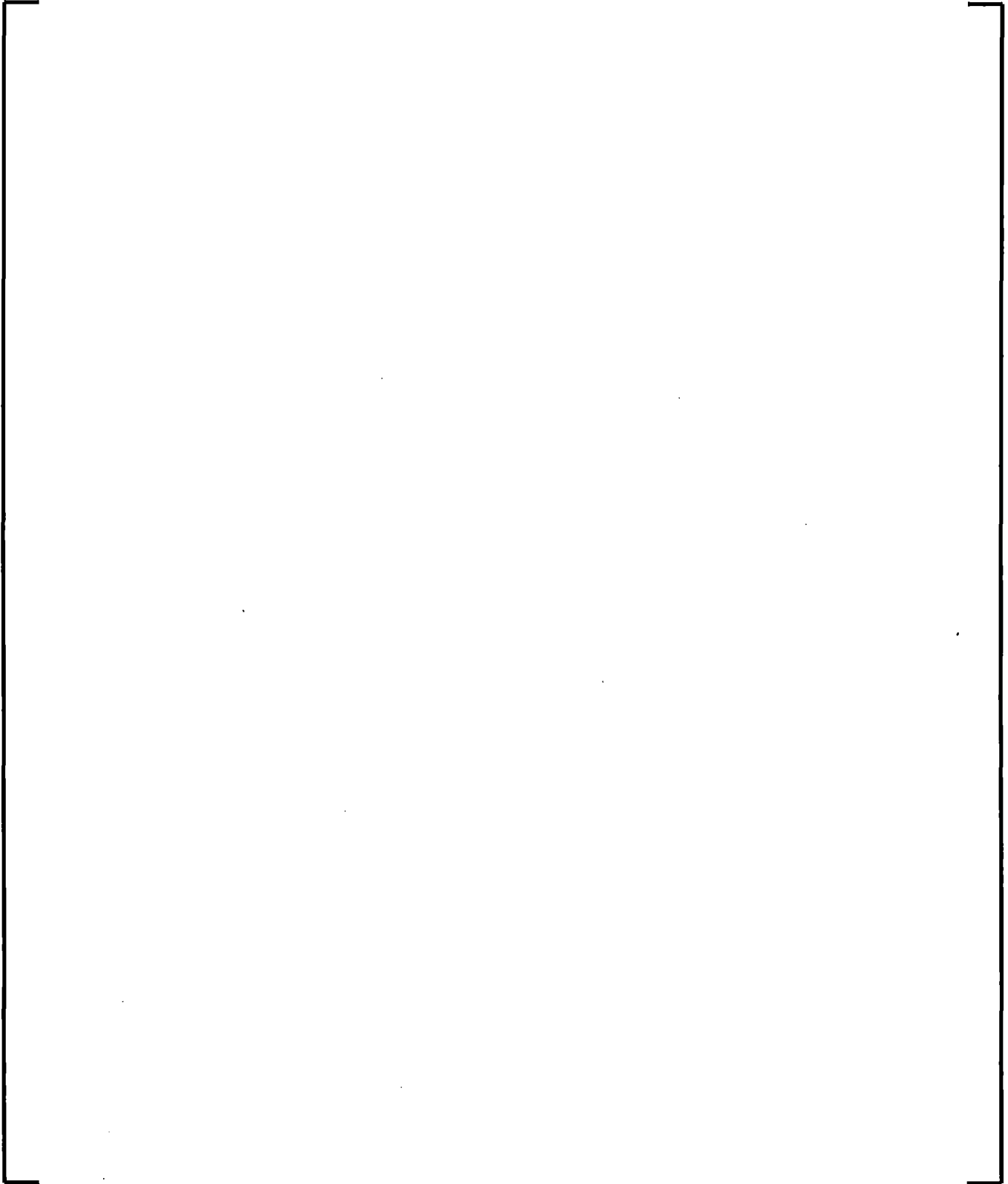
When the water level falls below the feedwater inlet, a special model takes into account the condensation due to the sub-cooled water injected into the saturated steam. This term is added to the vapor generation rate from Section 5.3.3 to determine the total evaporation/condensation in the downcomer. This condensation rate is calculated according to the following expression

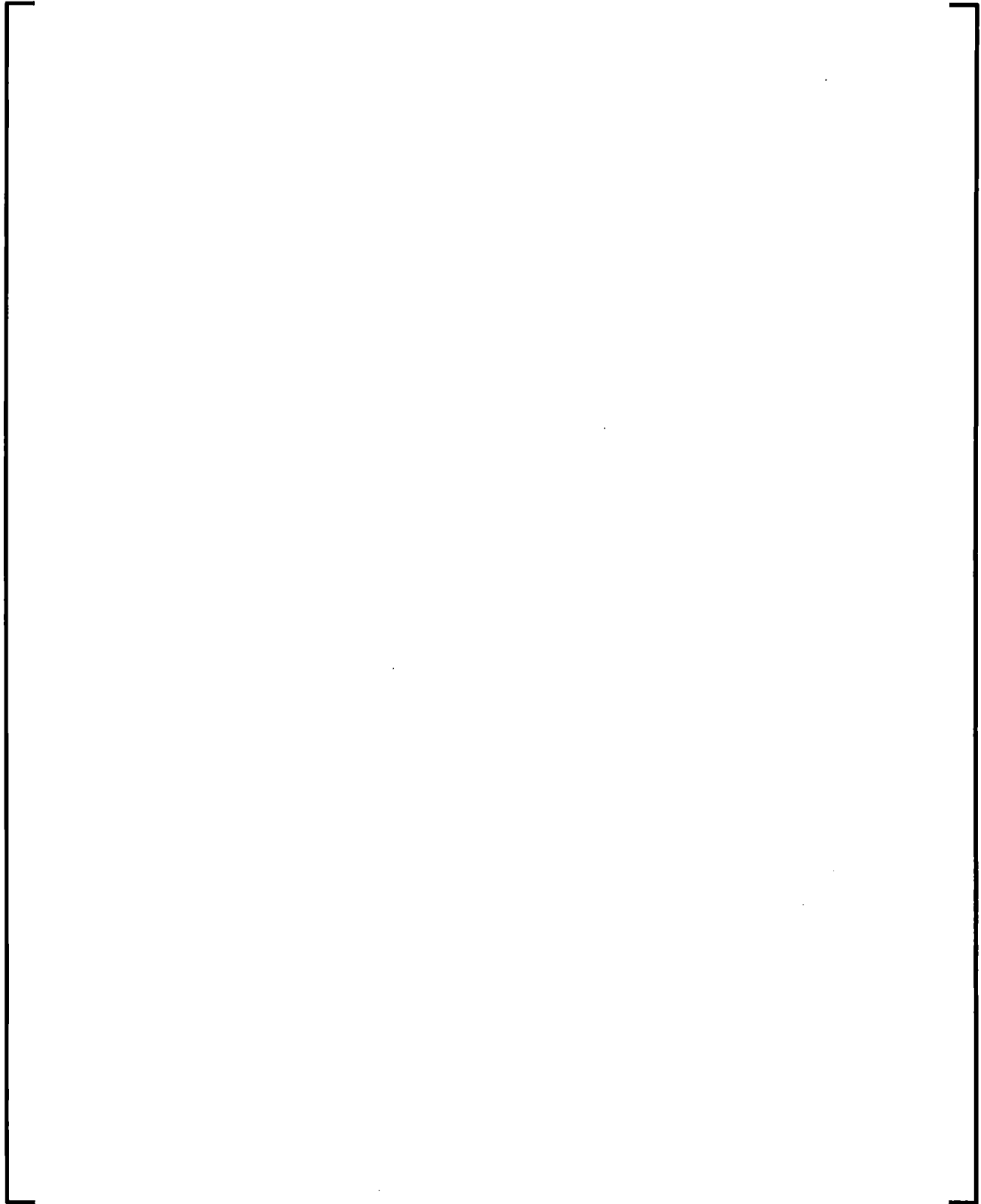
5.5.5 Dryout and Rewetting Model

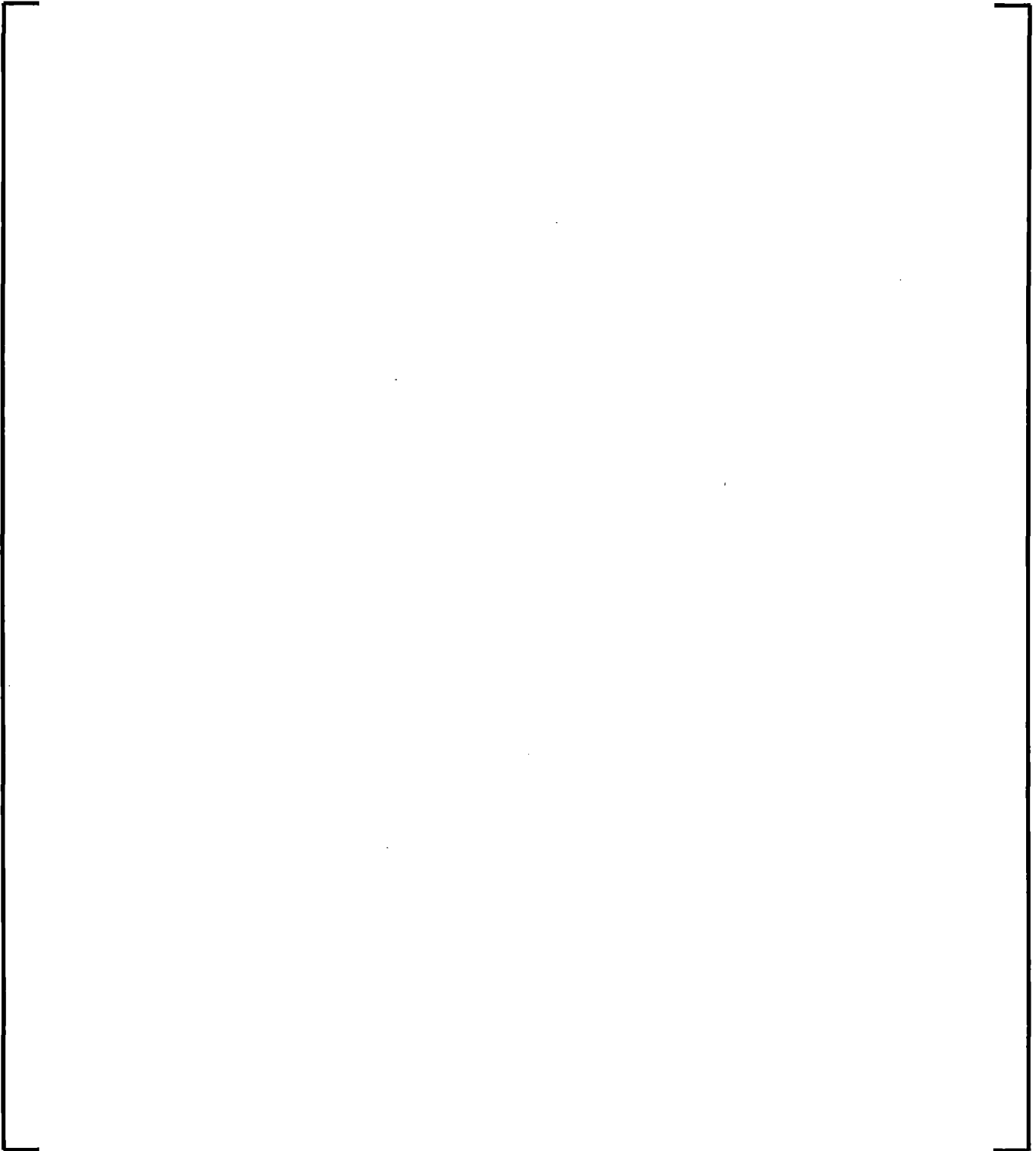
The Critical Power Reduced Order Model (CPRM) for dryout and rewetting is based on [

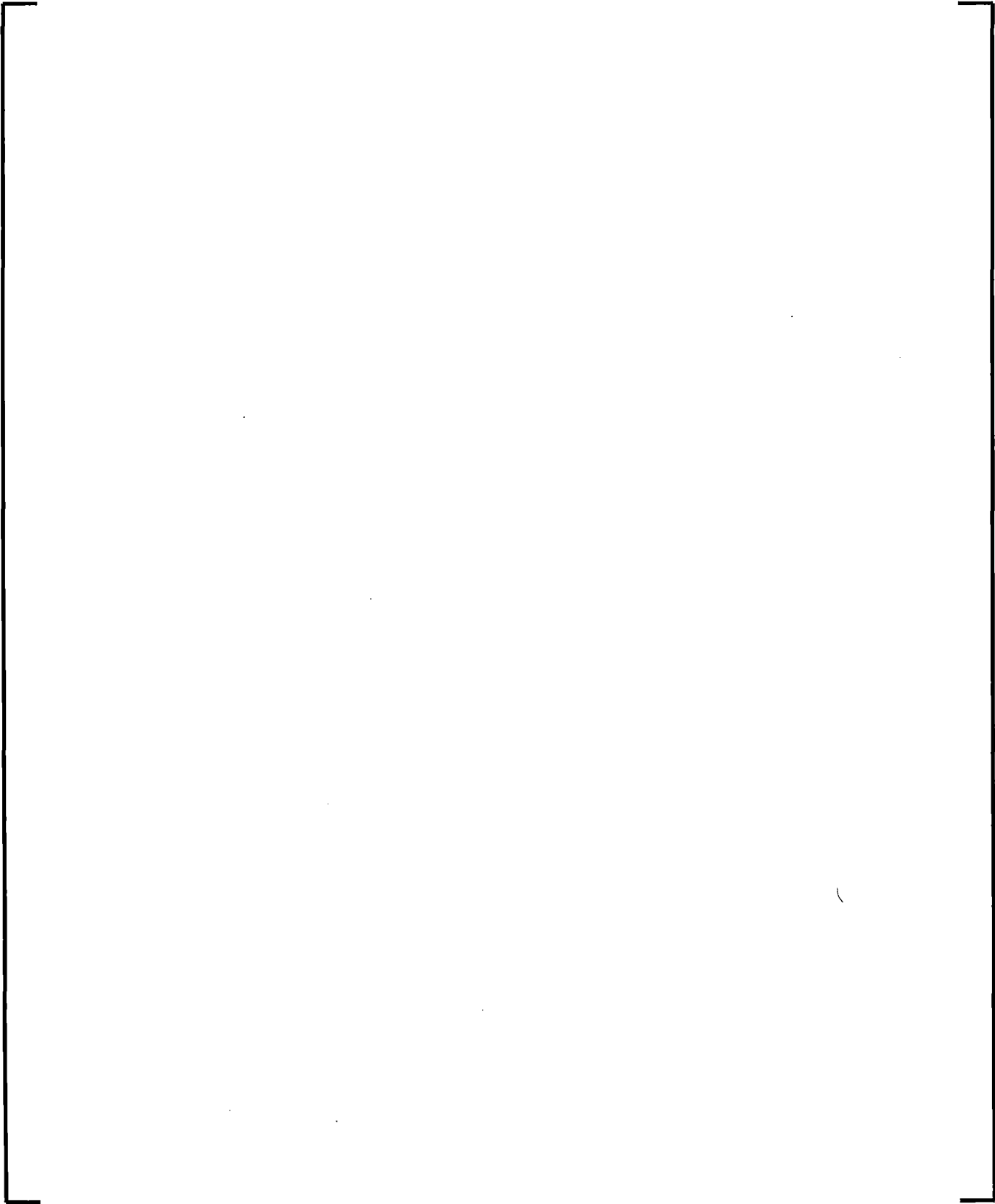
]

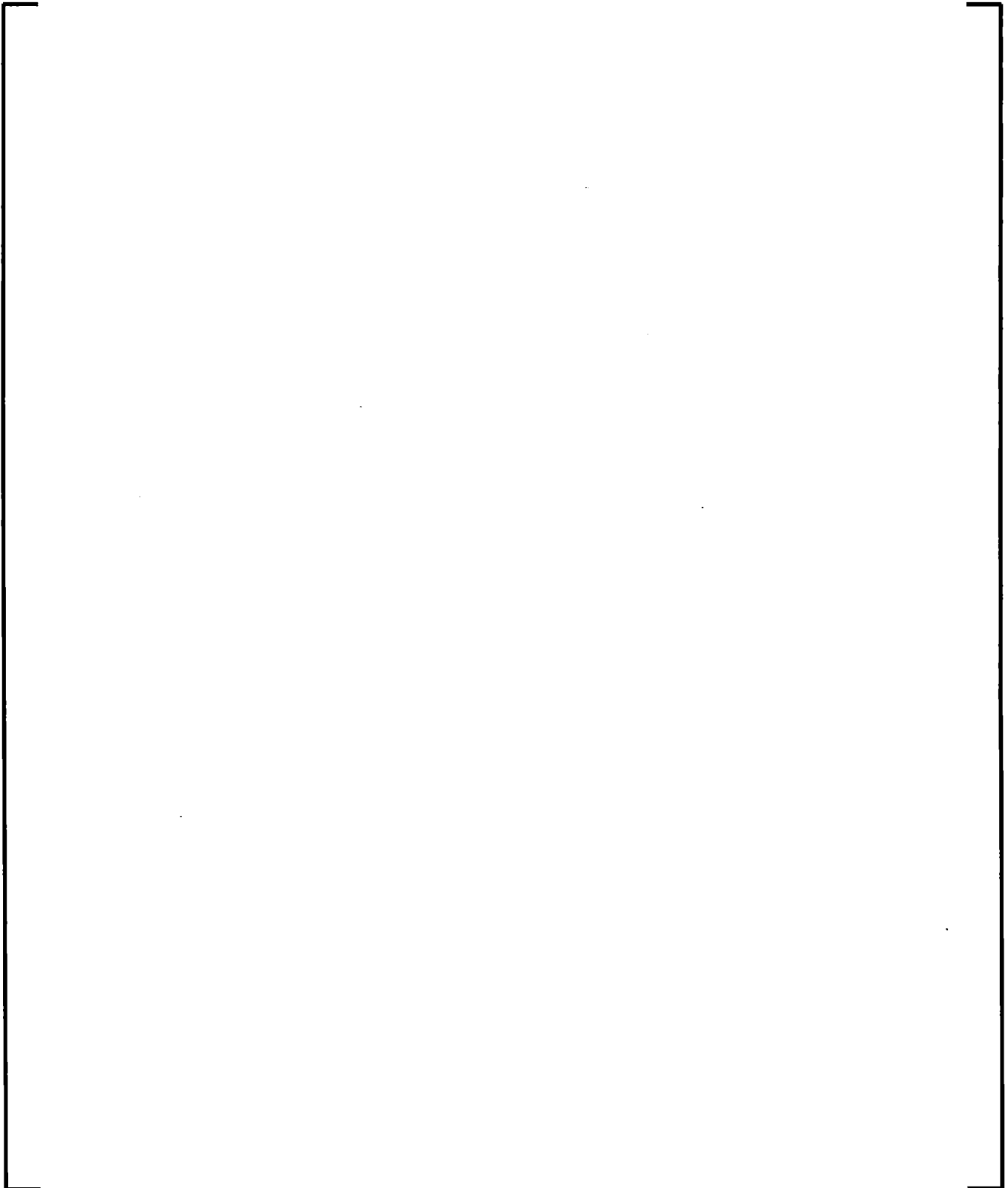


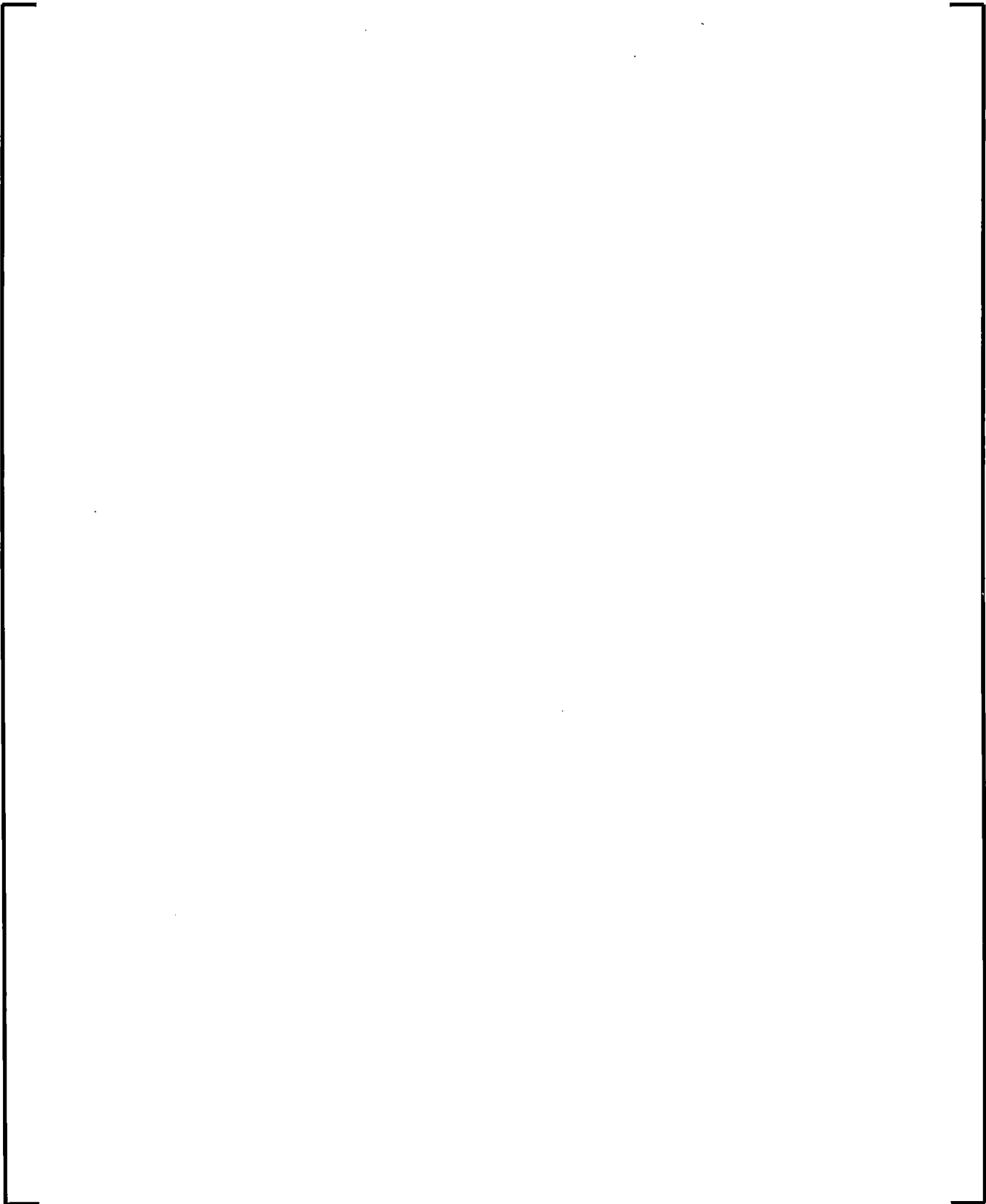












5.6 ***PLANT CONTROL AND PROTECTION SYSTEMS***

Below follows a short summary of the plant control and protection system models implemented in RAMONA5-FA:

- Pressure control system consisting of turbine control, bypass valve and safety and relief valve (SRV).
- Plant protection systems (PPS) including high-pressure coolant injection system (HPCI), control rod, main steam isolation valve (MSIV) and recirculation pump trips.
- Reactor core isolation cooling system (RCIC)
- Feedwater control system, for water level control
- Feedwater trip.

5.6.1 Pressure Control System

In a BWR, an increase in the vessel steam pressure results in an increase in steam flow through the steam line and the collapse of steam void in the reactor. The latter means that the water density increases and, hence, there is an increase in neutron moderation. This in turn leads to an increase in power, which has the effect of increasing pressure. In order to deal with this positive feedback a pressure regulator is provided. To maintain an approximately constant system pressure, a turbine control valve is provided. The bypass valve also directs the excess steam flow to the primary heat sink during load rejection events. Since the turbine and bypass flow controllers will influence the system response during many transients, it is important to have them properly represented in RAMONA5-FA.

5.6.1.1 Turbine Valve Regulator

The pressure regulator is composed of a pressure sensor transmitter, comparator, PID element, lag element, and a valve actuator. This model allows RAMONA5-FA to reasonably simulate the actual plant pressure control system.

5.6.1.2 Bypass Valve Regulator

The turbine bypass valve is not operative during normal plant operation. It opens to dump the excess steam to the condenser during abnormal transients such as turbine trip, load rejection. The bypass valve regulator is identical to the turbine control valve regulator. However, the operational characteristics may be quite different than the turbine control valve.

5.6.2 Feedwater Controller

The purpose of the feedwater controller is to determine the proper feedwater flow rate by comparing water level demand with level set point. If the error in the water level combined with the imbalance between steam and feedwater flow rates exceeds operational tolerance, proper action will be taken by the feedwater controller to correct this deficiency. The feedwater controller model employed in RAMONA5-FA is similar to the ones suggested in the literature with some adjustments and simplifications. In addition, RAMONA5-FA allows for an operator initiated reduction in water level in order to properly model the mitigation actions during an ATWS-I event.

5.6.3 Safety and Relief Valves

In a BWR, there are valves in the steam lines, which serve as safety and relief valves to maintain the system pressure below prescribed limits. RAMONA5-FA represents up to five different banks; each bank representing one or more safety or relief valves. Each bank can be activated on either steam line or dome pressure or at a user defined time.

5.6.4 Main Steam Isolation Valve (MSIV)

The purpose of the MSIV model is to predict the mass flow rate of steam through the valve during its closure. [

5.6.5 Plant Protection System (PPS)

The BWR plant protection system (PPS) is to assure that the consequences of all postulated conditions do not exceed the specified safety limit in the reactor system. It should provide the required protection by sensing the necessity and implementation of reactor scrams, pump trips, and turbine trip.

In RAMONA5-FA, the PPS functions include both manual and automatic modes. In the manual mode, the operator's action is simulated through a user specified "trip time", at which the desired shutdown system is activated. In the automatic mode, important system variables are processed through appropriate PPS subsystem trip functions for possible protective action in response to selected instrumentation signals. Following the PPS signal, a user specified trip time delay must be exceeded before PPS action is initiated.

5.6.6 Manual Operator Actions

Manual operator actions to reduce water level during an ATWS-I event are simulated in RAMONA5-FA through the feedwater control system. The time at which operator actions begin is specified by input, and is simulated by a reduction in the water level setpoint to a user specified value. [

] The feedwater pumps coast down until the feedwater controller takes control to maintain the water level at the new lower level.

5.7 *NUMERICAL TIME INTEGRATION*

This section summarizes the different time-integration techniques used to integrate the RAMONA5-FA differential equations and the intertwining of the numerical integration of the neutronics with that of the main hydraulics and the steam line integration.

5.7.1 Neutron Kinetics

[

]

5.7.2 Fuel Thermodynamics

[

]

5.7.3 Vessel Hydraulics

[

]

[

]

5.7.4 Coupling of the Neutronics and Hydraulics Integration

[

]

6.0 CODE VALIDATION

The RAMONA5-FA ATWS-I code theory is described in Section 5.0. The code calculates the transient thermal-hydraulic response of a BWR with a detailed core representation of one channel per fuel assembly. It applies a [

] There are no limitations with respect to flow direction, and the severe flow oscillations accompanied with inlet flow reversal can be simulated.

RAMONA5-FA ATWS-I applies [

] The steady state simulator provides automated input coupling for the hydraulic and neutron cross section parameters. [

] The dynamic functionality of the algorithms which is important in stability and oscillation calculations is verified by benchmarking to stability specific data.

The benchmarking of RAMONA5-FA ATWS-I is divided into two parts. The first part is focused on the pure thermal-hydraulic modeling and is accomplished by comparing the code results with the stability tests of various fuel designs performed at the KATHY loop as well as other publically available data. Both steady-state and transient benchmarks will be performed. The steady-state benchmarking includes measurement for void fraction in ATRIUM-10 and ATRIUM 10XM as well as FRIGG3. KATHY steady state pressure drop data will also be benchmarked. The measured decay ratio and frequency

for a large number of test points for ATRIUM-10 and ATRIUM 10XM are compared with the RAMONA5-FA ATWS-I calculated values. The agreement provides the needed evidence of the validity of the RAMONA5-FA ATWS-I thermal-hydraulic models.

The second part of the benchmarking is an integral exercise where both the thermal-hydraulic and the neutron kinetics are coupled in the simulation of oscillations that occurred in actual BWR plants. These benchmarks will be separated into linear stability and non-linear stability benchmarks. The linear stability benchmarks are the same used to benchmark the NRC-approved frequency domain stability code STAIF (Reference 21), and the original time-domain code RAMONA5-FA (Reference 7).

6.1 ***Test Suite and Acceptance Criteria***

The RAMONA5-FA ATWS-I code validation includes the following cases:

- Comparison to KATHY void fraction tests for:
 - ATRIUM-10
 - ATRIUM 10XM
 - FRIGG3
- Comparison to steady state pressure drop tests for:
 - KATHY ATRIUM-10
 - KATHY ATRIUM 10XM
- Comparison to KATHY loop stability tests. Comparisons include the decay ratio and frequency for all the runs in the test suite for the following fuel designs
 - ATRIUM-10
 - ATRIUM 10XM
- Comparison to KATHY dryout/rewet tests for ATRIUM 10XM and [].

- Benchmarking to all the linear instability tests in actual BWR plants included in the RAMONA5-FA test suite (Reference 7). These are:

- Benchmarking to the non-linear stability events in actual BWR plants. These include:
 - Oskarshamn turbine trip with non-linear oscillation
 - BWR A feedwater temperature transient with non-linear oscillation

The acceptance criteria are satisfied if the RAMONA5-FA ATWS-I code results agree with the experimental results. The criteria are chosen to be consistent with how this data is used in other approved methodologies. Quantitatively, the criteria are

- Calculated void fractions are within [] of the measured value.
- Calculated pressure drops are within [] of the measured value.
- Calculated decay ratios are within [] of the measured value. Conservative trends [] are acceptable.
- Calculated frequencies are within [] Hz of the measured values.
- For dryout/rewet cases, []

]

- For non-linear oscillations, []

]

6.2 *Benchmarking to Void Fraction Tests*

The FRIGG experiments, Reference 32 have been included in the validating database because of the broad industry use of these experiments in benchmarking activities, including TRAC, RETRAN, and S-RELAP5. The experiments include a wide range of pressure, subcooling, and quality from which to validate the general applicability of a void correlation. However, the experiments do not contain features found in modern rod bundles such as part length fuel rods and mixing vane grids. The lack of such features makes the data less useful in validating correlations for modern fuel designs.

Because of its prototypical geometry, the ATRIUM-10 and ATRIUM 10XM void data collected at KATHY was useful in validating void correlation performance in modern rod bundles that include part length fuel rods, mixing vane grids, and prototypic axial/radial power distributions. The characteristics of the void fraction validation database are listed in Table 6-1.

Figure 6-1 provides comparisons of predicted versus measured void fractions for the AREVA multi-rod void fraction validation database using the [] correlation. This figure shows reasonable predictions versus the measured data. The mean predictions fall within [] (predicted – measured) error with a mean error of [] and a standard deviation of [].

Table 6-1: Summary of Void Fraction Test Conditions

	FRIGG (Reference 32)	ATRIUM-10 KATHY	ATRIUM 10XM KATHY
Axial Power Shape	uniform	[]	[]
Radial Power Peaking	mild peaking	[]	[]
Bundle Design	circular array with 36 rods + central thimble	[]	[]
Pressure (psi)	435, 725, 1000, and 1260	[]	[]
Inlet Subcooling (°F)	5.7 to 56.99	[]	[]
Mass Flow Rate (lbm/s) (Based on mass flux assuming ATRIUM-10 inlet area)	10.14 to 42.56	[]	[]
Max Void at Measurement Plane (fraction)	0.848	[]	[]
Number of Data	69 tests, 314 points	[]	[]



**Figure 6-1: Validation of [] using FRIGG,
ATRIUM-10 and ATRIUM 10XM Void Data**

6.3 ***Benchmarking to KATHY Pressure Drop Tests***

Steady state pressure drop measurements have been performed for the ATRIUM-10 and ATRIUM 10XM at KATHY. The geometry was prototypic and includes all necessary features such as [

]. Pressure measurements were made at several elevations in the bundles. In addition measurements include both single phase and two phase statepoints. The characteristics of the pressure drop validation database are listed in Table 6-2.

Figure 6-2 provides comparisons of predicted versus measured pressure drops for the AREVA ATRIUM-10 multi-rod pressure drop validation. This figure shows that the majority of the predictions fall within [] (predicted – measured) error bands. The mean and standard deviation of the error were calculated using the method used in Reference 35. The single phase ATRIUM-10 data showed a mean error of [] and a standard deviation of []. The two phase ATRIUM-10 data showed a mean error of [] and a standard deviation of []. These statistics meet the NRC criteria for both average error and standard deviation.

Figure 6-3 provides comparisons of predicted versus measured pressure drops for the AREVA ATRIUM 10XM multi-rod pressure drop validation. This figure shows that the majority of the predictions fall within [] (predicted – measured) error bands. The mean and standard deviation of the error were calculated using the method used in Reference 35. The single phase ATRIUM 10XM data showed a mean error of [] and a standard deviation of []. The two phase ATRIUM 10XM data showed a mean error of [] and a standard deviation of [].

Table 6-2: Summary of Pressure Drop Test Conditions

	ATRIUM-10 KATHY	ATRIUM 10XM KATHY
Axial Power Shape	[]	[]
Bundle Design	[]	[]
Pressure (bar)	[]	[]
Inlet Temperature (°C)	[]	[]
Mass Flow Rate (kg/s)	[]	[]
Number of Two Phase Data Points	[]	[]
Number of Single Phase Data Points	[]	[]



**Figure 6-2: Validation of Pressure Drop Prediction versus KATHY ATRIUM-10
Measured Data**



**Figure 6-3: Validation of Pressure Drop Prediction versus KATHY ATRIUM 10XM
Measured Data**

6.4 ***Benchmarking to KATHY Stability Tests***

Several measurement campaigns were performed in the KATHY loop under natural circulation configuration to quantify the stability characteristics of ATRIUM-9, ATRIUM-10, and ATRIUM 10XM BWR fuel designs. The results of these measurements were used for developing and validating AREVA's stability methodologies. Of particular interest here is the ATRIUM-10 stability test series (Bundle ID STS-49.1) and the ATRIUM 10XM test series (Bundle ID STS115.1). [

]

The ATRIUM-10 tests were performed during the period May 31-June 17, 1999. The test bundle STS-49.1 was characterized by a down-skew power profile with [

] From this

data, decay ratios and frequencies were calculated.

The ATRIUM 10XM tests were performed during the period October 15-October 23, 2009. The test bundle STS-115.1 was characterized by a down-skew power profile with [

] From this

data, decay ratios and frequencies were calculated.

The data collected from the stability testing of the ATRIUM-10 and ATRIUM 10XM bundles in the KATHY loop are used for benchmarking RAMONA5-FA ATWS-I. The operating conditions of power and inlet subcooling were varied and data were collected for each operating point. [

]

The number of ATRIUM-10 data points used in this benchmarking is [] while the number of ATRIUM 10XM data points used in this benchmarking is []. The measured operating parameters for each test point are used as input to RAMONA5-FA ATWS-I. The decay ratio and frequency for each test point are compared with the corresponding measured values.

The following figures depict good agreement between the measured and calculated decay ratios and frequencies.



Figure 6-4: Validation of Decay Ratio Prediction versus KATHY Measured Data



Figure 6-5: Validation of Frequency Prediction versus KATHY Measured Data

6.5 ***Benchmarking to KATHY Dryout/Rewet Tests***

For stability and severe oscillation testing of ATRIUM 10XM, a full scale electrically heated test section is used. The axial power shape is bottom-peaked [

]. The heated rods include full-length and part-length rods. [

]

The procedure in the pure thermal-hydraulic testing is similar to the previous stability testing campaigns with ATRIUM-9 and ATRIUM-10. [

]

Information about dryout behavior is extracted from the pure thermal-hydraulic stability testing by simply allowing the flow oscillations to increase, and apply additional power increase steps as needed. Cyclical dryout and rewetting were observed in these tests by recording the responses of the many thermocouples attached to the heater rods at different elevations. [

]

It is well-known from numerical and theoretical studies of density waves in BWRs that the reactivity-to-power feedback has a destabilizing effect. By implementing such feedback in the KATHY test loop, the loop is operated at conditions closely resembling the actual conditions in an unstable BWR. With the power feedback turned on, [

] oscillations of the flow and now power to reach high amplitudes with significant inlet flow reversal []

[

]

The test results were studied and important data were extracted. These data allowed the transient extraction of [

] The measured and extracted information from the tests were essential in developing the post-dryout models, and serve to benchmark it.

The entire test run database was reviewed with regard to dryout occurrence under oscillation. All the test runs that were identified as experiencing dryout at any spacer, with or without failure to rewet, are processed and used for the benchmarking of post-dryout models. [

]

The post-dryout models were originally developed and validated using the SINANO code, Reference 34. These models have been further improved as described in Section 5.9.5, and were validated with the SINANO code. The models from the SINANO code have been integrated within the RAMONA code system, and the same benchmarks were performed with RAMONA to ensure the models were properly integrated.

Figure 6-6 through Figure 6-20 show the results of the benchmarking using CPROM coefficients consistent with the ATRIUM 10XM design discussed in Appendix A. All plots compare predicted temperatures at the spacer to the measured temperatures. In some instances nodes above and below are shown to better highlight the model behavior.

Figure 6-6 through Figure 6-20 provide a qualitative evaluation of the accuracy of the post-dryout models. In order to provide a quantitative evaluation of model accuracy, the benchmarks were re-analyzed with [

] and demonstrates that models can accurately reproduce the data.

In order to validate the post-dryout models for fuel designs besides ATRIUM 10XM, [

] Results of these cases are plotted in Figure 6-22 and Figure 6-23.

Table 6-3: Dryout and rewetting ATRIUM 10XM KATHY test runs

--



Figure 6-6: Limiting Temperature for KATHY ATRIUM 10XM []



Figure 6-7: Limiting Temperature for KATHY ATRIUM 10XM []

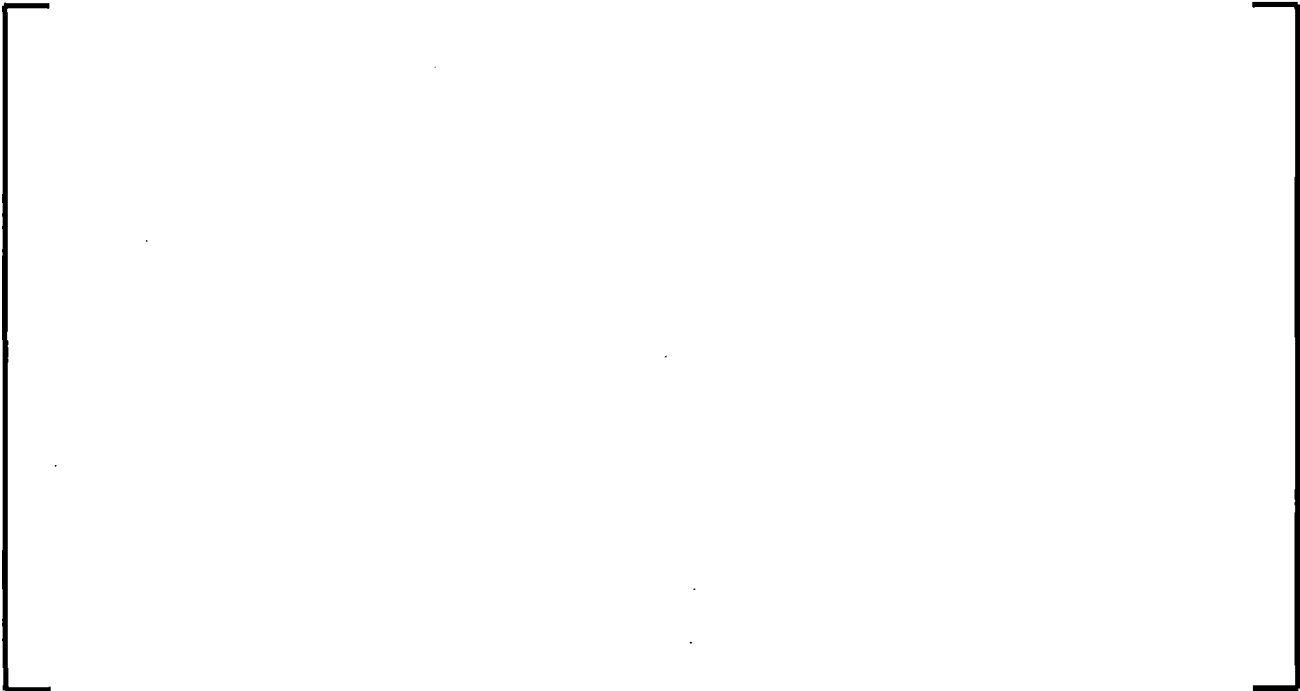


Figure 6-8: Limiting Temperature for KATHY ATRIUM 10XM []



Figure 6-9: Limiting Temperature for KATHY ATRIUM 10XM []



Figure 6-10: Limiting Temperature for KATHY ATRIUM 10XM test []



Figure 6-11: Limiting Temperature for KATHY ATRIUM 10XM []



Figure 6-12: Limiting Temperature for KATHY ATRIUM 10XM []



Figure 6-13: Limiting Temperature for KATHY ATRIUM 10XM []



Figure 6-14: Limiting Temperature for KATHY ATRIUM 10XM []



Figure 6-15: Limiting Temperature for KATHY ATRIUM 10XM []



Figure 6-16: Limiting Temperature for KATHY ATRIUM 10XM []

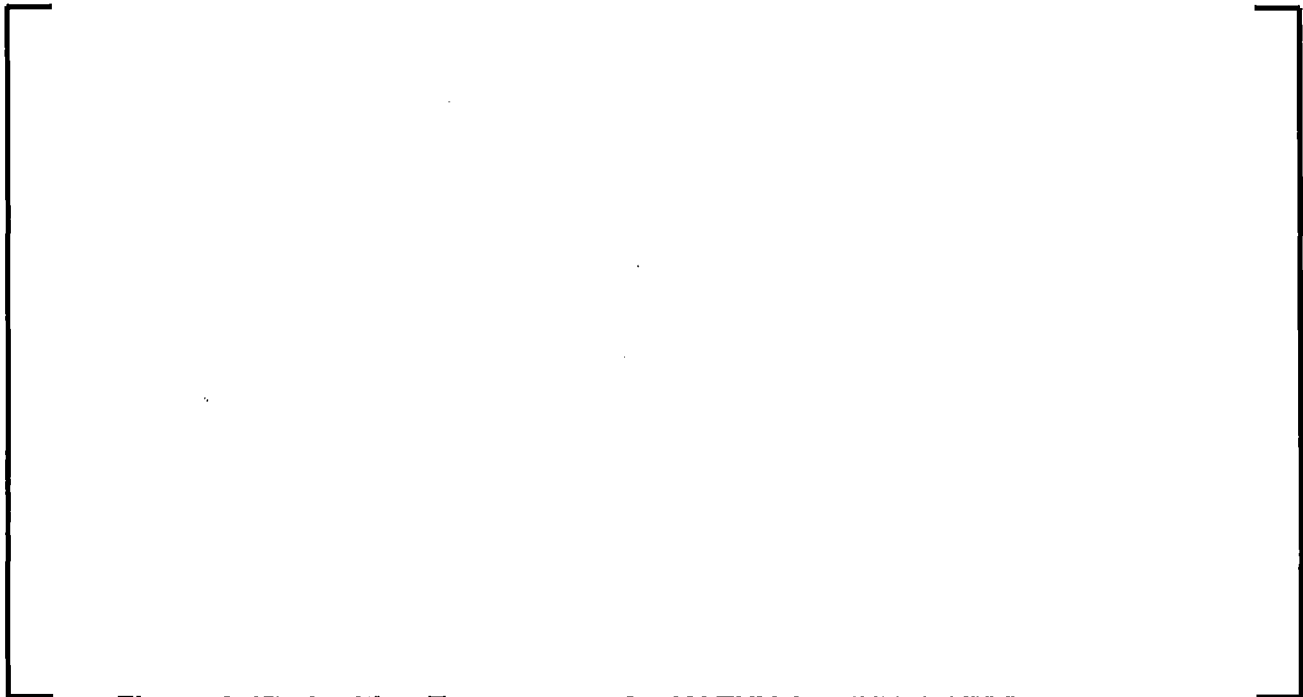


Figure 6-17: Limiting Temperature for KATHY ATRIUM 10XM []



Figure 6-18: Limiting Temperature for KATHY ATRIUM 10XM []



Figure 6-19: Limiting Temperature for KATHY ATRIUM 10XM []



Figure 6-20: Limiting Temperature for KATHY ATRIUM 10XM []



Figure 6-21: Limiting Temperature for KATHY ATRIUM 10XM []



Figure 6-22: Limiting Temperature for KATHY []



Figure 6-23: Limiting Temperature for KATHY []

6.6 *Benchmarking to Linear Reactor Stability Benchmarks*

In order to validate the functions and additions to the RAMONA5-FA ATWS-I code, several sets of linear stability reactor benchmarks were performed. [

]

utilize neutronic input taken from the benchmark material used to qualify the frequency domain code STAIF (Reference 21).

6.6.1 []

[

]

*

[

]

[

]

6.6.2 []

[

]

6.6.3 []

[

]

* [

]

6.6.4 []

[

]

6.7 ***Benchmarking to Non-Linear Reactor Benchmarks***

In order to validate the functions and additions to the RAMONA5-FA ATWS-I code, several sets of non-linear stability reactor benchmarks were performed. These benchmarks include:

- Oskarshamn Non-Linear Instability
- BWR A Feedwater Transient with Non-Linear Instability

A description of the benchmark analyses is given in the following sections along with the RAMONA5-FA ATWS-I calculated decay ratios and frequencies.

6.7.1 **Oskarshamn Nonlinear Instability**

On February 25, 1999 as maintenance work was being performed on a switchyard outside of Oskarshamn Unit 2, the power supply to a bus bar was interrupted for 150 ms. A load rejection signal was sent to the main breaker that connects the unit to the grid. This signal caused the turbine to trip, however due to a failure in the relay circuit, this signal was not transmitted to the reactor protection system. The system continued at power until operators initiated a partial scram. Following the partial scram, power and flow were decreased. The feedwater temperature continued to decrease causing reactor power to further increase until the system crossed the stability boundary. The reactor continued to oscillate until a high power scram was reached.

The Oskarshamn-2 non-linear stability was analyzed with RAMONA5-FA ATWS-I. Two separate scenarios were evaluated. In the first scenario, the measured pump speed was imposed and the recirculation flow was calculated based on the specified pump performance curves. The plots of relevant parameters to actual measured data for this scenario are given in Figure 6-24, Figure 6-25, and Figure 6-26. The results show good agreement with measured values with just a slight underestimation of the event growth rate. However, Figure 6-26 shows that the code overestimates the final recirculation flow during the final portion of the event. A second scenario was then run in which the pump speed versus time was modified to produce a recirculation flow approximately equal to the measured value. The results of this evaluation are given in Figure 6-27, Figure 6-28, and Figure 6-29. The results of this scenario show a very good agreement with the measured power results.

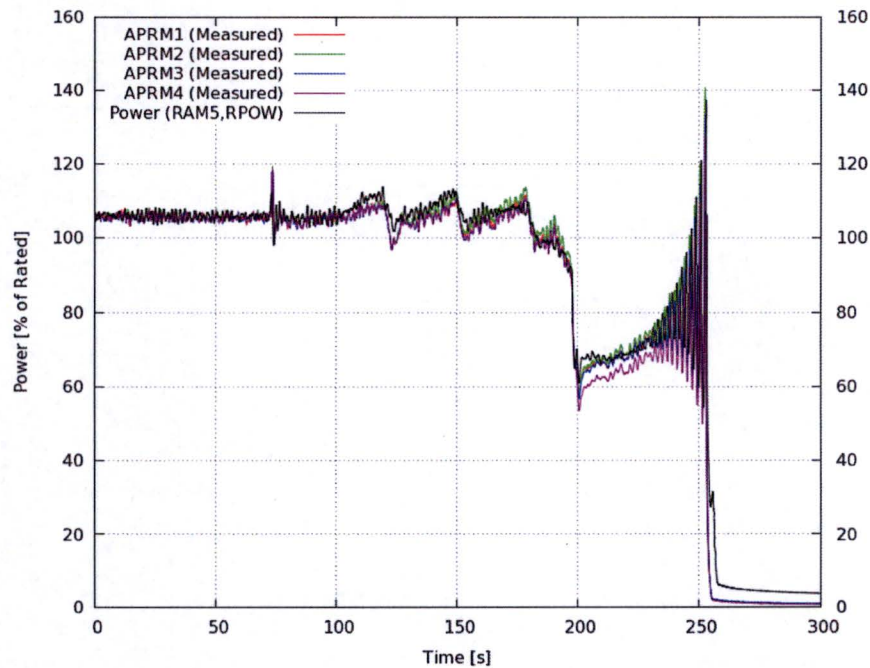


**Figure 6-24: Oskarshamn-2 Non-Linear Stability Simulation
Core Power, Imposed Pump Speed**

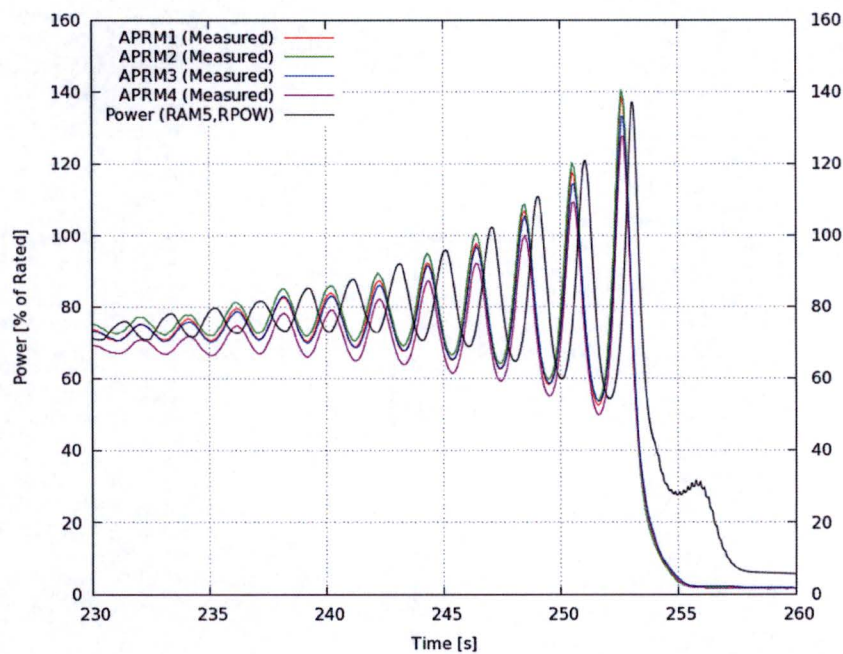


**Figure 6-25: Oskarshamn-2 Non-Linear Stability Simulation
Core Power - Zoom, Imposed Pump Speed**

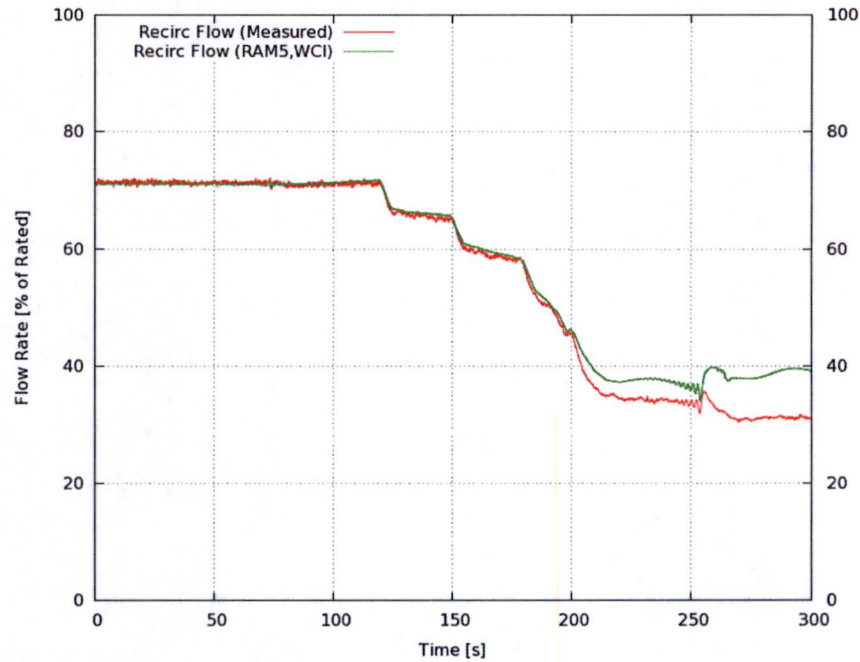


**Figure 6-26: Oskarshamn-2 Non-Linear Stability Simulation
Recirculation Flow, Imposed Pump Speed**

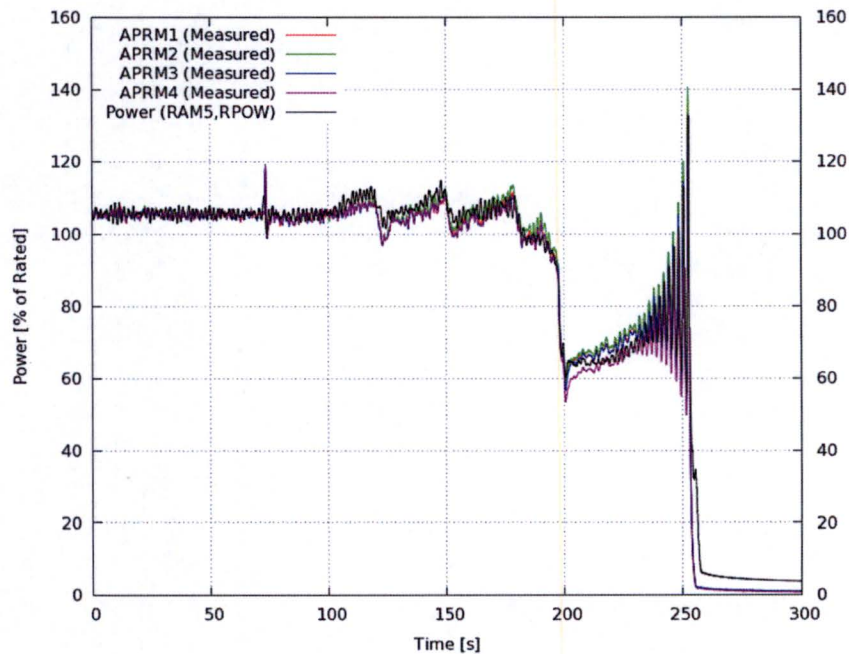


**Figure 6-27: Oskarshamn-2 Non-Linear Stability Simulation
Core Power, Match Recirculation Flow**

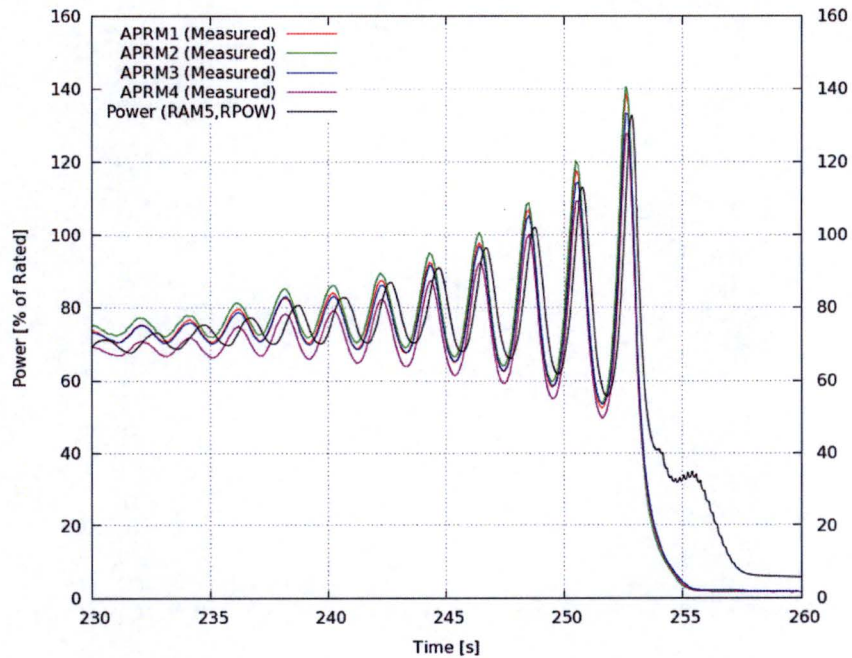


**Figure 6-28: Oskarshamn-2 Non-Linear Stability Simulation
Core Power - Zoom, Match Recirculation Flow**

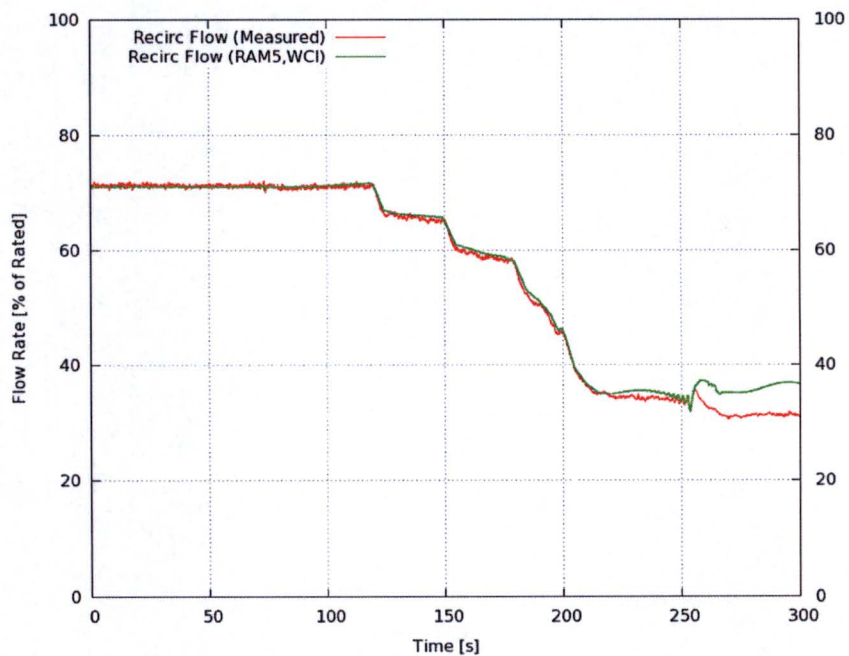


**Figure 6-29: Oskarshamn-2 Non-Linear Stability Simulation
Recirculation Flow, Match Recirculation Flow**

6.7.2 BWR A Feedwater Transient with Non-Linear Instability

[

] was analyzed with RAMONA5-FA ATWS-I. The plots of relevant parameters to actual measured data for this scenario are given in

Figure 6-30. The results show very good agreement between the measured and calculated []



Figure 6-30: BWR [] Transient Non-Linear Stability Simulation

7.0 **SAMPLE PROBLEMS**

In addition to the benchmarking described in the previous section, the general core performance against theoretically predicted trends was also investigated. This is accomplished by running a sample ATWS-I transient and performing checks to demonstrate the ability of the code to generate very large oscillations in power and flow and demonstrate large amplitude inlet flow reversal in some bundles. Sensitivity calculations for key parameters are examined.

The sample problem is based on the Brunswick BWR4 reactor. A full core of ATRIUM 10XM was modeled, and both TTWB and 2RPT transients were simulated. [

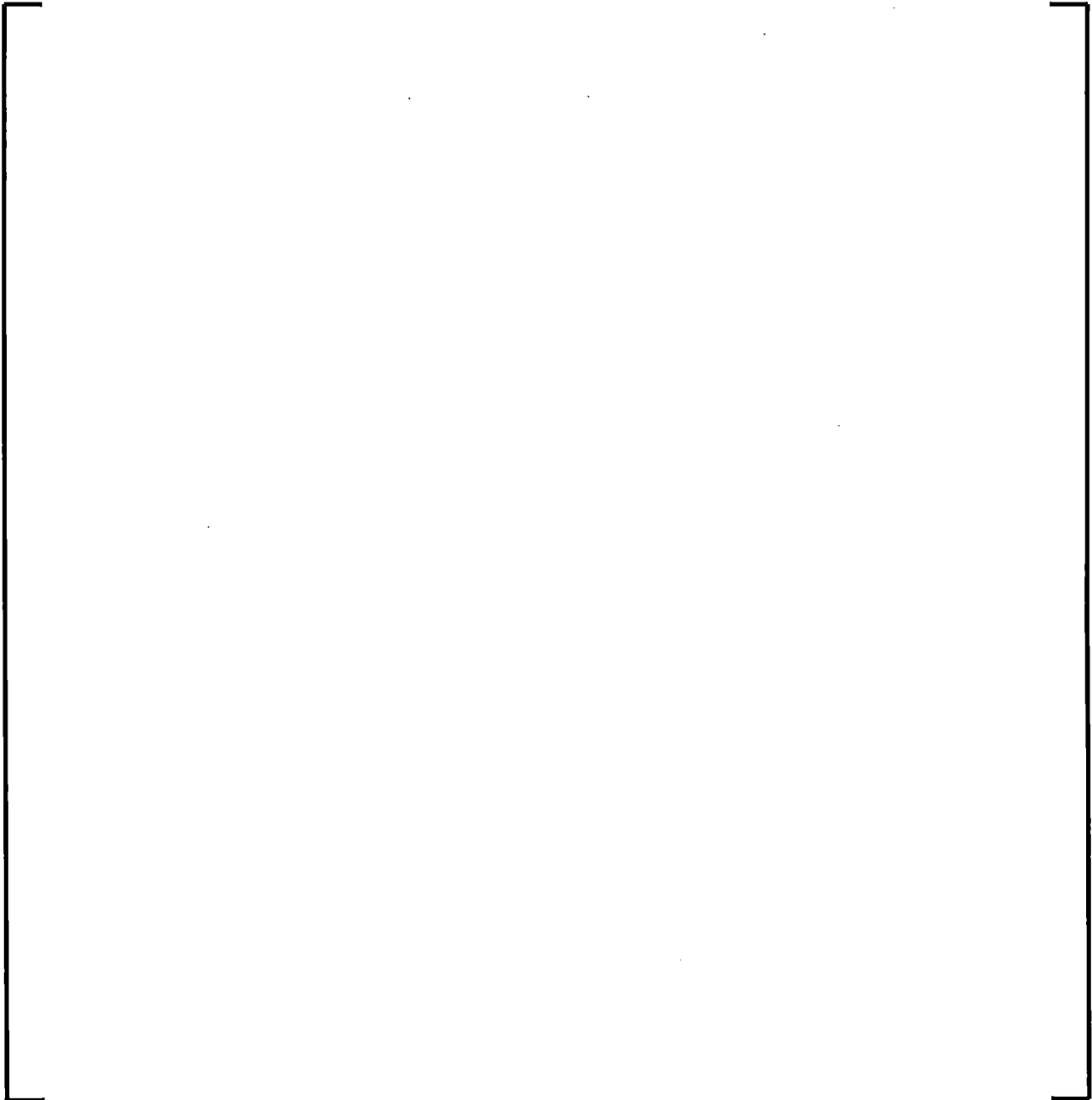
]

7.1 ***Turbine Trip***

A turbine trip with bypass was simulated [

]

Numerous sensitivity studies have also been performed to examine the sensitivity of the models to various operational variables, as well as modeling variables. The sensitivity to operational variables includes:



To examine the effect of model variations, the following sensitivity studies were performed.



The results for the [] sensitivity studies are presented in Table 7-1.

Table 7-1: TTWB Sensitivity Study Results

A large, empty rectangular box with a black border, intended for the content of Table 7-1. The box is currently blank.



Figure 7-1: TTWB Base Case Core Power



Figure 7-2: TTWB Base Case Core Inlet Flow



Figure 7-3: TTWB Base Case Core Inlet Subcooling



Figure 7-4: TTWB Base Case Limiting Channel Inlet Flow



Figure 7-5: TTWB Base Case Vessel Water Level



Figure 7-6: TTWB Base Case Limiting Channel PCT

7.2 *Two Recirculation Pump Trip*

A 2RPT was simulated [

Table 7-2: 2RPT Sensitivity Study Results



Figure 7-7: 2RPT Base Case Core Power



Figure 7-8: 2RPT Base Case Core Inlet Flow




Figure 7-9: 2RPT Base Case Limiting Channel Inlet Flow



Figure 7-10: 2RPT Base Case Core Inlet Subcooling



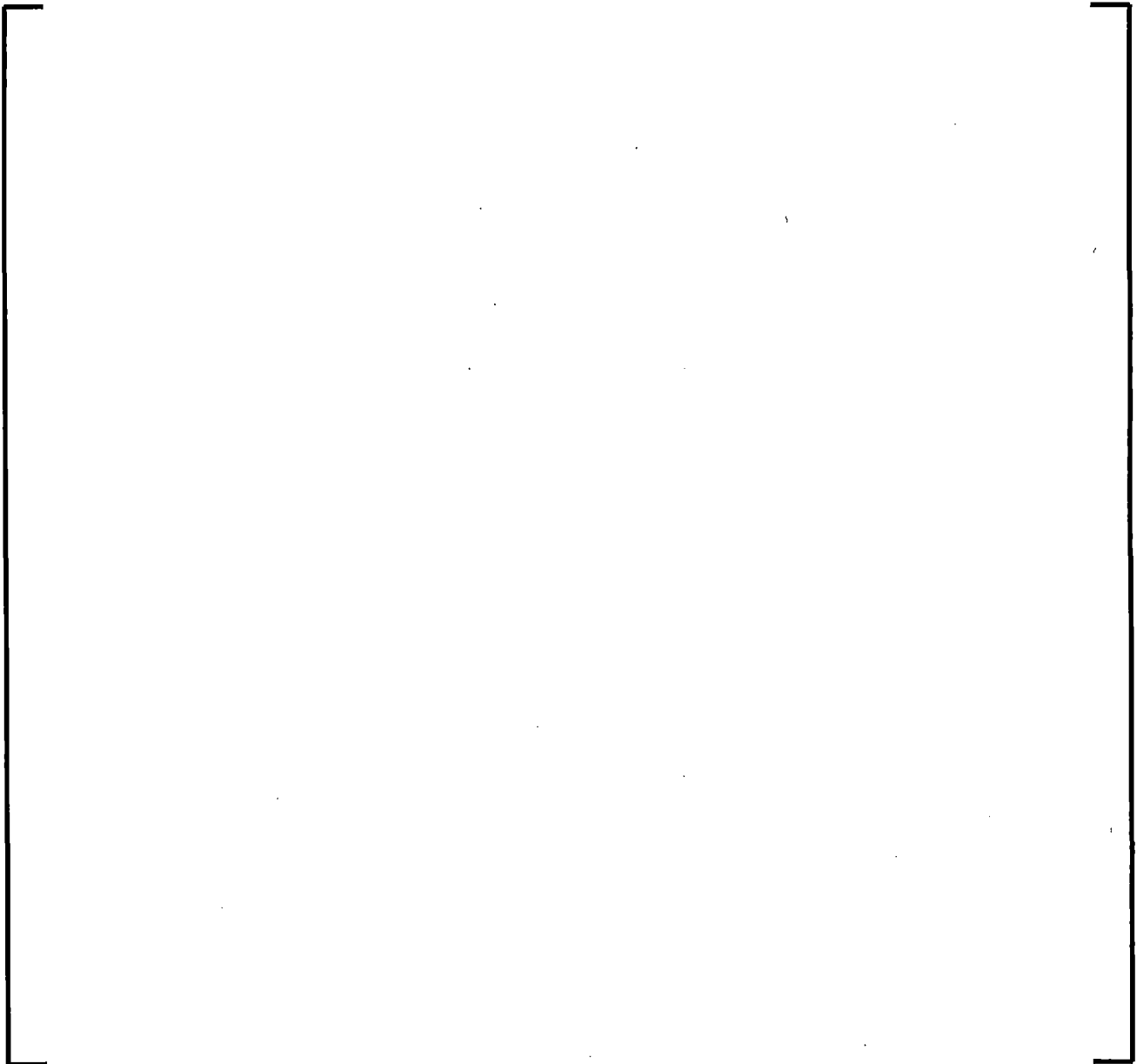
Figure 7-11: 2RPT Base Case Vessel Water Level

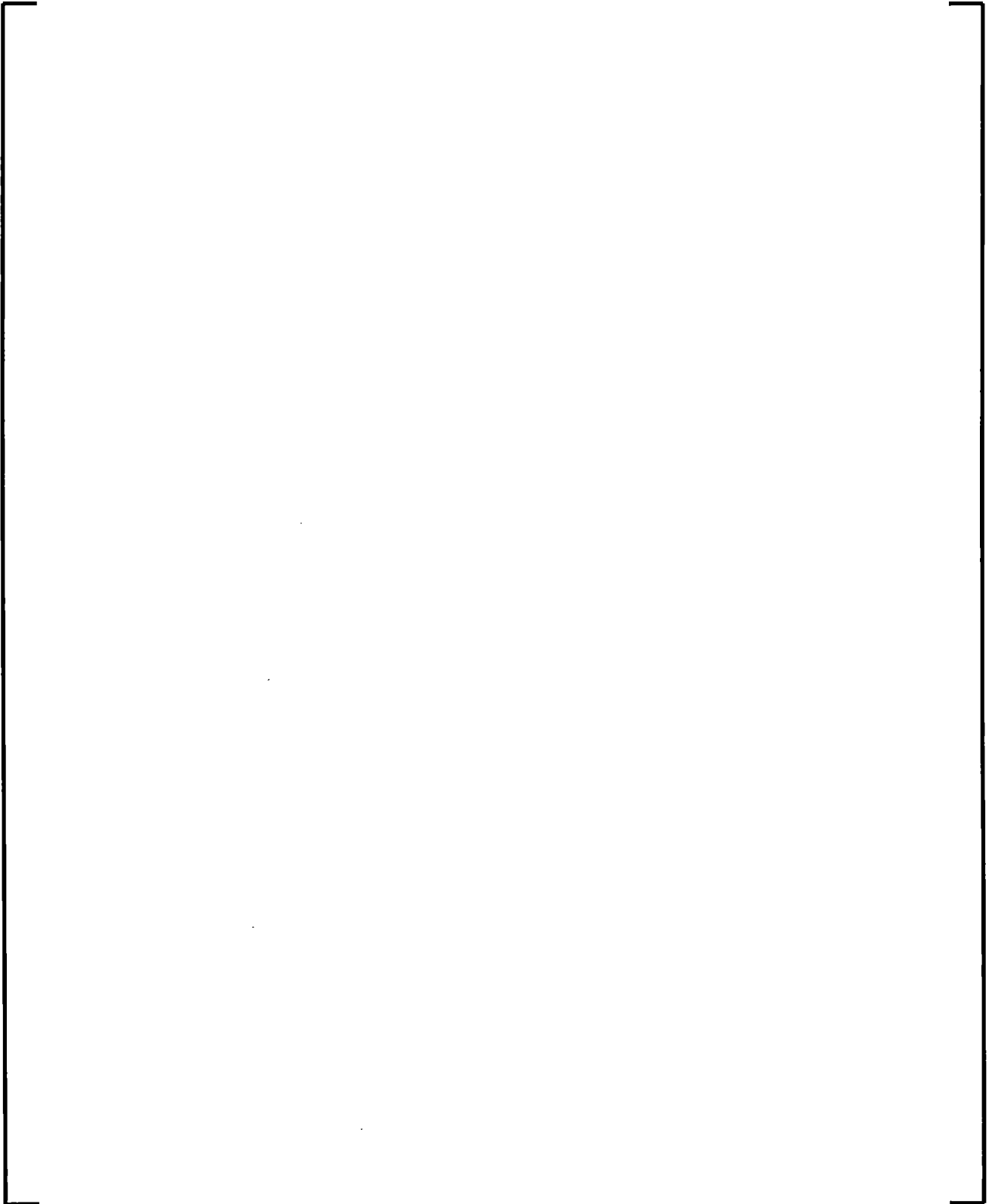


Figure 7-12: 2RPT Base Case Limiting Channel PCT

8.0 CALCULATION PROCEDURE

The RAMONA5-FA ATWS-I evaluation entails the analysis of simulated ATWS events at several state points throughout that cycle. This section is devoted to the general description of the methodology, the procedure for performing this calculation, and the limitation and conditions of the methodology which is presented in Table 8-1. In summary, the application procedure includes the following elements:





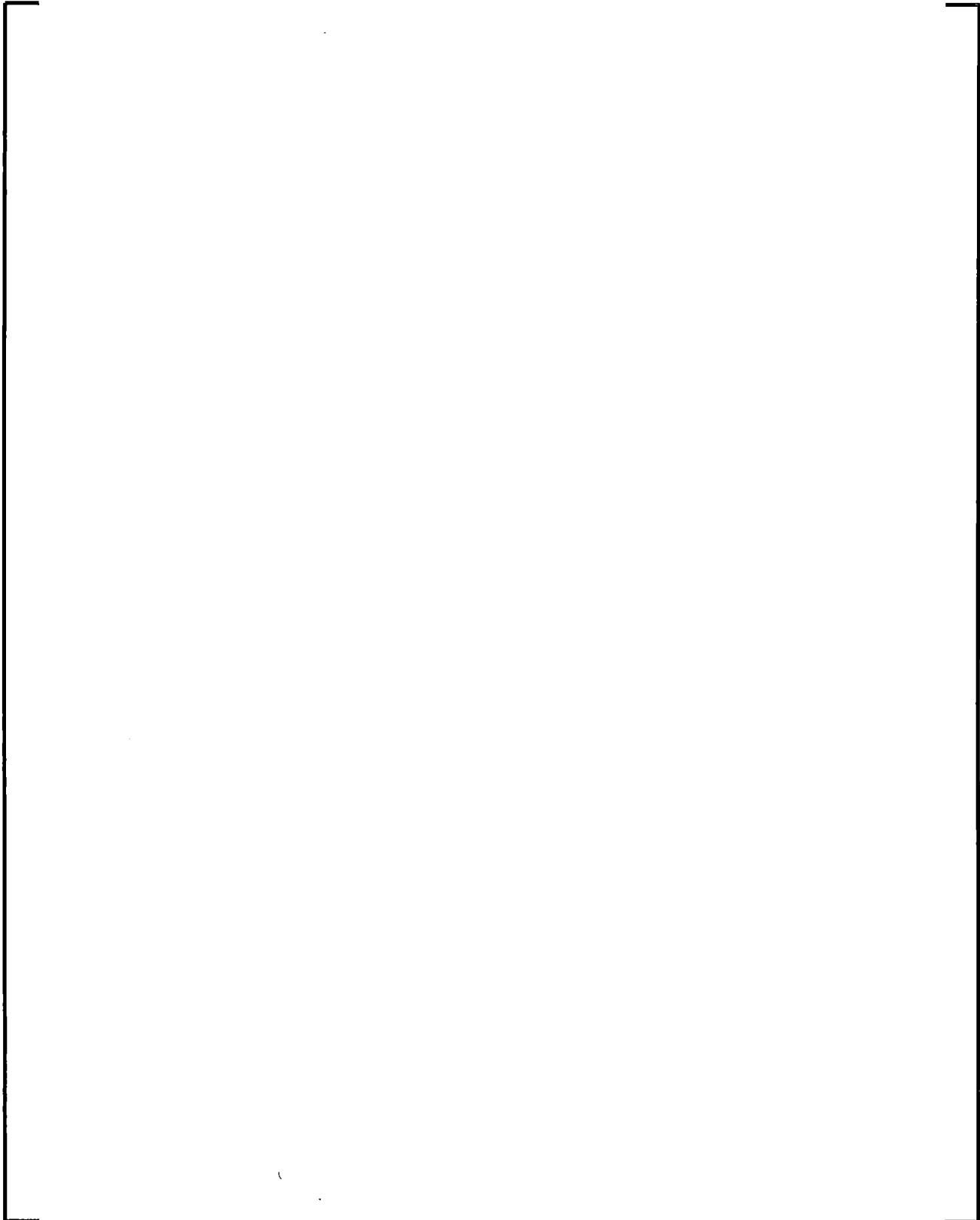


Table 8-1: ATWS-I Limitation and Conditions

--	--

9.0 REFERENCES

1. "ATWS Rule Issues Relative to BWR Core Thermal-Hydraulic Stability," NEDO-32047-A, Class I June 1995.
2. W. Wulff et al., "BWR Stability Analysis with the BNL Engineering Plant Analyzer," NUREG/CR 5816, BNL/NUREG-52312, October 1992.
3. USNRC Standard Review Plan, *15.8 Anticipated Transient Without Scram*, NUREG-0800, Revision 2, March 2007.
4. FQM, Revision 3, *AREVA NP Fuel Sector Quality Management Manual*, AREVA NP, June 2008.
5. J. March-Leuba, "Density-Wave Instabilities in Boiling Water Reactors," NUREG/CR-6003, ORNL/TM-12130, September 1992.
6. Carsten Lange et al., "Comments on local power oscillation phenomenon at BWRs," *Progress in Nuclear Energy* 60 (2012) 73-88.
7. BAW-10255(P)(A) Revision 2, "Cycle-Specific DIVOM Methodology Using the RAMONA5-FA Code," AREVA NP, May 2008.
8. A. Wysocki, J. March-Leuba, T. Downar, and A. Manera, "TRACE/PARCS Analysis of Out-of-Phase Power Oscillations With a Rotating Line of Symmetry," *The 15th International Topical Meeting on Nuclear Reactor Thermal- Hydraulics*, NURETH-15, paper 457, Pisa, Italy, May 12-17, 2013.
9. Y. M. Farawila and D. W. Pruitt, "A Study of Nonlinear Oscillation and Limit Cycles in Boiling Water Reactors – I: The Global Mode," *Nuclear Science and Engineering*: 154, 302-315 (2006).
10. Y. M. Farawila and D. W. Pruitt, "A Study of Nonlinear Oscillation and Limit Cycles in Boiling Water Reactors – II: The Regional Mode," *Nuclear Science and Engineering*: 154, 316-327 (2006).
11. Y. M. Farawila, "Application of Modal Neutron Kinetics to Boiling Water Reactor Oscillation Problems," *Nuclear Science and Engineering*: 129, 261 (1998).

12. Hideaki IKEDA et al., "Nonlinear Behavior under Regional Neutron Flux Oscillations in BWR Cores," J. Nuclear Science and Technology, Vol. 38, No. 5, p. 312-323 (May 2001).
13. D. W. Pruitt, D. R. Tinkler, and Y. M. Farawila, "Considerations for Bypass Boiling during BWR Power Oscillations," Trans. Am. Nucl. Soc., Vol. 99, pp. 739-740 (Nov. 2008).
14. D. W. Pruitt, K. R. Greene, F. Wehle, R. Velten, J. Kronenberg, A. Beisiegel, and Y. M. Farawila, "Stability and Void Fraction Measurements for the ATRIUM 10XM BWR Fuel Bundle," Proceedings of 2010 LWR Fuel Performance Top Fuel WRFPM, Orlando, Florida, Sept. 26-29, 2010.
15. F. Wehle, R. Velten, J. Kronenberg, A. Beisiegel, D. Pruitt, K. Greene, and Y. Farawila, "Full Scale Stability and Void Fraction Measurements for the ATRIUM 10XM BWR Fuel Bundle," 2011 Jahrestagung Kerntechnik, Berlin, Germany, May 17-19 2011.
16. [
-]
17. W. Wulff, "Simulation of Two-Phase Flow in Complex Systems," Nuclear Technology Vol. 159, September 2007.
18. ANF-88-101(P), *MICROBURN-B: A Two-Group, Three Dimensional BWR Nodal Simulator Code*, Advanced Nuclear Fuels, July 1988.
19. Byung-Oh Cho, "Nodal Methods for Calculating Nuclear Reactor Transients, Control Rod Patterns, and Fuel Pin Powers," Ph.D. Thesis, Oregon State University, OSU-NE-9108, June 1991.
20. EMF-2158(P)(A) Revision 0, "Siemens Power Corporation Methodology for Boiling Water Reactors: Evaluation and Validation of CASMO-4/MICROBURN-B2," Siemens Power Corporation, October 1999.
21. EMF-CC-074(P)(A) Volume 4 Revision 0, *BWR Stability Analysis – Assessment of STAIF with Input from MICROBURN-B2*, Siemens Power Corporation, August 2000.

22. EMF-3028P-A Volume 2 Revision 4, "RAMONA5-FA: A Computer Program for BWR Transient Analysis in the Time Domain Volume 2 -- Theory Manual," AREVA NP Inc., March 2013.
23. American National Standard for Decay Heat Power in Light Water Reactors, ANSI/ANS-5.1-1979.
24. W. Wulff, et al., "A Description and Assessment of RAMONA-3B Mod. 0 Cycle 4 A Computer Code with Three-Dimensional Neutron Kinetics for BWR System Transients," BNL-NUREG-51748, January 1984.
25. []
26. Moody, L. F., "An Approximate Formula for Pipe Friction Factors," *Mechanical Eng.* 69, pp 1005-1006, December 1947.
27. []
28. []
29. W. Wagner and H.-J. Kretzschmar, "International Steam Tables – Properties of Water and Steam Based on the Industrial Formulation IAPWS-IF97," second edition 2008 Springer-Verlag Berlin Heidelberg.
30. ANP-10262PA Revision 0, "Enhanced Option III Long Term Stability Solution", AREVA NP, May 2008.
31. NUREG/CR-6743, LA-UR-00-3122, "Phenomenon Identification and Ranking Tables (PIRTS) for Power Oscillations Without Scram in Boiling Water Reactors Containing High Burnup Fuel," September 2001.
32. O. Nylund et al., "Hydrodynamic and Heat Transfer Measurements on A Full-Scale Simulated 36-Rod Marviken Fuel Element with Non-Uniform Radial Heat Flux Distribution," FRIGG-3, R-494/RL-1154, November 1969.

33. BAW-10247PA Revision 0, *Realistic Thermal-Mechanical Fuel Rod Methodology for Boiling Water Reactors*, AREVA NP, February 2008.
34. ANP-3274P Revision 3, *Analytical Methods for Monticello ATWS-I*, February 2017.
35. XN-NF-79-59(P)(A), *Methodology for Calculations of Pressure Drop in BWR Fuel Assemblies*, October 1983.

Appendix A Steady State Dryout Correlation CPROM

Abstract

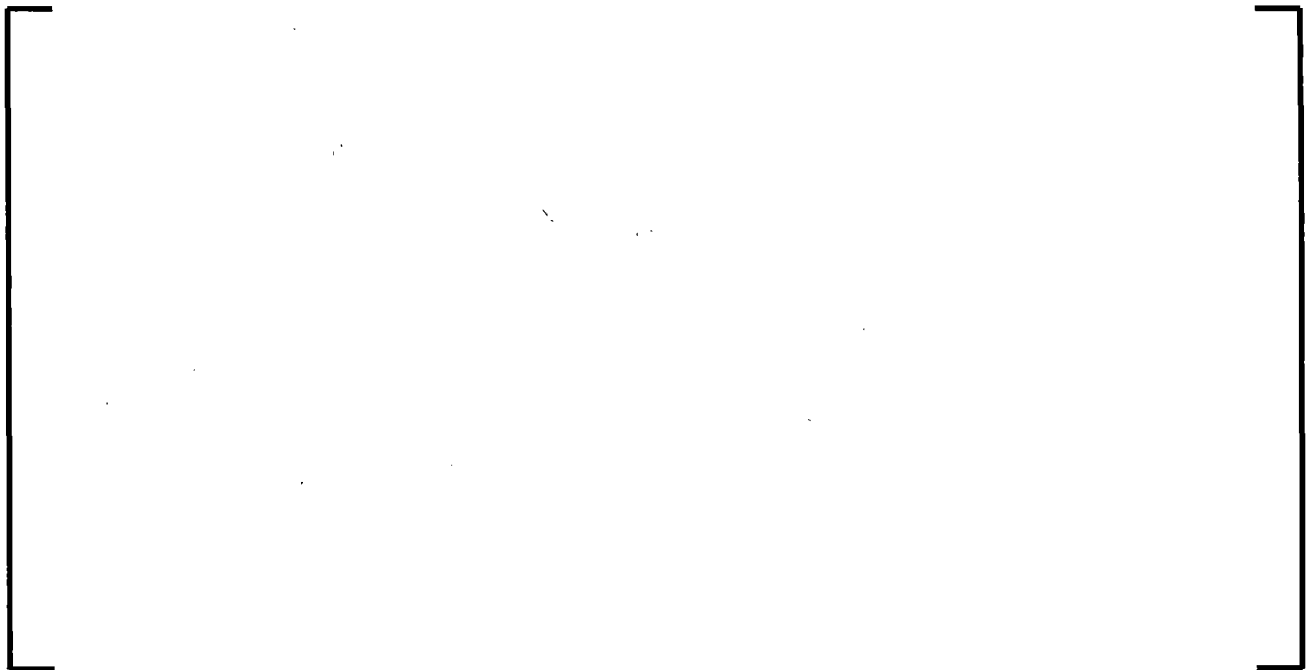
A new dryout correlation is presented. This correlation, named Critical Power Reduced Order Model (CPROM), has been developed based on AREVA correlation development guidelines similar to dryout licensing correlations such as ACE. The CPROM correlation range of applicability is wide [

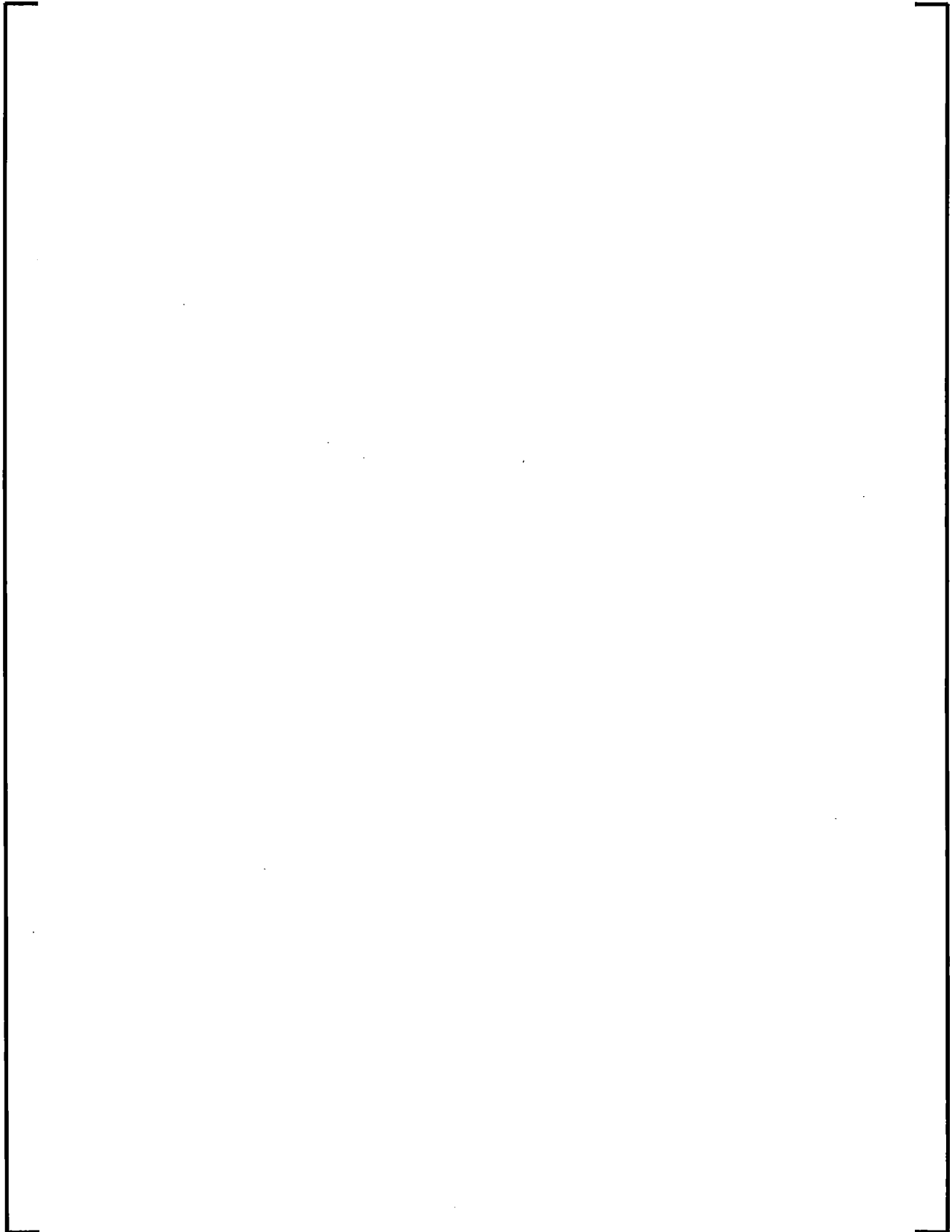
] making it well-suited to fitting into transient models of post-dryout that include cyclical dryout and rewetting with possible failure to rewet. CPROM is an integral part of the RAMONA5-FA transient model described in Section 5.5.5.

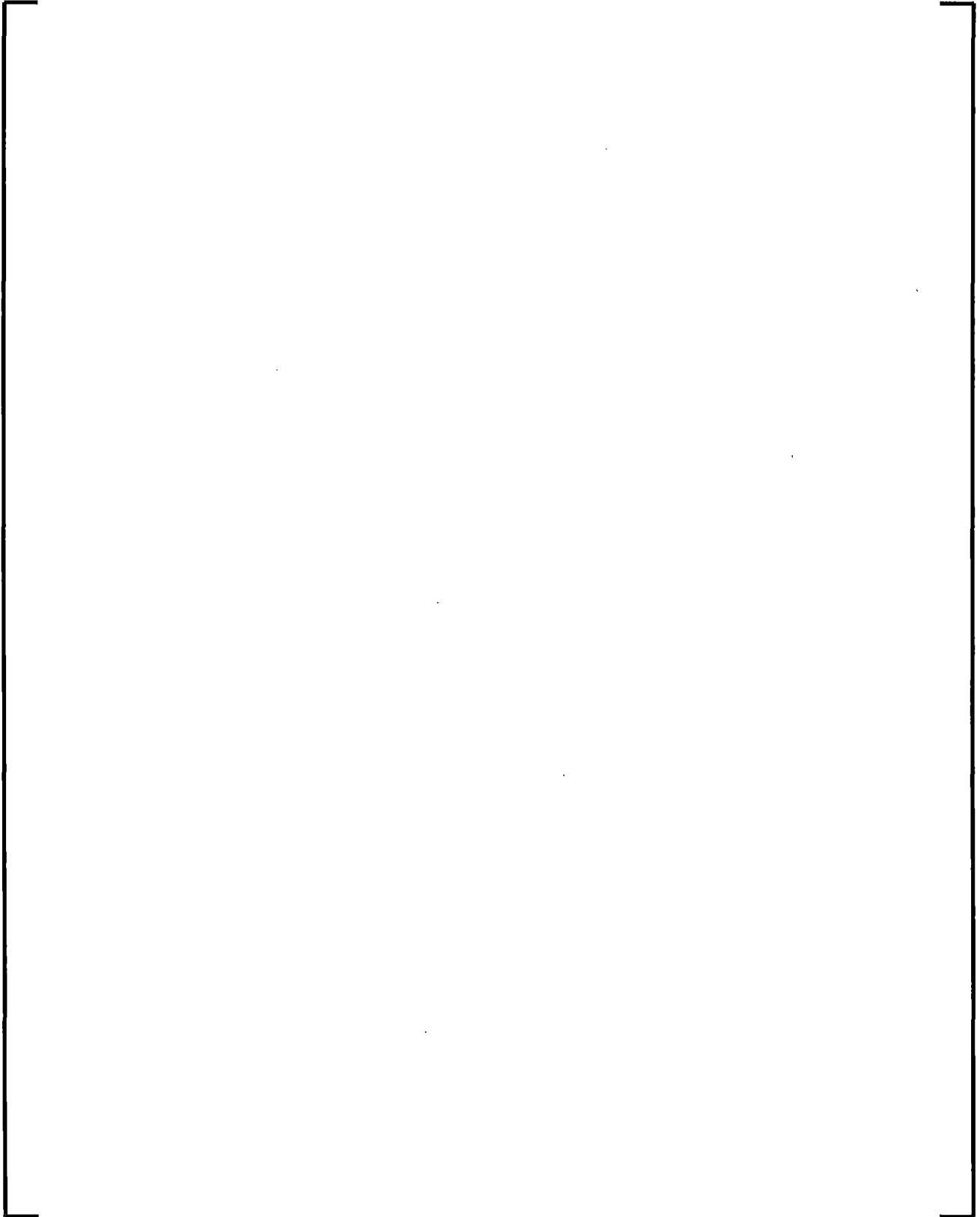
A.1 *Description of CPROM Correlation*

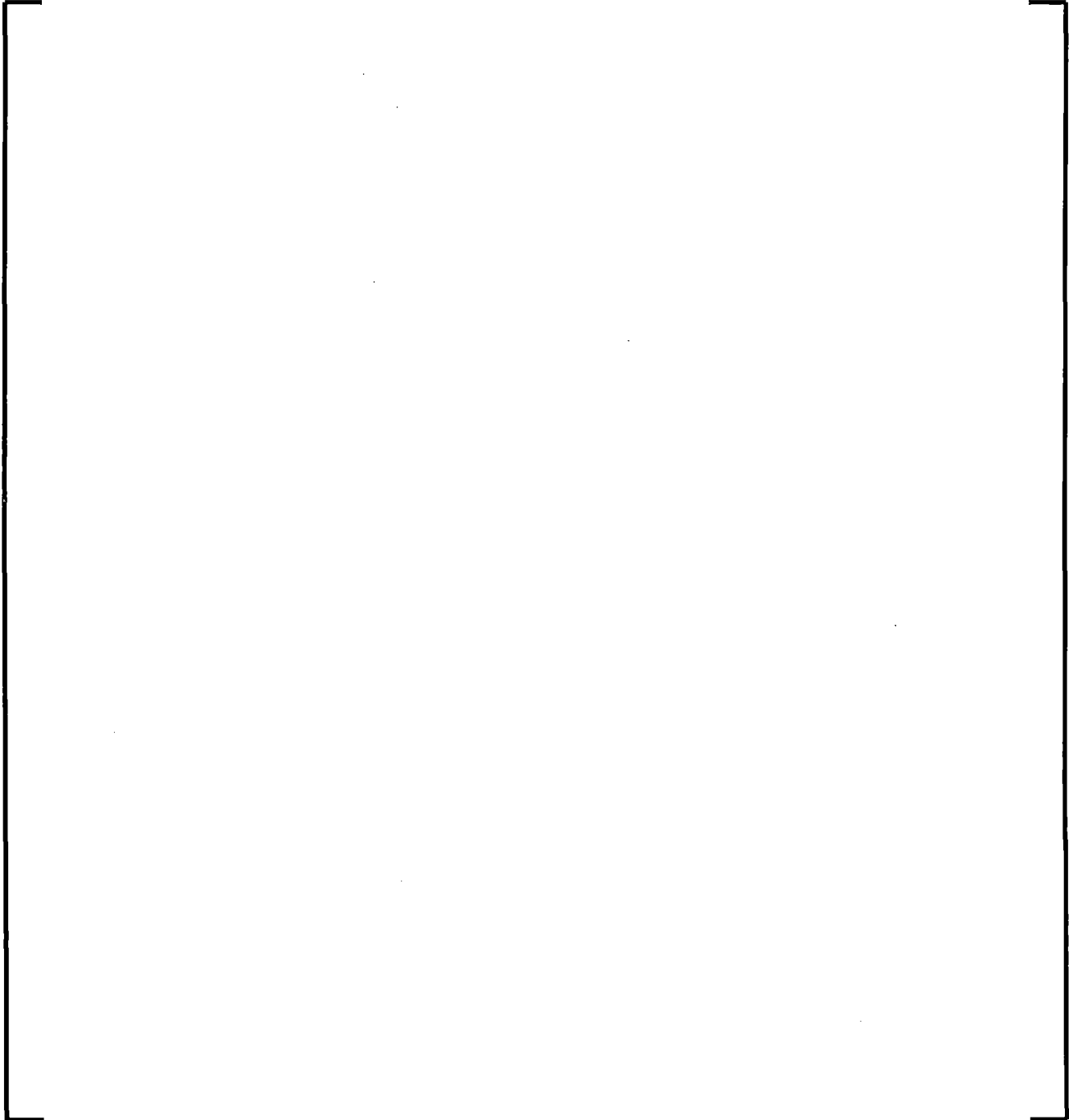
A dryout correlation of the critical heat flux type is developed. [

]









A.2 CPROM Correlation for ATRIUM 10XM



I

[illegible]

[

1

[

]



Figure A-1: Calculated versus measured critical power,
[]



FigureA-2: []



Figure A-3: []



Figure A-4: []



Figure A-5: []



Figure A-6: []

Table A-2: Statistics [

[illegible]

Table A-3: Statistics [

I

I

E

1

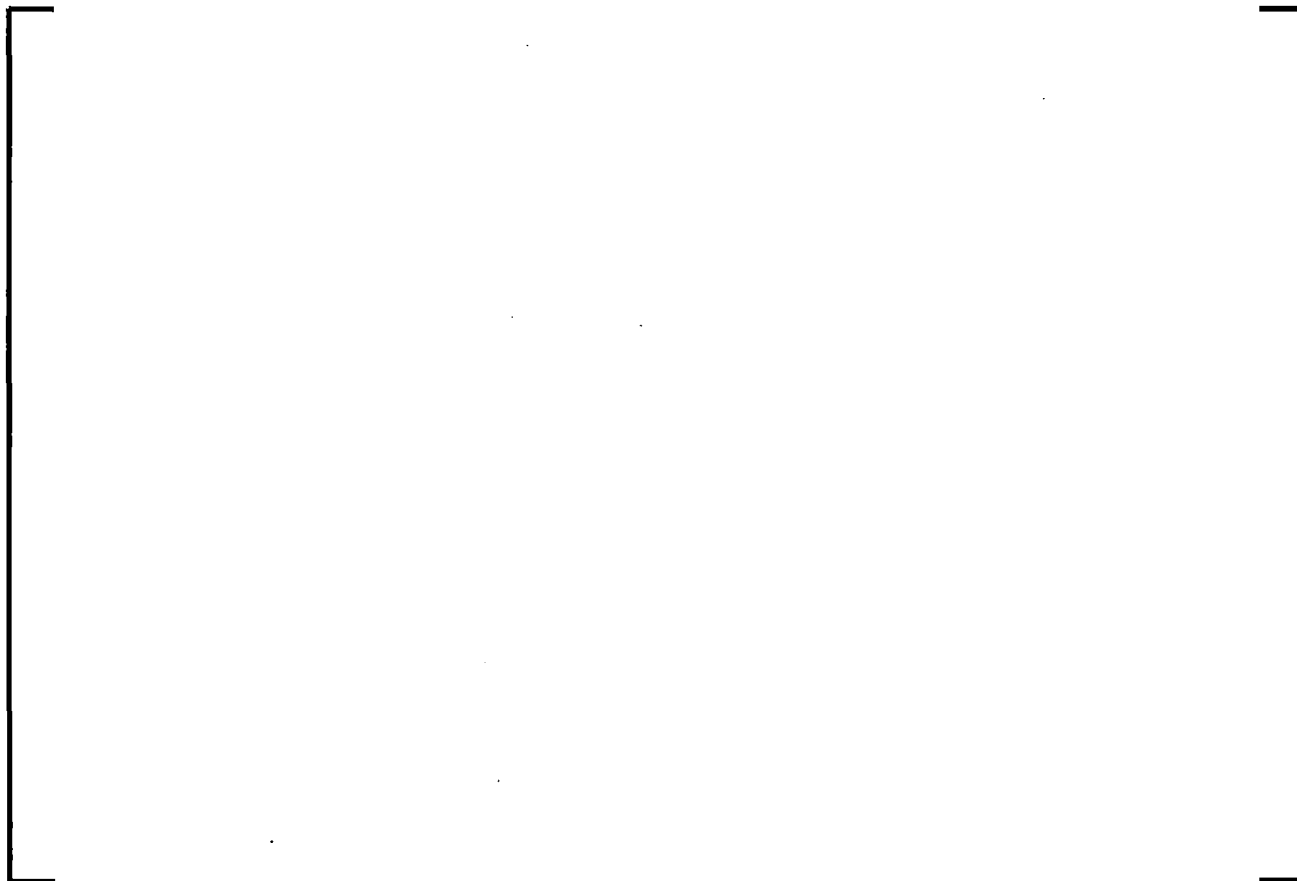


Figure A-7: Calculated versus measured critical power,
[]



Figure A-8: []

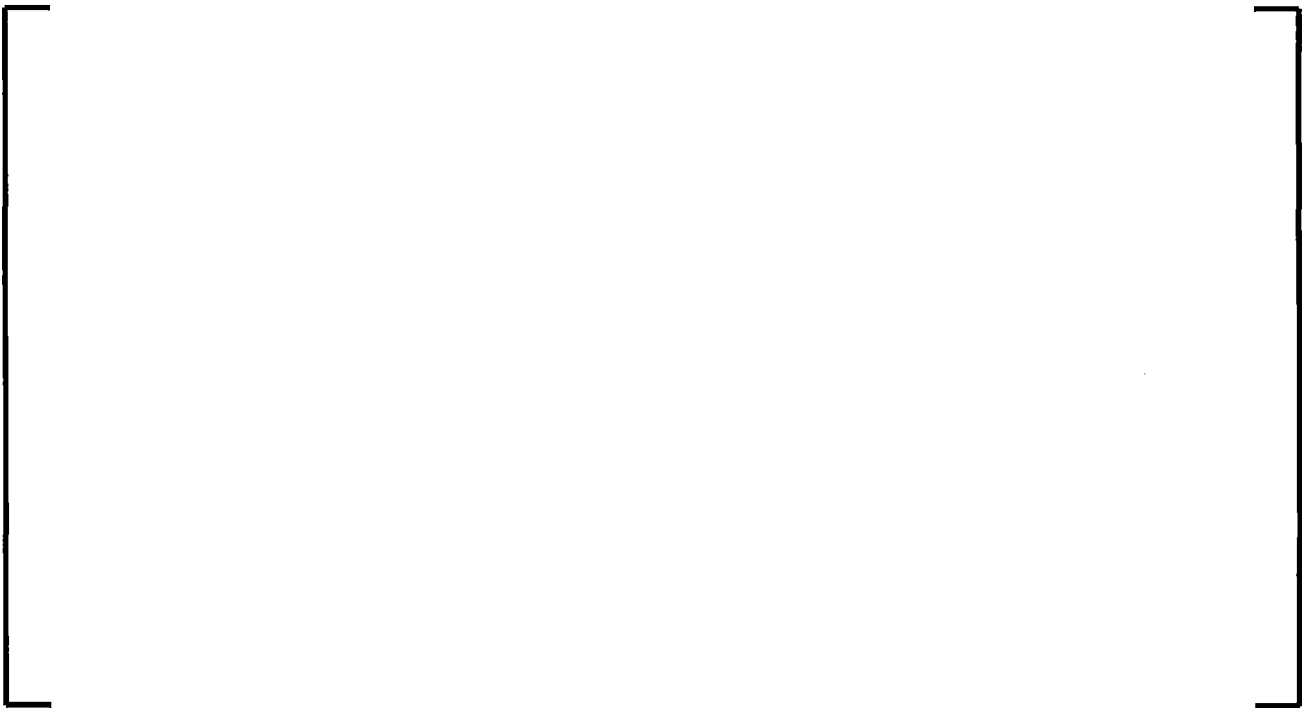


Figure A-9: []



Figure A-10: []



Figure A-11: []



Figure A-12: []

Table A-6: Statistics []



Table A.2: Stationing 5

[illegible]

The figure below shows comparison of the calculated and measured critical power for the combined data set. The mean critical power ratio is [] and the standard deviation of the calculated versus measured critical power for the entire database is [] and the number of data points is [].



Figure A-13: Calculated versus measured critical power

A.3 *CFROM BOUNDS OF APPLICABILITY*

The bounds of applicability are determined by the data available to benchmark the correlation. For ATRIUM 10XM, the [

A.4 CPROM COEFFICIENT GENERATION FOR NEW FUEL DESIGNS

In order to properly generate CPROM coefficients for new fuel designs, the following requirements must be met.



Appendix B Heat Transfer Data from KATHY Loop Stability Testing of ATRIUM 10XM

Abstract

Essential elements of the RAMONA5-FA model pertaining to the heat transfer coefficient behavior under wetted and dry conditions are extracted from measured data. The data set used for this purpose is the stability testing of the ATRIUM 10XM BWR bundle represented in full scale electrically heated module in the KATHY test facility. The testing conditions include steady state where the flow rate fluctuates only at the noise level. They also include very large unstable oscillations where significant inlet flow reversal occurs. The power level was kept constant under manual control for some tests. For other test runs, a feedback loop (SINAN module) determined the power input to the bundle and the resulting coherent power and flow oscillations of large amplitude provided a close simulation of the realistic conditions under ATWS-I transient.

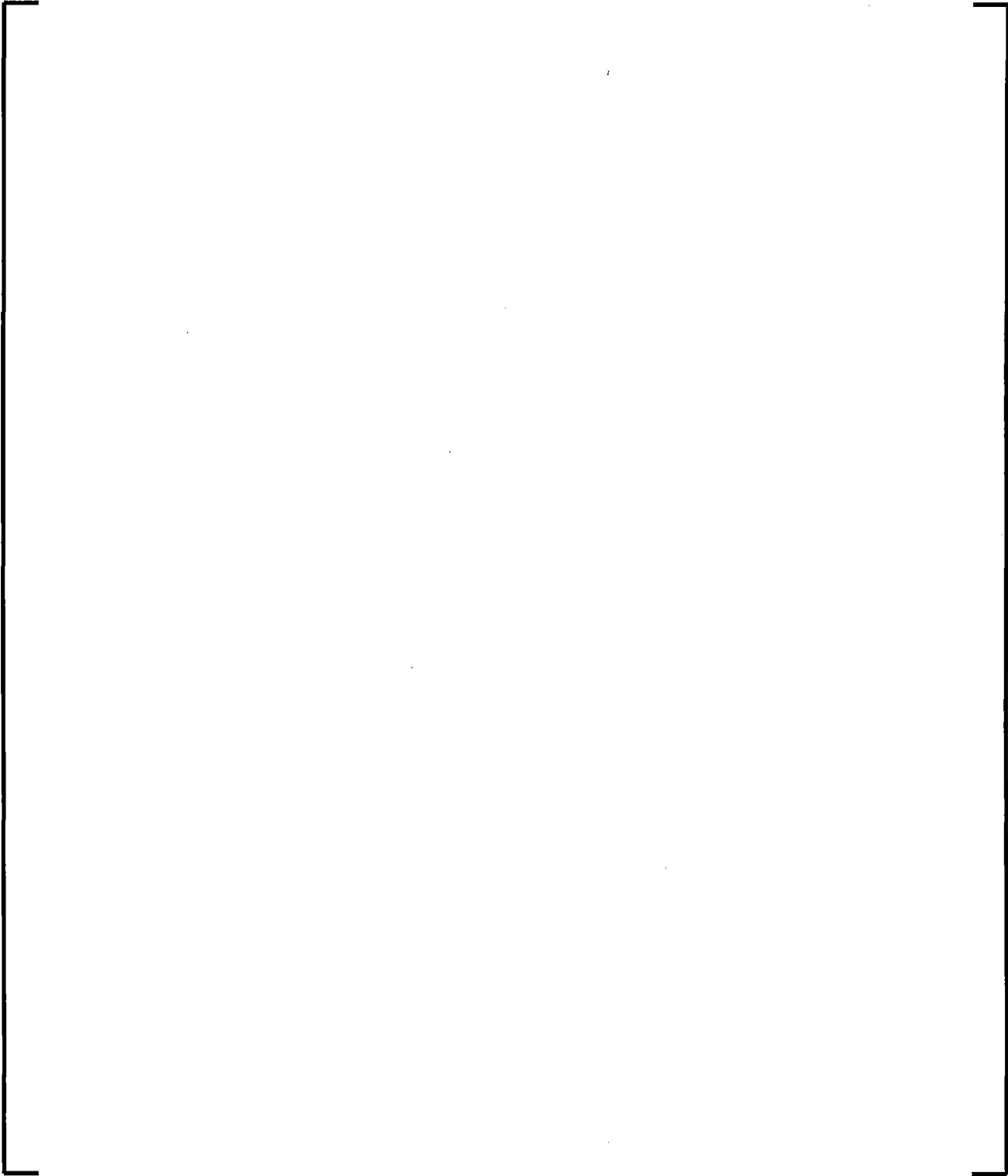
The following sections provide the heat transfer parameters determining the wet and dry conditions and [

]

B.1 *Summary of Heat Transfer Coefficient Data and Observations*

The needed measured data include the test section power, pressure, inlet flow rate, inlet subcooling and the temperature of the heater rods. [

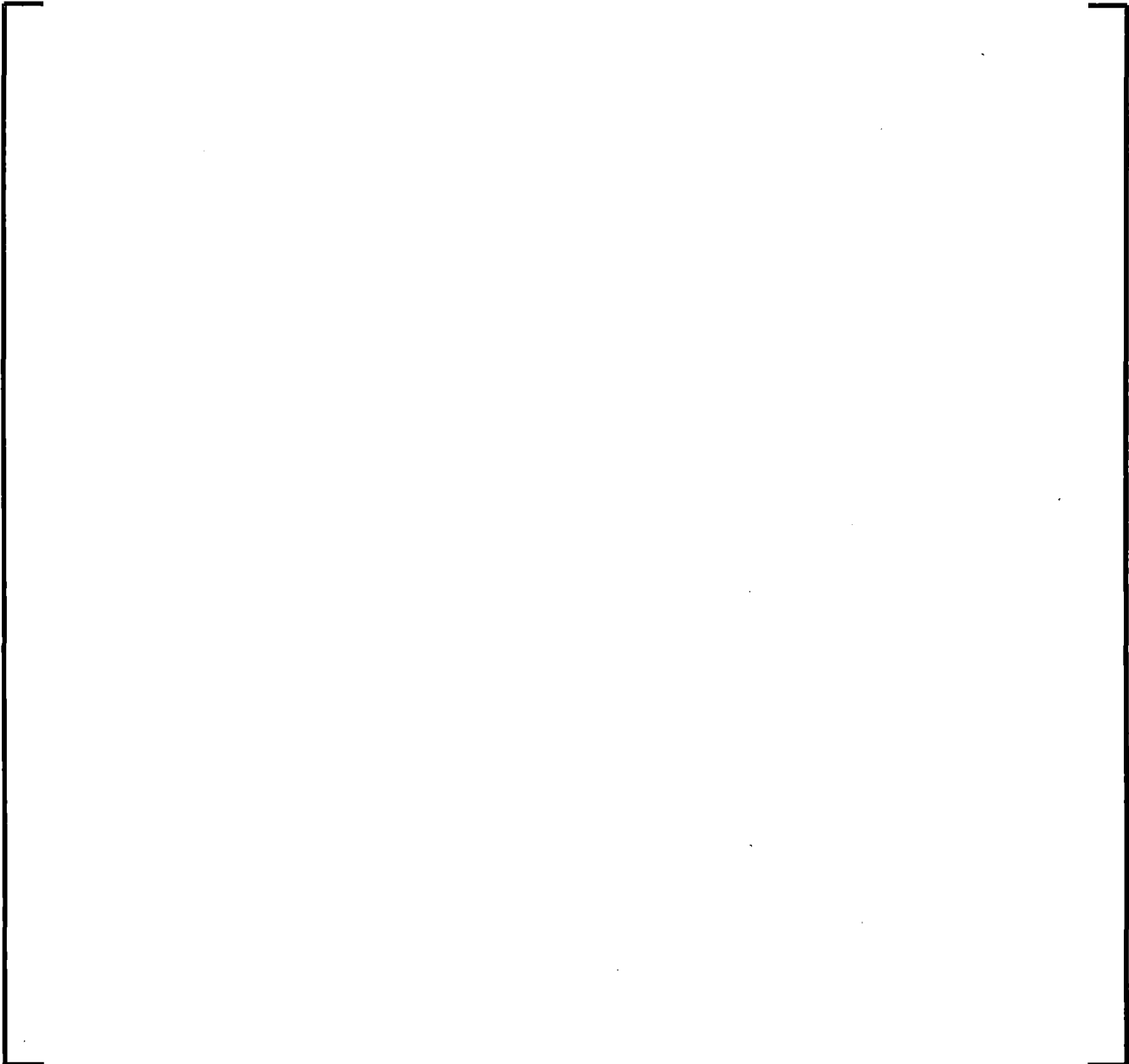
]



B.2 *Heat Transfer Coefficient under Wetted Conditions*

The heat transfer extracted at the initial testing time, where wet conditions are guaranteed, are fit to the [].

B.3 []



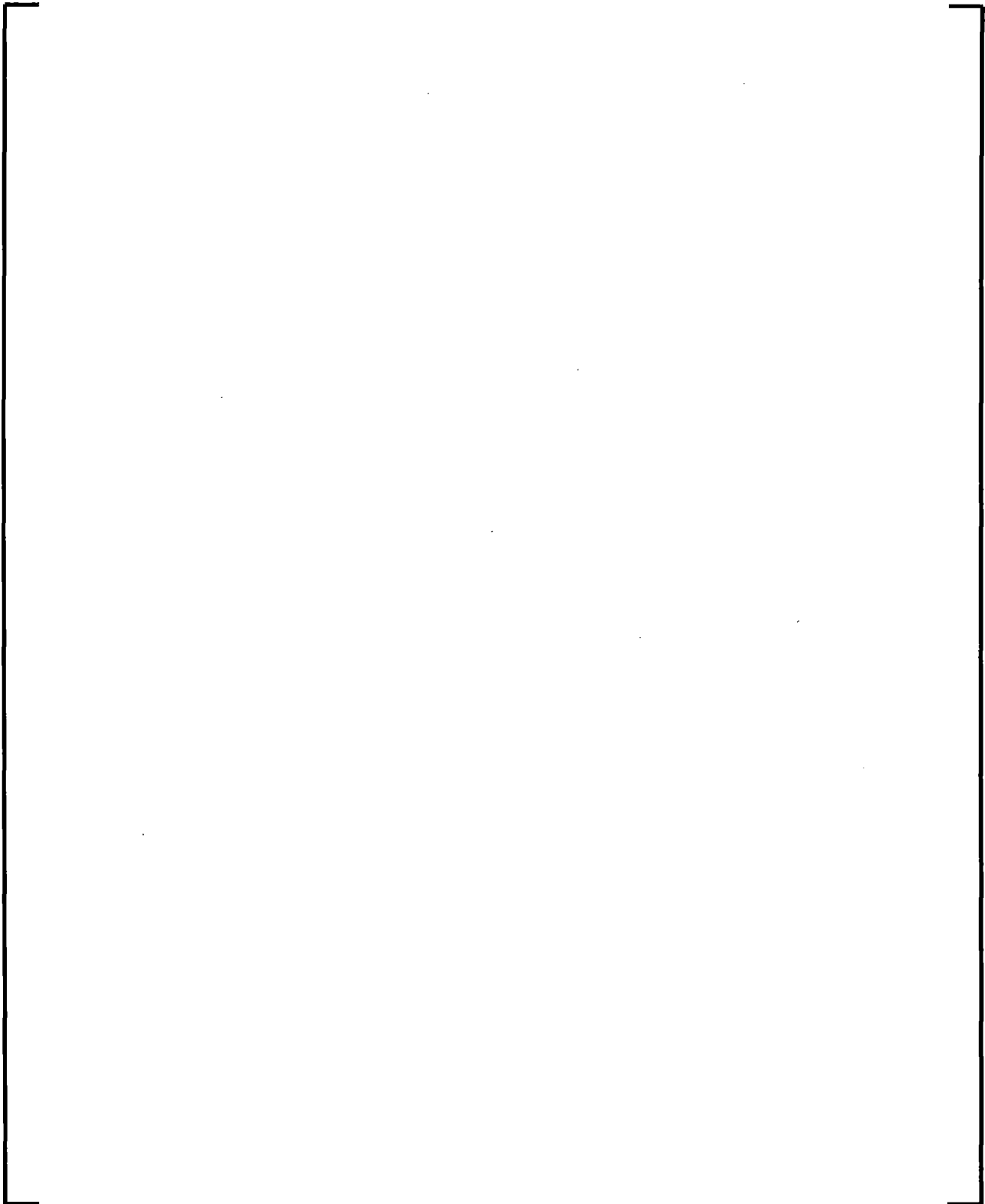




Figure B-1: [

]

B.4 *References*

B.1. [

]

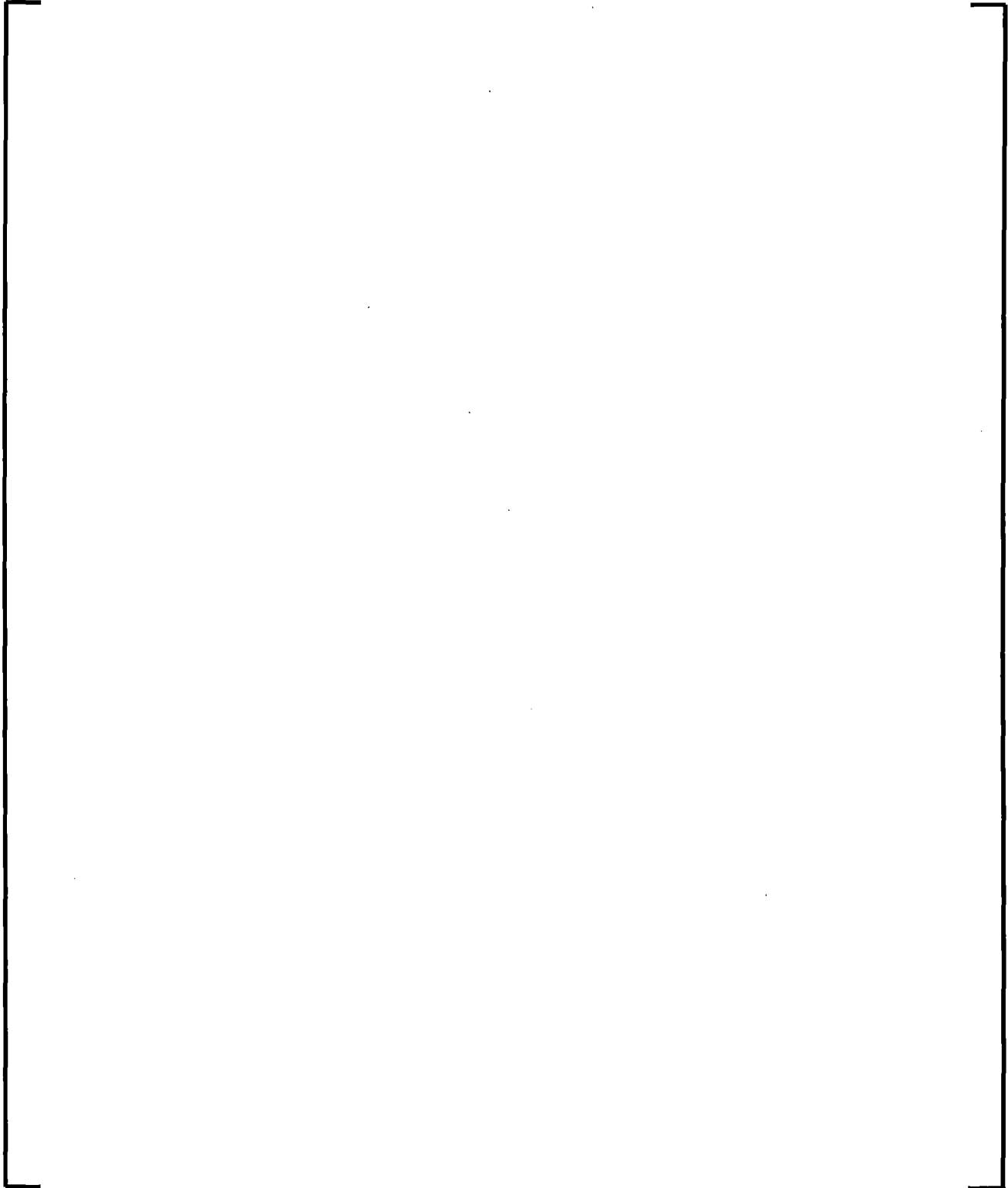
B.2. [

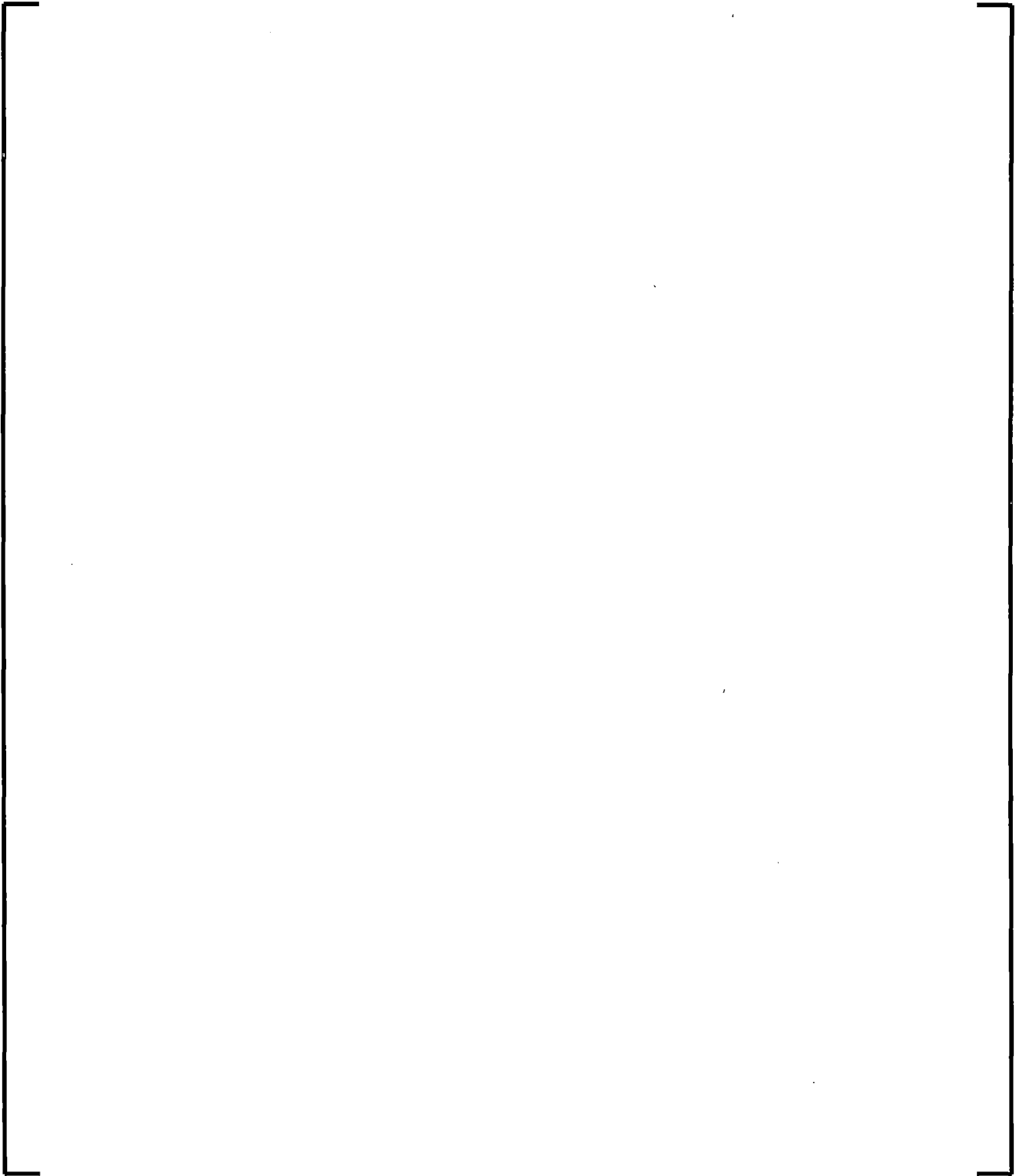
]

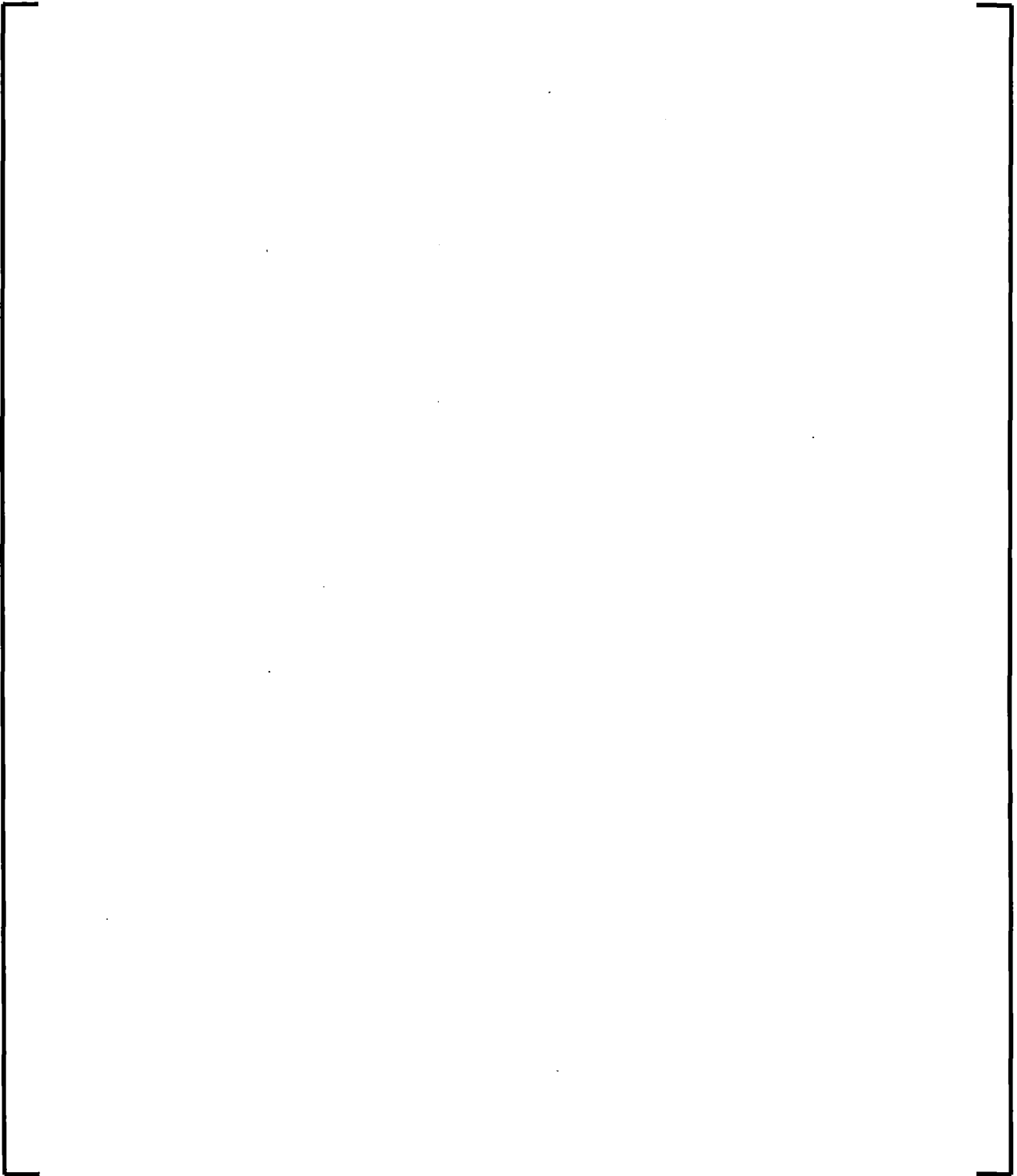
B.3. [

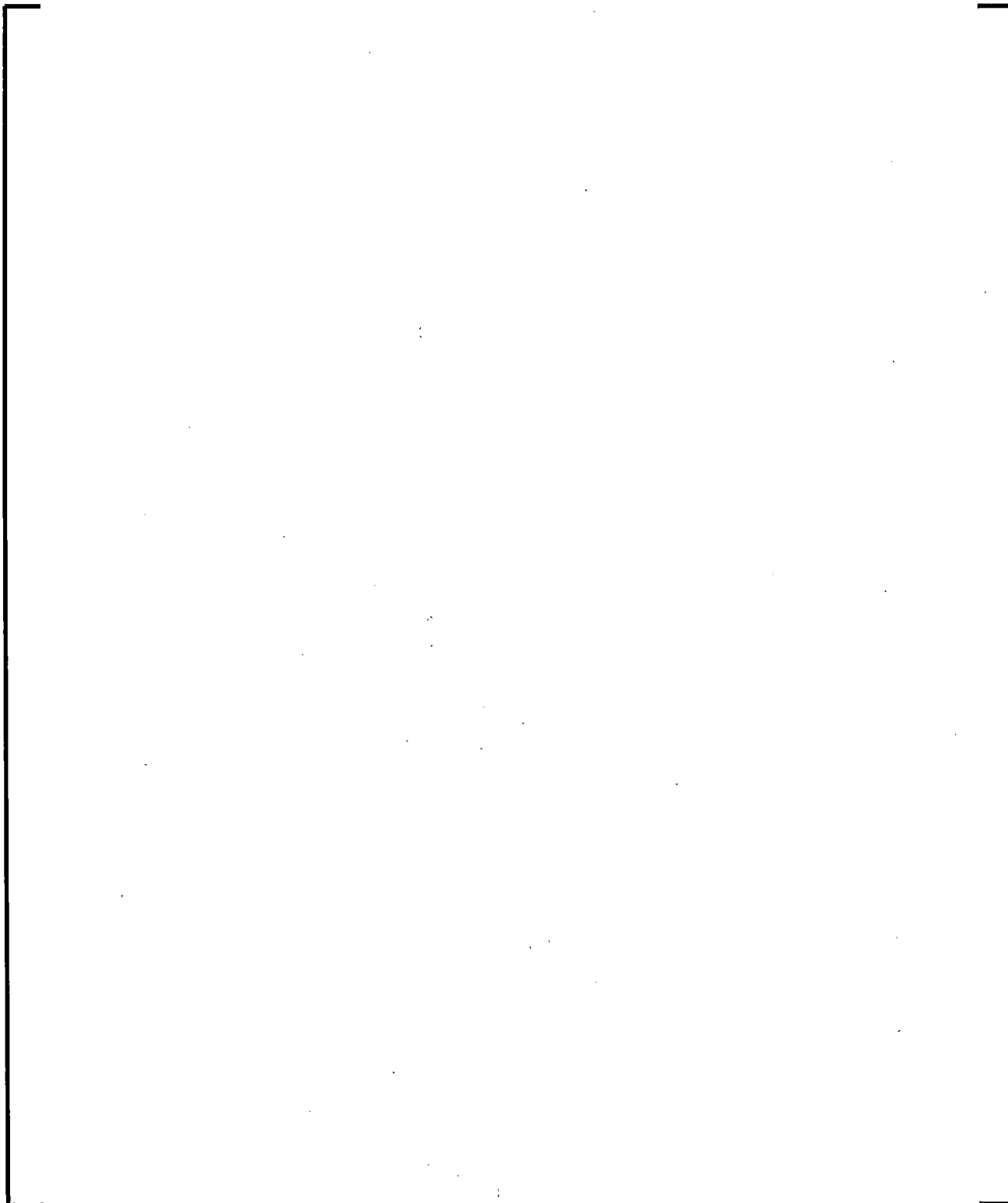
]

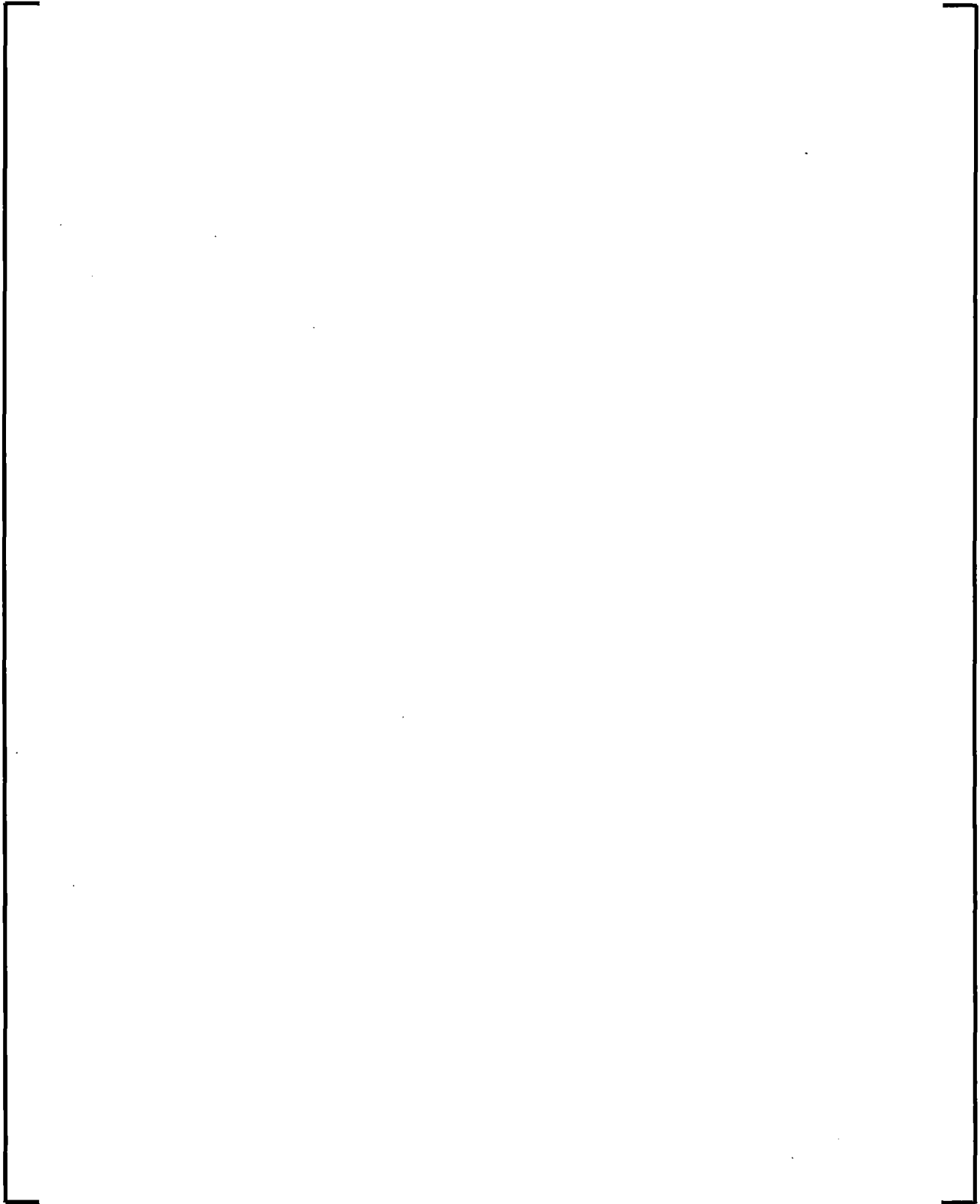
Appendix C Investigation of the Dynamic Effects of Interfacial Friction

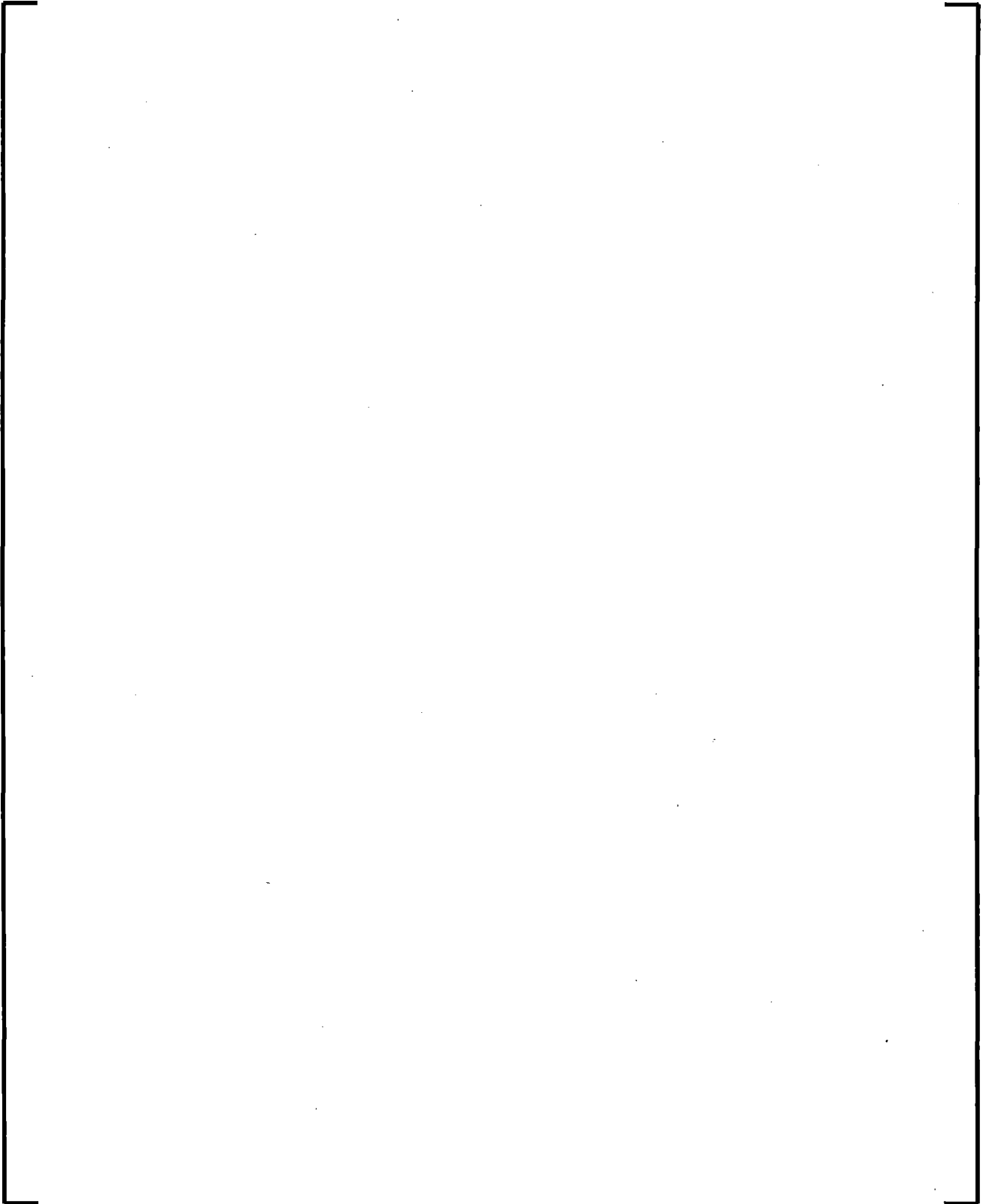


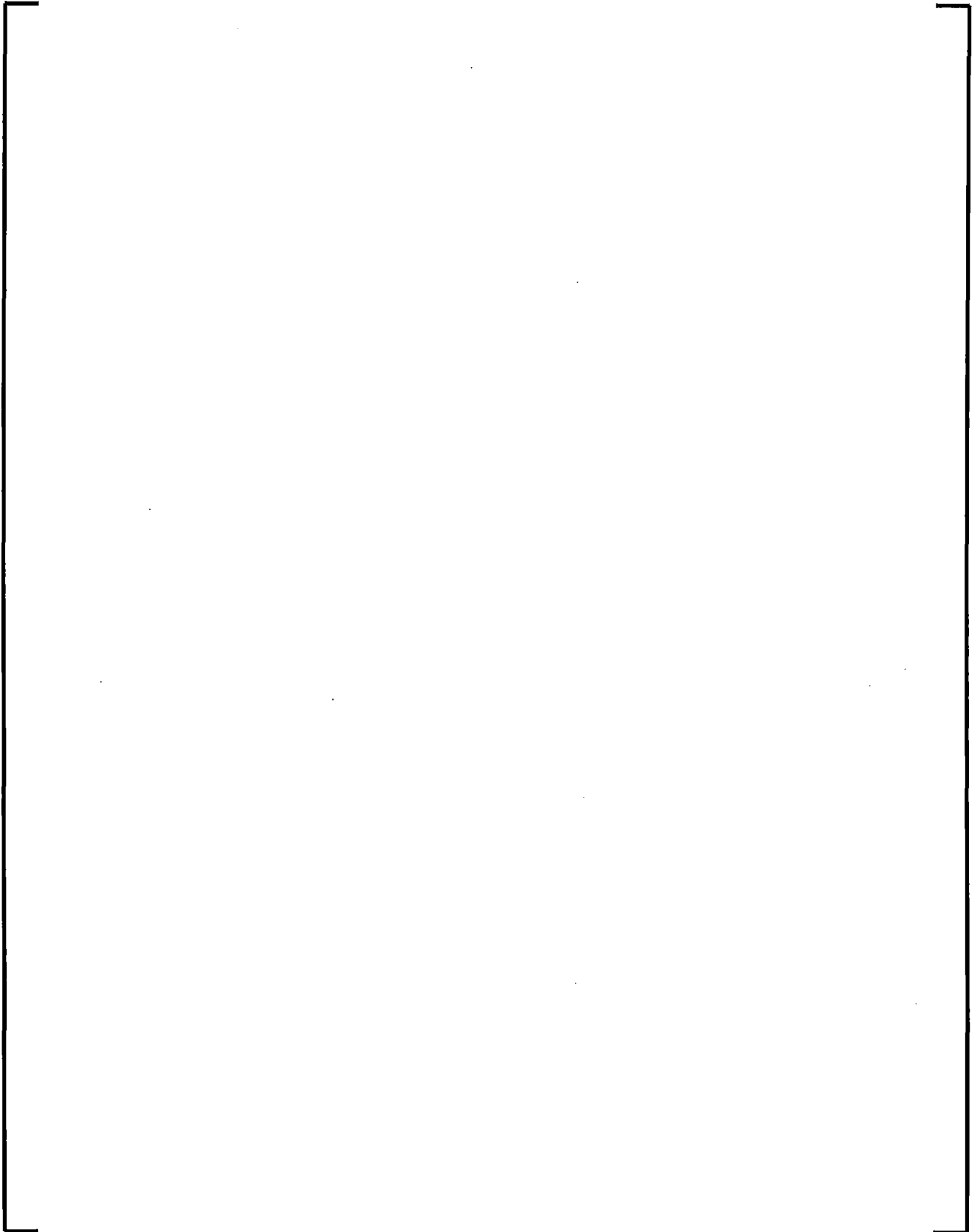


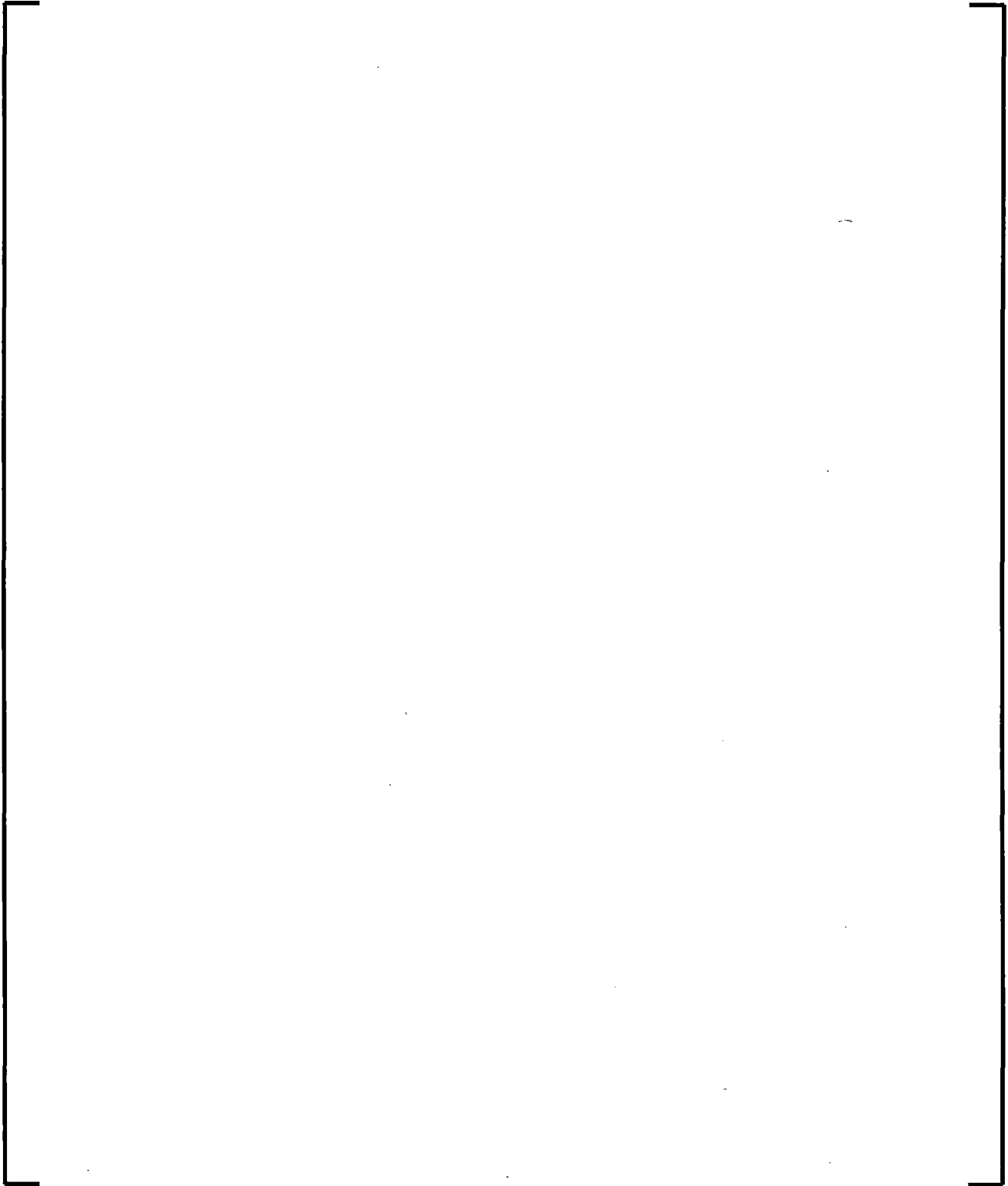


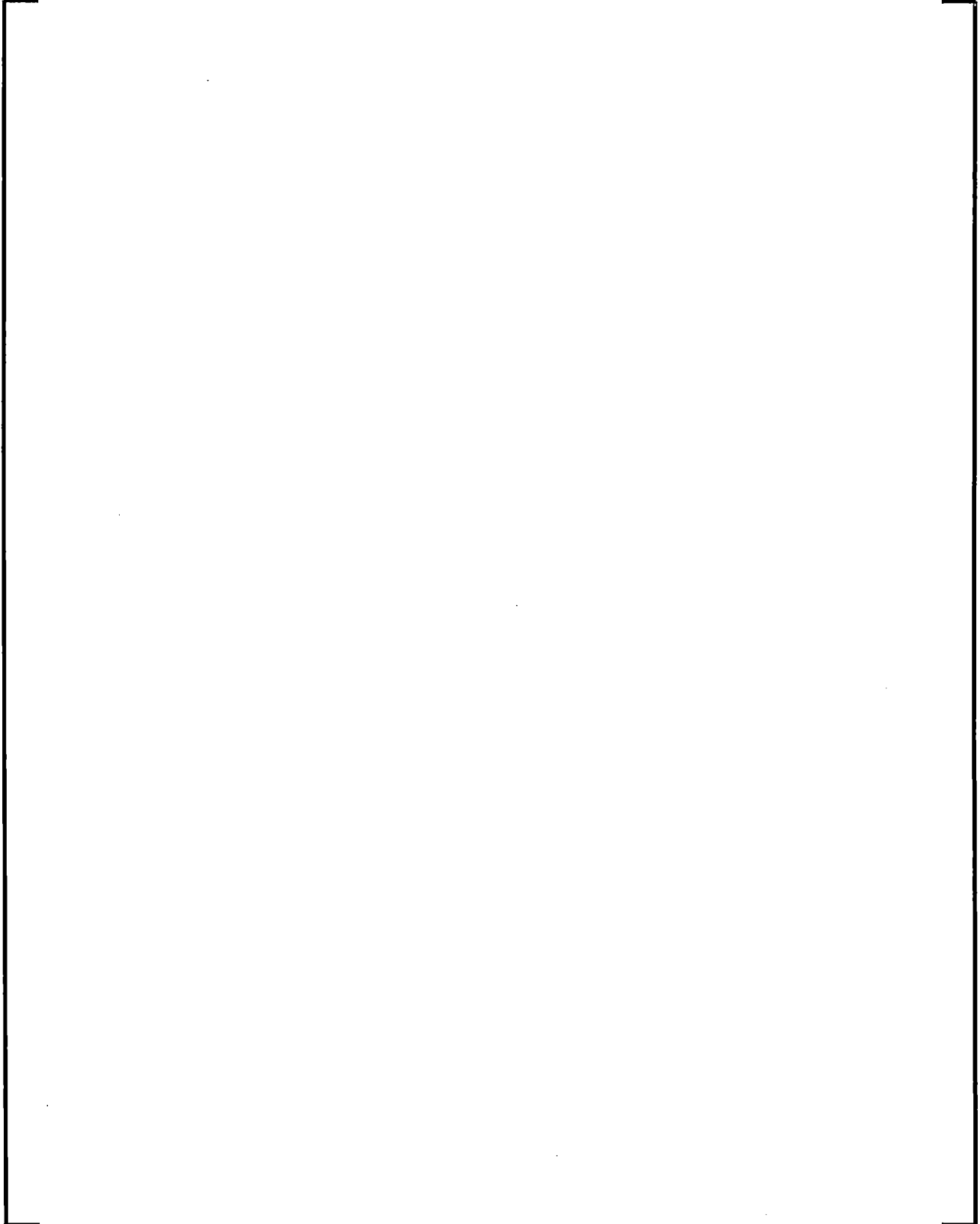












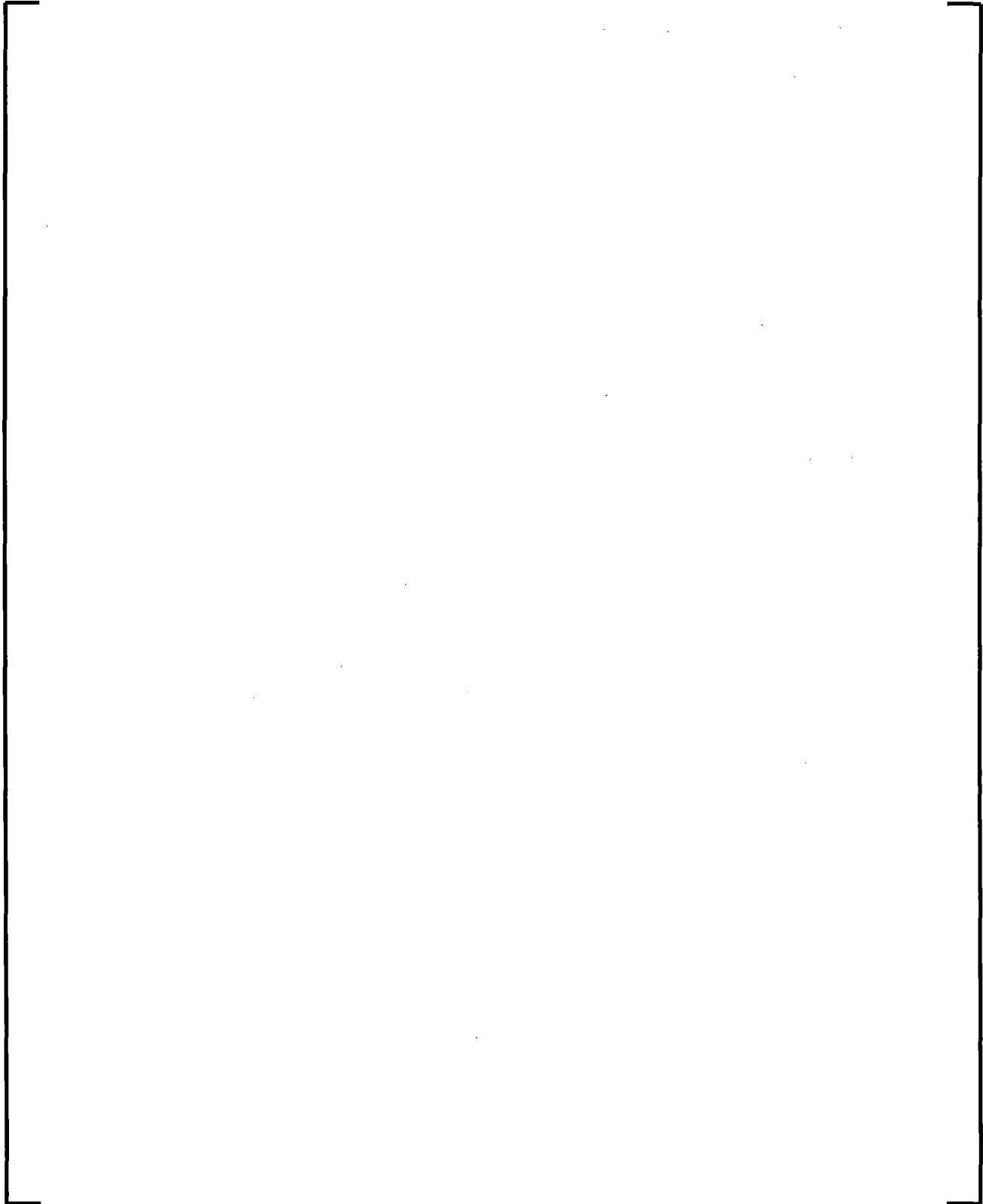




Figure C-14: Oskarshamn Core Power, Interfacial Friction Sensitivity



Figure C-15: BWR A Core Power, Interfacial Friction Sensitivity